Vaal University of Technology

INVESTIGATION OF THE PERFORMANCE OF FIBRE REINFORCED POLYMER RE-BARS IN STRUCTURAL FOUNDATIONS

by

LABANA BELTRAN BTech (Eng)

Dissertation submitted in fulfilment of the requirements for the Degree of **Magister Technologiae** in the Department of Civil Engineering and Building, Faculty of Engineering and Technology, Vaal University of Technology.

Supervisor: Dr. R. Salim Wanjala, BSc (Hons) Eng, MSc, PhD

Co – supervisors: Prof J.M. Ndambuki BSc (Hons) Eng, MSc, PhD

Prof L.M. Masu BSc (Hons) Eng, MSc, PhD

June 2011

Declaration

I declare that this dissertation is my own unaided work, except where specific acknowledgement is made in the form of a reference. The dissertation is being submitted for the degree of Magister Technologiae: Civil Engineering at the Vaal University of Technology, Vanderbijlpark. It has not been submitted before for any examination.

LABANA BELTRAN

_____ day of _____ 2011

Acknowledgements

I would like to express my sincere gratitude to my supervisor and co-supervisors, Dr Salim Wanjala, Prof Leonard Masu and Prof Julius Ndambuki respectively for their support, guidance, helpful criticism and patience throughout the course of this work.

The financial support from Vaal University of Technology is greatly appreciated.

Special thanks go to Stephen Nyende Byakika with whom we shared many ideas and challenges. I would like to thank the staff at the Department of Civil Engineering and Building for their assistance and time that we shared.

I am also very grateful to my family for the support and encouragement during my study and particularly grateful to my parents, Prof Labana Lasay'Abar and Mrs Thabu Malu for their guidance and love. My sincere thanks go to my friends, Alain Ndaya, Ms T. Serote, Cedrick Lumbu, Olivier Mukobo and many others, thanks to all you guys. I would like to thank my fiancée Gloria Munda for the support, patience and for always being there.

Finally, I thank God for enabling me to go through this course.

Dedication

This dissertation is dedicated to my family and my fiancée Gloria Munda.

Abstract

This research focused on the structural performance of Fibre Reinforced Polymer (FRP) re-bars in structural foundation compared to steel reinforcement re-bars. The corrosion of steel re-bars is the main reason of deterioration of reinforced concrete. However, use of FRP re-bars as alternative reinforcement will address the deterioration of reinforced concrete. Carbon and Glass Fibre Reinforced Polymer re-bars were used as reinforcing bars and traditional steel reinforced concrete was used as the reference. Thirty six specimens of reinforced concrete bases were tested for flexural capacity at different ages.

The simulation of Soil Bearing Pressure of this study was derived from the model of beam finite length on elastic foundation. The foundation base was treated as a beam while the soil was modelled as series of timber elements acting as springs. The mathematical model to reflect the model was as documented by Timoshenko (1976:18) and Den Hartog (1952:160).

Results showed that stress in the steel re-bars of reinforced concrete was higher than that of Carbon Fibre Reinforced Polymer (CFRP) and Glass Fibre Reinforced Polymer (GFRP) re-bars by 227 MPa (5.99 percent) and 284 MPa (7.61 percent), respectively. The stress in CFRP re-bars was 57 MPa or 1.53 percent higher compared to GFRP re-bars of FRP reinforced concrete. Furthermore, the experimental ultimate moments of CFRP and GFRP reinforced concrete foundation – bases on the 28^{th} day were 23.917 kNm (79.0 percent) and 23.529 kNm (77.7 percent) higher than the theoretical ultimate moments, respectively. However, steel reinforced concrete foundation – bases had the higher calculated deflection than FRP reinforced concrete.

With high resistance to corrosion as a property, FRP re-bars appeared to be a better alternative reinforcement to steel in corrosion in an aggressive environment.

Table of contents

List of Figures

List of Tables

Notation

A Area of reinforcement

A_f Cross-sectional area of FRP re-bars

A_s Cross-sectional area of Steel re-bars

D_w Width of timber element

E Bridge voltage

E_A Anodic electrode potential

E_C Cathodic electrode potential

E_c Modulus of elasticity of concrete

E_f Modulus of elasticity of FRP re-bars

E_r Modulus of elasticity of reinforcement

E_s Modulus of elasticity of Steel re-bars

E_T Modulus of elasticity of timber

$E_{h.frp}$ Modulus of elasticity in the hoop direction

$E_{\sec 0}$ Secant modulus of elasticity at the compressive strength of unconfined concrete

Fe^{2+} Concentration of iron ions

F_C Compression force

F_T Tensile force

F_u Ultimate tensile capacity

F_1 Tensile force in FRP re-bars at 20 percent of tensile strength

F_2 Tensile force in FRP re-bars at 50 percent of tensile strength

I_c Second moment of area of concrete section

L Span of reinforced concrete foundation – base specimen

M Bending moment

M_o First moment of area

M_u Ultimate moment

O_2 Concentration of oxygen

P Concentrated load

R Radius of concrete core

b Breadth of reinforced concrete specimen; Width of the beam

c' Normalised ultimate strain of unconfined concrete

d Depth of reinforcement

d_b Equivalent diameter of FRP re-bars

e Electromotive force

e_o Output voltage

f_c Cube compressive strength of concrete

f_{cu} Ultimate cube compressive strength of concrete

f_c' Cylinder compressive strength of concrete

f_{cd} Characteristic compressive strength of concrete

f_{co}' Compressive strength of unconfined concrete

$f_{l,a}$ Actual maximum confining pressure

f_f Tensile strength of FRP re-bars

f_{fk} Characteristic tensile strength of FRP re-bars

f_{fu} Ultimate tensile strength of FRP re-bars

f_s Tensile strength of high Steel re-bars

f_{su} Ultimate tensile strength of high Steel re-bars

h Depth of reinforced concrete specimen

h_T Height of timber element

k Modulus of foundation

k_1 Strain enhancement coefficient for Steel jacket

k_2 Strain enhancement coefficient for FRP jacket

k_s Gauge factor

m Modular ratio

t Total thickness of the FRP jacket

x Depth of neutral axis

x_1 Age of reinforced concrete bases

y Ultimate loads

y_{CT} Distance between compressive force and tension force

y_{centre} Deflection at the centre of beam on elastic foundation

y_{end} Deflection at the end of beam on elastic foundation

α Exponent to be determined related to ultimate condition of the jacket for FRP – confined concrete

α_1 Ratio of the average concrete stress to the concrete strength

α_{cc} Factor related to the compressive strength of concrete equals to 1

β Exponent to be determined related to ultimate condition of the jacket for FRP – confined concrete

β_1 Equivalent rectangular stress block parameter

β_e Characteristic of beam on elastic foundation

γ_f Partial safety factor of FRP re-bars

γ_s Partial safety factor of steel re-bars

$\varepsilon_{h.rup}$ Hoop rupture strain of the FRP

ε_{co} Axial strain of unconfined concrete

ε_{ccu} Ultimate strain of the confined concrete

ε_c Strain in concrete

ε_{cu} Ultimate strain in concrete

ε_f Strain in FRP re-bars

ε_{fk} Characteristic tensile strain of FRP re-bars

ε_{fd} Design strain of FRP reinforcement

ε_{fu} Ultimate strain in FRP re-bars

ε_1 Strain in FRP re-bars at 20 percent of tensile strength

ε_2 Strain in FRP re-bars at 50 percent of tensile strength

ε_s Strain in Steel re-bars

ε_{su} Ultimate strain for Steel re-bars

ε_o Initial strain in concrete

ε_{OS} Output Strain

η_a Environmental conversion factor for different FRP re-bars

η Factor related to the compressive strength of concrete equals to 1

λ Factor related to the compressive strength of concrete equals to 0.8

ρ_f FRP reinforcement ratio

ρ_{fb} Balanced FRP reinforcement ratio

σ_x Corresponding stress in reinforcing bars

ψ_u Corresponding curvature of compression in concrete when rupture of FRP occurs.

CHAPTER 1: INTRODUCTION

1.1 General Background

Reinforced concrete is one the most used composite material in structural and civil engineering. The deterioration of concrete and the corrosion of steel are the disadvantages of this material. Different methods of reinforcement protection, such as carbonisation, increase of concrete cover and specific selection of aggregates, have been reported and are well documented (Ahmad, 2003:459; Alexander Mackechine, 2003:20). However, the economic aspects of corrosion of steel re-bars on the lifetime of structures and the degradation of reinforced concrete in marine structures and bridges subjected to de-icing salts has become an environmental issue; the above cited methods are not adequate and they have their limitations.

In the past decade, a new approach was adopted to deal with the corrosion of steel by using an alternative reinforcement. The high resistance to corrosion, high longitudinal strength, high fatigue endurance and high specific stiffness of Fibre Reinforced Polymer (FRP) made them an appropriate material for this purpose regardless of their relatively high manufacturing cost compared to steel re-bars as well as their high initial application costs. Despite these advantages over steel re-bars, the ultimate tensile strength of FRP re-bars decrease with bar diameter and they are brittle materials.

Fibre Reinforced Polymer (FRP) is a composite material constituted of resin (known as matrix) and fibres. The fibres are the primary load-carrying components and the resin provides a continuous protection medium of fibre. Manufactured by pultrusion method, FRP re-bars are commercialized worldwide in three types namely as Carbon (CFRP), Glass (GFRP) and Aramid (AFRP). They are produced in different forms (sheets, re-bars, grids, prestressing tendons and laminates) for different applications such as external and internal reinforcement. In the present study, CFRP and GFRP re-bars were used as internal reinforcement and they were chosen due to their availability in the local market.

Over the last two decades, FRP reinforcements for structural elements in construction have aroused the interest of civil and structural engineers as well as the composites industry. Civil engineers are driven by the potential performance benefits offered by these materials and the enthusiasm of academics and researchers for developing new materials (Humphreys, 2003:1-3; Shanmuganathan, 2003:26). The composites industry is driven by the desire to participate in what is arguably the world's largest industry (Humphreys, 2003: 1-3). Nowadays, theoretical studies and experimental program-data are available on the applications of FRP reinforced concrete such as beams, suspended slabs and pavement.

To date some design guidelines and standards have been published worldwide to provide information on the use of Fibre Reinforced Polymer materials in the construction industry. These design guidelines are based on reports of theoretical studies and experimental programs on FRP reinforced concrete conducted in the past. However, the necessity to address the non-ductility of Fibre Reinforced Polymer re-bars and the insufficient experimental data on the long time behaviour of concrete reinforced with FRP re-bars are some obstacles for the full implementation of Fibre Reinforced Polymer as internal reinforcement materials.

1.2 Problem Statement

The lack of ductility of FRP re-bars is critical in the behaviour of concrete reinforced with them. This can consequently lead to a lack of plasticity in the reinforced concrete member and make elements fail in a brittle manner. The currently available design formulae for designing FRP reinforced concrete elements as adopted by many design codes were originally developed with regard to that of steel reinforced concrete. Hence a new approach is needed to attend to the lack of ductility in the design philosophy of FRP reinforced concrete.

To date many experimental programs and theoretical studies have been done on concrete reinforced with FRP re-bars members such as beams, columns and slabs. The flexural, shear, bond of FRP re-bars or cracking and deflection behaviour of beams, columns and slabs have been addressed and reports have been published as

guidelines. More recently (ACI 440.1R, 2006:120), FRP re-bars were used in concrete pavement as dowel bars. However, more research is needed to understand the mechanical characteristics of this new technology and there are still many aspects to be investigated to provide reliable design rules to be implemented in codes of practice (Ceroni et al., 2006:857). Despite the extraordinary progress made in research of this new material, to date adequate research has not been done to fully exploit the potential of this composite material (Pilakoutas et al., 2007:38). Scanty evidence exists on the flexural behaviour and deflections of isolated foundations despite its interaction effects on the reinforced concrete member and the soil bearing pressure.

In this application, the theoretical approach developed for beam and slab suspended was considered by taking into account the interaction between the reinforced concrete member and the soil bearing pressure.

1.3 Main Objective

The main objective of this research was to investigate the structural behaviour of Fibre Reinforced Polymer reinforced concrete foundation – bases and compare it to that of steel reinforced concrete foundation – bases.

Although some researchers in Japan, North America and Europe are working in teams to develop the design codes, to date, in Africa (except in Egypt) and particularly in South Africa, there are no standard codes developed locally for the use of Fibre Reinforced Polymers in civil engineering. Thus the main objective of this research is to investigate and compare strength and flexural behaviour of Fibre Reinforced Polymer reinforced concrete at the ultimate limit state in the design of foundation. Of particular interest is the comparison of FRP reinforced concrete to steel reinforced concrete strength characteristics, mechanical behaviour, deflection and stress.

1.4 Specific Objectives

In order to achieve the research objective, the study sought to:

a. Analyse the strain behaviour of FRP materials and their implications;
b. Evaluate the stress-strain behaviour of FRP and steel reinforced concrete foundations and their implications;
c. Analyse the load carrying capacity and the moment capacity of FRP and steel reinforced concrete foundations.

The study also focused on the new areas of applications of this advanced composite in reinforced concrete pavement, especially in the isolate foundation considered as slab not suspended.

1.5 Scope

Many conferences and journal publications have focussed on the use of Fibre Reinforced Polymer in the design of beams or slabs. However, few research studies have been conducted on FRP reinforced concrete foundation – bases. This study focused on the application of this advanced composite in reinforced concrete isolated foundation bases. The structural properties investigated in this research were the strain behaviour of materials, namely, concrete, FRP and steel reinforcing bars as well as the stress behaviour and moment capacity.

Considering the properties of Fibre Reinforced Polymer (such as its high specific stiffness, high specific strength and anti-seismic behaviour), it was anticipated that the foundations designed with Fibre Reinforced Polymer reinforcement would be superior in performance to the steel reinforcement, especially in an aggressive environment. The research also provided more insight into the performance of Fibre Reinforced Polymer. Hence this study would help in improving the existing design methods used in Fibre Reinforced Polymer in buildings and pavements.

1.6 Outline of the dissertation

The dissertation has six chapters. Chapter 1: Introduction. Chapter 2: Literature Review; presents the development in used FRP in the civil engineering field. Chapter 3: Research Materials, equipment and methods. Chapter 4: Modelling Approach; the theoretical approach used to analyse the moment capacity of foundation and the simulation of bearing pressure of soil are presented. Chapter 5: Presentation and Discussion of Results. Chapter 6: Conclusions and Recommendations.

CHAPTER 2: LITERATURE REVIEW

2.1 Introduction

This chapter explores the use of Fibre Reinforced Polymer (FRP) in different applications in civil engineering. The first part explored the properties and advantages of using FRP in different projects of structural engineering and the second part discusses the importance of FRP investigation.

2.2 Fibre Reinforced Polymer

FRP composites shown in Figure 1, also known as advanced composite materials, are made from combined fibres and resin so that each constituent retains its original properties. The effects of fibre reinforcement depend on the type and content of the fibre and the properties of the resin (known as matrix). The fibres are the primary load-carrying component having low-weight, high-strength, and high-stiffness properties. The resin provides a continuous medium protection of fibre reinforcement and transferring the stresses between fibres (Shanmuganathan, 2003:26).

Figure 1 FRP re-bars produced by Pultrall Company

2.2.1 Composition of Fibre Reinforced Polymer

2.2.1.1 Fibres

By definition, fibre is a general term for a filamentary material or any material with its length 100 times its diameter, typically 0.10 to 0.13 mm (ACI 440. 1R, 2006:25). There are three types of materials used as fibre elements; namely aramid fibres, carbon fibres and glass fibres.

a) Aramid Fibres

Aramid fibre is the generic name for aromatic polyamide fibres. The structure of organic aramid fibres gives higher strength and modulus in the fibre longitudinal direction. Since 1972, the aramid fibres are commercialised by company known as Du Pont under the trade name of Kevlar (William and Javad, 2006:654). Two varieties are produced: Kevlar 29 and Kevlar 49. Kevlar 29 is a low density, high strength aramid fibre designed for ballistic protection, ropes and cables; while Kevlar 49 is for plastic reinforcement (Lovell, 1999:27). In certain applications where light weights, high strength, stiffness, resistance to fatigue and stress rupture are important, the Kevlar aramid is used.

b) Carbon Fibres

The term carbon fibre describes fibres that have a carbon content of 80% to 95%. There are 40 different products of carbon fibres varying in modulus, strength, density and number of filaments per row. The fibres can be arranged in four classes: Ultra High Modulus (UHM), High Modulus (HM), Very High Strength (VHS) and High Strength (HS) (Lovell, 1999:28). Currently available carbon fibres are made using one of the three precursor materials: polyacrylonitrile (PAN) fibres, rayon fibres or pitch (Täljsten, 2006:13).

c) Glass Fibres

Glass fibre is an inorganic fibre that is manufactured through a melting process in which an appropriate mixture of raw materials, sand limestone and alumina, is

melted (Täljsten, 2006:12). There are six types of fibres developed for different applications. 'A' glass was the original fibre made from standard window glass; 'C' glass developed to provide improved resistance to acids for chemical plant; 'D' glass for electronic applications to provide a low dielectric constant and good transparency to radar frequencies; 'E' glass for resistance to acids and electrical insulation properties; 'S' glass for highest strength and 'R' glass as a European alternative to 'S' glass (Lovell, 1999:23).

Glass fibres for continuous fibre reinforcement are classified into three types (FIB Bulletin 14, 2001:130): E-glass fibres, S-glass and alkali resistant AR-glass fibres. The two most important types of glass used to produce glass fibres for composites are E (electrical) and S (high-strength) glasses.

The E glass is a lime-aluminium-borosilicate glass with zero or low sodium and potassium levels. Its basic composition ranges from 52 to 56 percent of Silica dioxide (SiO_2), 12 to 16 percent of aluminium oxide (Al_2O_3), 16 to 25 percent of Calcium oxide (CaO), and 8 to 13 percent of anhydrous boric acid (B_2O_3). The composition of S glass is 65 percent SiO_2, 25 percent Al_2O_3 and 10 percent of magnesium oxide (MgO). It has a higher strength-to-weight ratio and is more expensive than E glass (William and Javad, 2006:651).

The mechanical properties of fibres are presented in Table 1.

Table 1 Typical properties of fibres (Täljsten, 2006:14).

Fibre	**Elastic Modulus (GPa)**	**Tensile Strength (MPa)**	**Ultimate tensile strain (%)**
Glass			
E	72 – 77	2,000 – 3,700	3.0 – 4.5
S	80 – 90	3,500 – 4,900	4.2 – 5.4
AR	71 – 74	3,000 – 3,300	3.0 – 4.3
Aramid			
Low modulus	70 – 80	3,500 – 4,100	4.3 – 5.0
High modulus	115 - 130	3,500 – 4,000	2.5 – 3.5
Carbon			
PAN	230 – 600	2,500 – 6,000	0.9 – 2.0
Pitch	200 – 800	2,100 – 3,100	0.2 – 0.9

A new type of FRP composite has emerged that uses high-strength steel fibres and commonly known as Steel FRP (SFRP). The high-strength steel fibres have a linear elastic stress-strain relationship similar to carbon and glass fibres. The tensile strength of the SFRP is in the range of 2400 to 3100 MPa and an elastic modulus of 0.2 GPa. The steel fibres (also referred to as wires) are constituted with steel wires twisted together to form steel cords, each containing five to 13 wires. SFRP is currently being applied for strengthening concrete structures in a similar manner to other externally bonded FRP materials (ACI 440.1R, 2006:62).

2.2.1.2 Matrix

Matrix is the material that serves to bind the fibres together, transfer load to the fibres and protect them against environmental attack and damage due to handling (ACI 440. 1R, 2006:29).

The matrix has a strong influence on several mechanical properties of the composite such as transverse modulus strength, shear properties, and properties in compression (Täljsten, 2006:14). There are three polymetric matrix materials used regularly for the manufacturing of FRP: Polyester, vinylester and epoxy and their properties are shown in Table 2.

Table 2 Typical properties of commonly used matrix materials (Täljsten, 2006:14).

Matrix	Elastic Modulus (GPa)	Tensile Strength (MPa)	Ultimate tensile strain (%)
Polyester	2.1 – 4.1	20 – 100	1.0 – 6.5
Vinylester	3.2	80 – 90	4.0 – 5.0
Epoxy	2.5 – 4.10	55 – 130	1.5 – 9.0

2.2.2 Properties of Fibre Reinforced Polymer

FRP has much higher strength-to-weight ratio and higher ultimate tensile strength than steel. Other properties of FRP are: good resistance to corrosion, fire, and excellent durability. FRP is electrically and electro-magnetically neutral.

However, the mechanical performance of an FRP composite is affected by the volume and type of the fibre and resin; fibre orientation; dimension and quality control during manufacture; loading history and duration; and temperature and moisture. The last factor i.e. duration, temperature and moisture were related to the conservation of materials (Alsayed et al., 2000:132).

An exposure of FRP to sunlight causes damage as well as the degradation of properties in composites materials that may cause chemical reactions between ultraviolet rays and the polymetric matrices. In addition the durability of FRP re-bars is not a straight-forward subject, it tends to be more complex than corrosion of steel reinforcement, because degradation of the material could depend both on resin and fibres and their interface bond behaviour (Ceroni et al., 2006:857). Furthermore, the brittle linear-elastic behaviour of FRP reinforcements due to the lack of ductility is the mostly influencing factors in FRP reinforced concrete and the compressive behaviour of FRP re-bars has not been studied adequately and the tendency to buckle sooner than the steel bars has been noticed (Nicolae et al., 2008:17).

2.3 Reinforced Concrete in Aggressive Environment

The corrosion process of steel reinforcing bars has been widely reported in literature (Ahmad, 2003:459). Different methods have been proposed with a view to protecting the reinforcement against corrosion for over two decades. These methods are such as specific selection of aggregates, increase of concrete cover or cathodic protection.

As the mechanism of the deterioration of reinforced concrete depends on the characteristics of the materials and the environment (Adbulla, 2008: 13); a specific selection of aggregates contribute to make a dense concrete which forms a passive film around the embedded steel. However, increase of concrete cover prevents infiltration of aggressive ions such as chloride.

In addition, the principle of cathodic protection is in connecting an external anode to the metal to be protected and the passing of an electrical dc current so that all areas of the metal surface become cathodic and therefore do not corrode (Kean and Davies, 2003:2)

2.3.1 Deterioration of Reinforced Concrete

Different studies conducted on the deterioration of reinforced concrete show that there are two main reasons for its deterioration namely the exposure of rebar to the chloride and carbonation of concrete.

Ahmad (2003:460) demonstrated that the mechanism of corrosion of steel embedded in concrete is an electrochemical process. The surface of the corroding steel functions as a mixed electrode that comprises anodes and cathodes electrically connected through the body of steel itself, upon which coupled anodic and cathodic reactions take place. Concrete pore water functions as an aqueous medium.

When the concrete losses its initial pH of about 12.5 to 13.5 (Apostolopoulos and Papadakis, 2008:2318; Ahmad, 2003:459), the two reactions take place. The anodic reaction is the oxidation process, which results in dissolution or loss of metal and the cathodic reaction is the reduction process, which results in reduction of dissolved oxygen forming hydroxyl ions.

Referring to the anodic reaction, the anodic electrode potential, $E_{A,}$ is given by Equation 1:

$$E_A = -0.44 + 0.0296\, log[Fe^{2+}] \quad \text{[In Volts]} \tag{1}$$

where $\left[Fe^{2+}\right]$ is the concentration of iron ions in moles per litre of electrolyte, which is related to the mass concentration of $F_e(OH)_2$ per unit volume of concrete and the amount of capillary water per unit volume of concrete.

The cathodic electrode potential E_C in the cathodic reaction is given by Equation 2:

$$E_C = 1.229 + 0.0148\, log[O_2] - 0.0591\ \text{pH [In Volts]} \tag{2}$$

where O_2 is the concentration of oxygen, expressed in terms of molarity, and the amount of capillary water per unit volume of concrete.

The electromotive force, emf $(e)_{[\text{in Volts}]}$, of reinforcement corrosion cell, drives the corrosion current through the electrolyte from anode to cathode and is given by the following Equation 3:

$$e = 1.669 + 0.0148\, log[O_2] - 0.0591\ \text{pH} + 0.44 - 0.0296\, log[Fe^{2+}] \quad (3)$$

Therefore, the corrosion current, i.e. corrosion rate is affected in general by the:

a) pH of electrolyte in concrete which is affected mainly by the carbonation;

b) Availability of oxygen and capillary water and

c) Concentration of Fe^{2+} in concrete near the reinforcement.

Corrosion of steel is an expansive process, which fractures the surrounding concrete and weakens the steel as it rusts (rust component = $F_e(OH)_2$). Both the chloride ions and carbonation destroy the protective layer (i.e. passive film) around steel and deterioration in the form of corrosion of steel will start.

Chloride from the concrete ingredients or penetrated from the surrounding chloride-bearing environment can reach the reinforcement. In the case of highway structures and bridges as well as parking garages, de-icing salts (NaCl and $CaCl_2$) can cause the chloride ions ingression or the seawater in contact with concrete (Gailius and Kosior-Kazberuk, 2008:350).

In marine structures, there is no carbonation of concrete as concrete is totally water-saturated. Therefore chloride penetration is the only mode of exposure. Special concrete mixture should prevent chloride penetration for good protection of reinforcement.

In South Africa, recent study conducted by Alexander and Mackechine (2003:20) on durability of concrete in marine structures presents practical results in terms of design limits and mix design recommendations based on appropriate performance criteria. Results emphasized importance on selections of materials, mixed proportions, concrete grade, cover to reinforcement and quality control of concrete

during construction. This study focused on concrete material as part of solution to degradation of reinforced concrete.

Decrease in the pH of the concrete occurs when carbon dioxide reacts with the calcium hydroxide present in concrete. The diffusion of carbon dioxide follows concrete pores and the carbonation process starts at the surface of concrete and penetrates slowly to the interior of concrete. A state of reinforcement corrosion at various pH levels have been reported and is presented in Table 3:

Table 3 State of reinforcement corrosion at various pH levels (Ahmad, 2003:461).

pH of Concrete	State of reinforcement corrosion
Below 9.5	Commencement of steel corrosion
At 8.0	Passive film on the steel surface disappears
Below 7	Catastrophic corrosion occurs

In case of reinforced concrete foundation – base, it is more likely that deterioration by chloride ions takes place than carbonisation. As the foundation is surrounded by the soil, the carbon dioxide from the air cannot react chemically with the cement paste of the reinforced concrete and therefore not reduce the alkalinity of the concrete which is the first step of deterioration by carbonisation. However, the deterioration by chloride ions occurs when the anode has high chloride content and high moisture content (Aberdeen group, 2000:1). In most cases, the chloride ions are present in the contaminated groundwater.

According to the Aberdeen group (2000:2), if the steel in the foundation – base is discontinuous, as with anchors and dowel bars, there is less potential for anodes and cathodes and, therefore, less potential for strong corrosion cells to develop. However, if continuous pieces of metal span across the foundation – base, they will eventually be subjected to chloride-ion gradation, which could lead to the development of a corrosion cell.

2.3.2 Fibre Reinforced Polymer: An Environmental Solution

Normally construction technologies in civil infrastructures face many situations such as economic condition and global environmental challenges. The cost for the maintenance of structures in an exposed environment is very high.

To address corrosion problems, professionals have turned to enhanced protection of metallic reinforcement, such as epoxy-coated steel bars, cathodic protection, and increased concrete cover thickness. While effective in some situations, such remedies may still be unable to completely eliminate the problems of steel corrosion (Zhou et al., 2002:1).

Since the corrosion products occupy several times the volume of the original steel, tremendous tensile stresses are exerted on the surrounding concrete as the steel corrodes. When these stresses exceed the tensile strength of the concrete, cracking and delamination develops (Abdulla, 2007:13). Since FRP has good resistance to corrosion, these stresses do not exceed the tensile strength of the concrete, therefore no cracks are developed.

One of the successful environmental experiences is the construction of Okinawa Park Road Bridge of two span continuous girder bridge with total span length of 37.76 m and width of 3.5 m (Figure 2). It is one of the FRP bridges in the world and emphasizes the use of this advanced material in big scale project. It was erected in the parking area of Ikei-Hirakawa roadway surrounded by the sea environment: corrosive condition. After 8 years of continuous inspection, no degradation was observed except for some corrosion of the stainless bolts used in the connections (Sugiura et al., 2008:308).

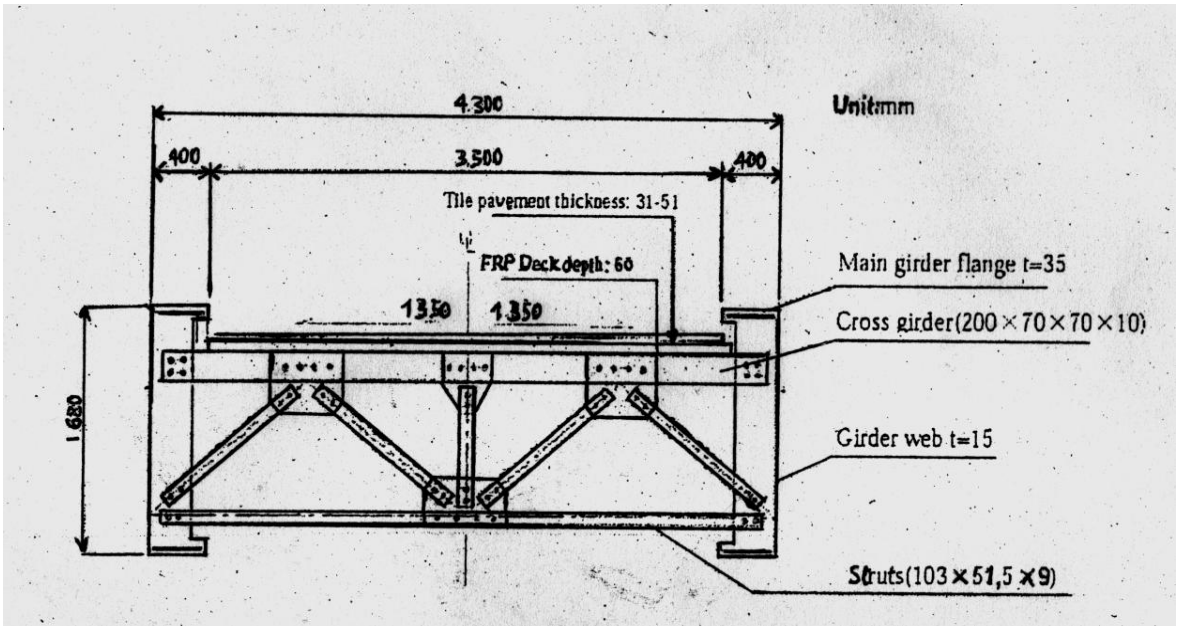

Figure 2 Cross Section of Okinawa park road footbridge (Sugiura et al., 2008:308).

In fact, the FRP are better for the environmental problems as demonstrated by the following projects: one cited in the precedent paragraph and other in the repair of cracking and spalling of concrete columns in a building at the University of Sherbrooke, Canada (Shanmuganathan, 2003:30). Glass FRP (GFRP) where sheets were used to strengthen and protect two reinforced concrete columns where the steel reinforcement had corroded significantly and it was the main cause of the concrete cracking and spalling. The repair work was carried out under cold and snowy conditions (Shanmuganathan, 2003:30).

2.4 Different application of Fibre Reinforced Polymer

Presently, there are eight design guidelines available for construction with FRP worldwide. These documents are:

i. Guide for the Design and Construction of Concrete Structures Reinforced with Fiber-Reinforced Polymer Bars (CNR-DT 203/2006, 2007).
ii. Guide for the Design and Construction of Structural Concrete reinforced with FRP bars (ACI 440.1R-06, 2006).

iii. The use of Fiber Reinforced Polymer (FRP) in the construction fields (Egyptian code of practice, 2005).
iv. FRP Reinforcement for reinforced concrete Structures (FIB: Task Group 9.3, 2005).
v. Guide for Design and Construction of Concrete Reinforced with FRP bars (ACI 440. 1R-03, 2003).
vi. Design and construction of buildings components with fiber-reinforced polymers (CAN/CSA-S6-02, 2002).
vii. Canadian High Bridge Design Code (CAN/CSA-S6-00, 2000) and
viii. Recommendations for Design and Construction of Concrete Structures using Continuous Fiber Reinforcing Materials (Japan Society of Civil Engineers (JSCE), 1997).

The Egyptian code of practice for the use of Fiber Reinforced Polymer (FRP) in the construction fields (Egyptian Ministry of Housing, Utilities and Urban development, 2005) was the first FRP code issued in Africa.

The ACI Guidelines, the CNR design code and the Egyptian FRP code were used as reference and code of practice for the design of FRP reinforced concrete in the present research. These guidelines were selected due to the fact that they were most updated documents issued.

a) To date, an advanced composite bridge systems, a 137 m long cable-stayed bridge supported by a 46 m high A-frame pylon (Figure 3), was designed at the University of California in San Diego (UCSD). The design proposed the use of carbon shell system for the pylon legs and edge longitudinal girders supported by a dual cable plane system. In the transverse direction, partially grouted carbon tube cross-beams were employed, which in turn supported longitudinally spanning prefabricated E-glass or reinforced concrete deck panels (Van Den Einde et al., 2003:400).

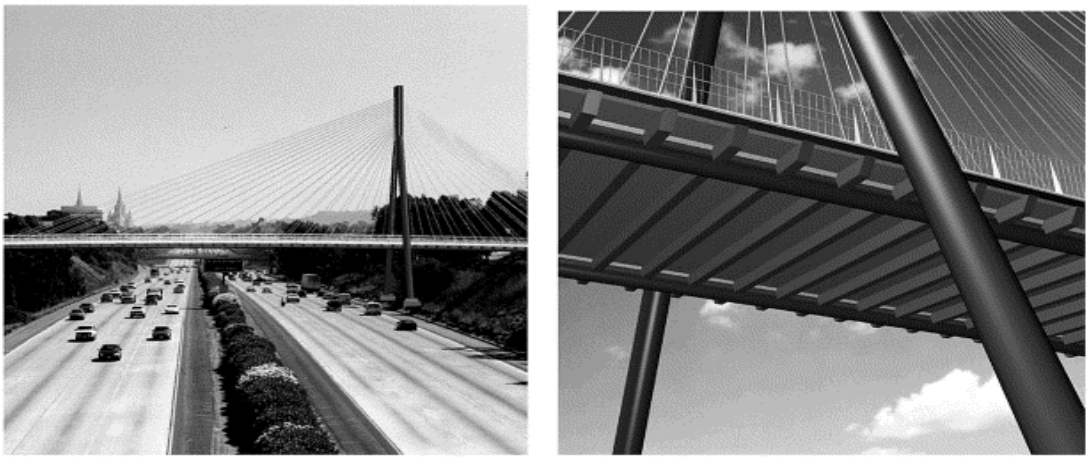

Figure 3 The I-5/Gilman Advanced Technology Bridge (Van Den Einde et al., 2003:400).

b) Another application of FRP in structural engineering is the construction of the first bridge in composite materials shown in Figure 4 in Denmark in 1997. The bridge was constructed with glass fibre reinforced polymer for the pedestrians and cyclists and it crosses over a railway line, with a span of 40 meters and a weight of 12 tons (Shanmuganathan, 2003:31).

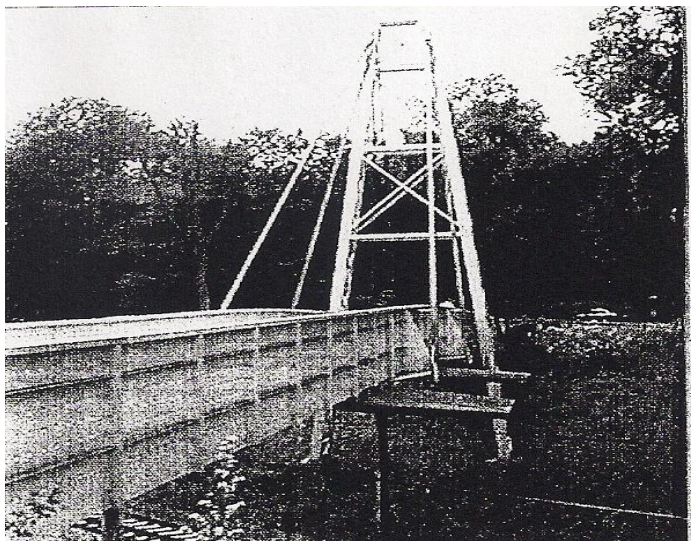

Figure 4 Fiberline Bridge, Kolding, Denmark (Shanmuganathan, 2003:31)

c) Fibre Reinforced Polymers are well used in strengthening of existing concrete structures. One of the successful projects of strengthening with advanced materials in

the world is the repair of six silos reinforced concrete in Boston, USA shown in Figure 5 (www.spsrepair.com).

The silos have specifications of 45.72 meters high and 7.01 metres diameter; there was an error in construction of the silos implying loss of shear resistance longitudinally and vertically. After an evaluation on the possibilities of reconstruction and strengthening with different methods, the choice was to use Fibre Reinforced polymers. 16.09 km of materials were used; with 4 million of Dollars (approximately 28 million Rands) saved and 18 months of construction for replacement avoided as advantages in this project.

Figure 5 Silo Reinforced Concrete, Boston, Massachusetts,

USA (www.spsrepair.com).

More recently, two studies have been conducted on the use of FRP re-bars in the pavement applications (ACI 440.1R, 2006: 120). The first project carried out the use of FRP dowel bars in highway concrete pavement construction and results of this research have shown that GFRP dowels are able to carry the shear transfer across the pavement joint. The second study focused on the GFRP-reinforced continuously reinforced concrete pavement section, where the results have shown that the stress level in concrete was reduced with GFRP re-bars (ACI 440.1R, 2006:120).

The main objectives of the modern engineer in attempting to modify the properties of concrete by the inclusion of fibres (as steel, FRP) are as follows (Hannant, 2003:6/1):

i. To improve the rheology or plastic cracking characteristics of the material in fresh state or up to about 6 hours after casting.

ii. To improve the tensile or flexural strength.

iii. To improve the impact strength and toughness.

iv. To control cracking and the mode of failure by means of post-cracking ductility and

v. To improve durability.

The emphasis on new structural material for the 21st century is based on the advanced composites materials that have specific characteristics as high specific strength, excellent durability, corrosion resistance, excellent fatigue behaviour, etc. (Humphreys, 2003:3), rather than steel and concrete.

The performance durability of FRP reinforcements is considered by some authors to be a possible solution to the problem of corrosion of steel reinforcement and primary factor in reduced durability of concrete structures (Humphreys, 2003:3). The ability of materials that posses high specific strength and high specific stiffness to produce structures with low self-weight will be more beneficial than steel in some applications. The large range of constituent materials potentially allows design of a material which exhibits very good resistance to long-term deficiencies which can result from environmental influence of moisture, ultraviolet radiation, chemical attack (alkaline solution), dynamic loading, freeze thaw cycles and deterioration of material properties through physical aging (Humphreys, 2003:7).

2.4.1 Fibre Reinforced Polymer as External Reinforcement

Real life situations do arise where it becomes important to increase the load carrying capacity of a structure in service. Structures such as bridges require continuous

maintenance and due to exposure to adverse environmental conditions, the strengthening of structures is needed.

Historically, engineers provided for this increased strength by either casting additional reinforced concrete, dowelling in additional reinforcement or by externally post-tensioning structures. More recently, attaching steel plates to the surface of the tension zone by use of adhesives and bolts has been used to strengthen concrete structures (Arya et al., 2001:1243).

Although these techniques can effectively increase the element load carrying capacity, they are often susceptible to corrosion damage which results in failure of the strengthening system. Consequently, non-corrosive innovative strengthening systems, such as FRP strips, that have the potential for extending service lives of reinforced concrete structures and reducing maintenance costs are required to replace old strengthening systems (Maaddawy and Soudki, 2007:5). As FRP plates used for external bonding are relatively thin, neither the weight of the structure nor its dimensions are significantly increased. In fact, the requirements for the maintenance of FRP are low (Arya et al., 2001:1244).

The success of structural rehabilitation measures with advanced composite materials has led to the development of new lightweight structural concepts utilizing FRP shells and tubes to form new structural systems. FRP/Concrete composite systems have been developed for use in new lightweight bridge systems due to their simplification in construction and excellent short- and long-term structural characteristics (Van Den Einde et al., 2003:390).

Van Den Einde et al (2003: 397) reported that Seible et al (1998) developed the first modular FRP-concrete composite structural system. It consisted of concrete filled carbon shell system using prefabricated filament – wound carbon/epoxy thin shells filled on-site with concrete as shown in Figure 6.

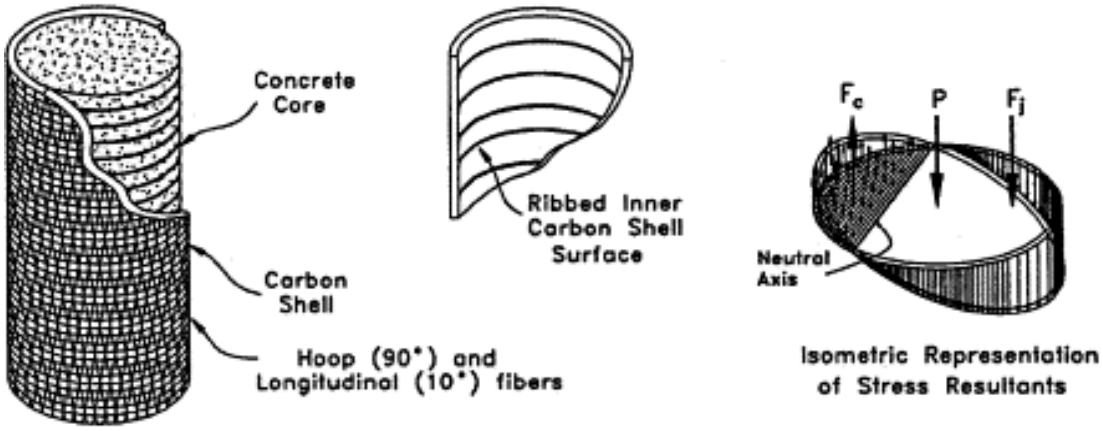

Figure 6 Concrete filled Carbon Shell System (CSS) (Van Den Einde et al, 2003: 397).

The most common use of FRP in structural engineering is the strengthening of the reinforced concrete on different types of structures for example in buildings and bridges. Research has been done in this perspective and these applications are grouped as follows (Arya et al., 2001:1246): flexural strengthening of beams and slabs, flexural and compressive strengthening of columns and shear strengthening of beams and columns.

2.4.1.1 Flexural strengthening

In this application, the design of FRP strengthening is relevant to flexural strengthening of beams and slabs for the two limit states as shown in Table 4. It appears that the bonding of FRP to the tension face increases the flexural strength of concrete elements.

Table 4 Limit states of reinforced concrete (Arya et al., 2001:1247).

Ultimate (ULS)	**Serviceability (SLS)**
Strength Bending Shear Plate separation	Deflection Cracking

It is important to note that there are other relevant limit states such as fatigue, creep, rupture and durability that can be considered for flexural strengthening. Structures that cannot resist working loads without collapsing should normally be considered suitable for strengthening.

In the same philosophy to upgrade reinforced concrete slabs deficient in flexural strength, two methods have been developed: (a) the mechanically-anchored unbounded fibre reinforced polymer (MA-UFRP) and (b) the externally-bonded fibre reinforced polymer (EB-FRP) which is the most popular and in which the FRPs strips are bonded to the tension face of the flexural element by a structural adhesive (Maaddawy and Soudki, 2007:444).

Maaddawy and Soudki (2007:445) examined the potential use of mechanically-anchored no bonded FRP (MA-UFRP) system to upgrade suspended reinforced concrete slabs deficient in flexural strength. In their study, a total of six slabs were used. One slab was used as a control while the other five slabs were strengthened with either EB-FRP or MA-UFRP systems. The test results showed that MA-UFRP system resulted in up to 43% enhancement in the slab flexural strength.

Furthermore, using the CFRP composites in the form of strips; which offers a cost-effective technique for the flexural strengthening, Vasquez found that the ultimate strength of the slab was increased to more than twice of the weakened slab with cut-out (Van Den Einde et al., 2003:394).

Täljsten (2006:42) has developed different formulae for the strengthening in bending moment. From his research the design for FRP strengthening in bending moment for beams depends on the modes of failure.

2.4.1.2 Flexural and Compressive Strengthening of Columns

In the case of the retrofit of reinforced concrete columns subject to either static or seismic load, Lam and Teng (2002:789) investigated degree of accurate stress-strain of FRP-confined concrete. To achieve the goal, FRP sheets (or jacketing) were used to wrap the columns as external confinement. From their work the following

Equation 4 for the ultimate condition of the jacket (this equation takes into account the stiffness of the FRP sheets) was proposed:

$$\frac{\varepsilon_{ccu}}{\varepsilon_{co}} = c^{'} + k_2\left(\frac{E_{h.\,frp}t}{E_{\sec o}R}\right)^{\alpha}\left(\frac{\varepsilon_{h.rup}}{\varepsilon_{co}}\right)^{\beta} \tag{4}$$

where c' is the normalised ultimate strain of un-confined concrete; k_2 is the strain enhancement coefficient; and α and β exponents are determined using test results from the open literature (Lam and Teng, 2002:793); R is the radius of the concrete core (mm); $E_{h.\,frp}$ is the elastic modulus in the hoop direction (GPa), denoted by E_{frp}; t is the total thickness of the FRP jacket (mm); $\varepsilon_{h.rup}$ is the hoop rupture strain of the FRP (%); $E_{\sec o}$ is the Secant modulus of elasticity at the compressive strength of unconfined concrete (GPa); ε_{co} is the axial strain of unconfined concrete (%) and ε_{ccu} is the ultimate strain of the confined concrete (%), denoted by ε_{cu}.

In Lam and Teng (2002), a database containing the test results of 81 plain concrete circular specimens wrapped with FRP is presented and the secant modulus of elasticity at the compressive strength of unconfined concrete is calculated from Equation 5:

$$E_{\sec o} = \frac{f'_{co}}{\varepsilon_{co}} \tag{5}$$

where f'_{co} is the compressive strength of unconfined concrete (MPa). Assuming the exponents α and β as equal to unity, then Equation 4 reduces to:

$$\frac{\varepsilon_{ccu}}{\varepsilon_{co}} = c^{'} + k_2\frac{f_{l,a}}{f_{co}^{'}} \tag{6}$$

where $f_{l,a}$ is the actual maximum confining pressure given by Equation 7:

$$f_{l,a} = \frac{E_{h.\,frp}t\varepsilon_{h.rup}}{R} \tag{7}$$

So that the ultimate strain is directly and only related to the actual confinement ratio

$\frac{f_{l,a}}{f_{co}^{'}}$ as ε_{co} is generally taken as a constant.

When steel is used for confined concrete, the strain enhancement factor k_2 is $5k_1$ (Täljsten, 2006:109).

In Japan, after the Hyogoken – Nanbu earthquake (17 January 1995) that caused extensive damages to civil infrastructures, a lot of research activities concentrated in using FRP jacketing for reinforced concrete columns to repair the structures damaged. From these instants, the Task Committee on FRP hydrid bridges of the Japan society of Civil engineers are currently working on a draft for the standard design guideline of FRP footbridge and almost completed (Suguira et al., 2008:305; Matsui et al., 2009:1).

2.4.1.3 Shear Strengthening of Beams and Columns

Research has demonstrated that the external bonded FRP laminates increase the shear strength of reinforced concrete columns by wrapping with a continuous sheet of FRP to form a complete ring around the member (Arya et al., 2001:1248; Täljsten, 2006:100).

However, the shear strengthening of beams is likely to be more problematic since they are normally cast monolithically with slabs (Arya et al., 2001:1248). The design of shear strengthening systems made from FRP follows the same procedure used in conventional reinforced concrete. The FRP laminates are also used in increasing of shear capacity of brick walls.

2.4.2 Fibre Reinforced Polymer as Internal Reinforcement

The fundamental design methodologies for FRP Reinforced Concrete are similar to those of the conventional steel reinforced concrete (ACI 440.1R, 2006:37). The similarities and differences are reviewed below.

2.4.2.1 Flexural Strength

There are two modes of failure considered in different design codes: the crushing of concrete in compression and the breakage of FRP reinforcement in tension. The representation of stress-strain distribution for the two modes of failures is shown in Figure 7(a) and Figure 7(b) for singly FRP composite element (Newhook et al., 2002:126; ACI 440.1R, 2006:101).

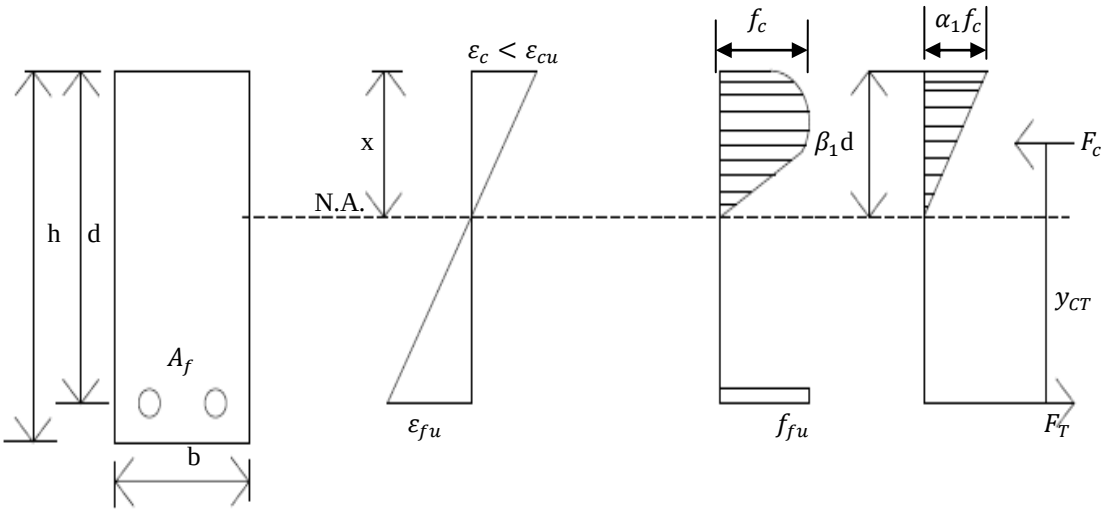

Figure 7(a) Stress-strain distribution in flexure: Failure by rupture of FRP.

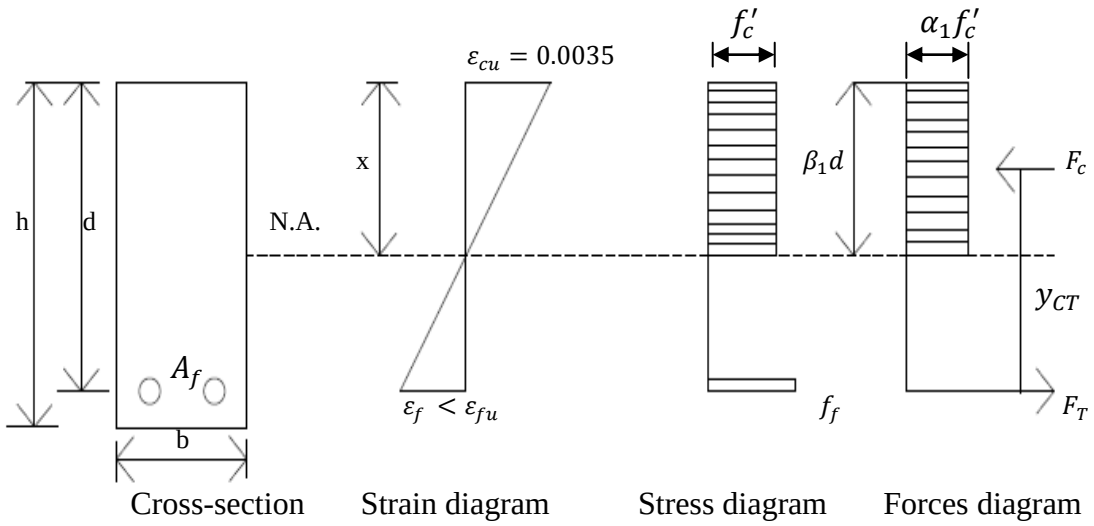

Figure 7(b) Stress-strain distribution in flexure: Failure by crushing of concrete.

From Figure 7, A_f is the cross-sectional area of FRP re-bars (mm^2); h is the depth of the reinforced concrete specimen (mm); d is the depth of reinforcement (mm); b is the width of reinforced concrete beam (mm); x is the distance from extreme compression fibre to neutral axis (mm); ε_c is the strain in concrete (%); ε_{cu} is the ultimate strain in concrete (%); ε_f is the strain in FRP re-bars (%); ε_{fu} is the ultimate strain in FRP re-bars (%); f_c is the compressive strength of concrete (MPa); f_c' is the cylinder compressive strength of concrete (MPa); f_f is the tensile strength of FRP re-bars (MPa); f_{fu} is the ultimate tensile strength of FRP re-bars (MPa); α_1 is the ratio of the average concrete stress to the concrete strength; β_1 is the equivalent rectangular stress block parameter; F_C is the compression force in compression zone (kN) and F_T is the tensile force (kN) in FRP re-bars.

When rupture of the FRP reinforcement in tension occurs, failure of the member is sudden and brittle due to the fact that FRP is not ductile. The current design philosophy in all the design codes accepts that the ultimate failure will be governed by concrete crushing mode for flexural member reinforced with FRP bars. This is due to the fact that a flexural member does exhibit some plastic behaviour before failure (Pilakoutas et al., 2007:32; Egyptian FRP code, 2005:5-3).

Similar to FRP reinforced concrete, steel reinforced concrete have two types of failures namely concrete crushing and tension failure. Steel re-bars show a plastic behaviour up to failure of reinforced concrete and the steel reinforced concrete develop a ductile curvature response (MacGregor & Wight, 2006:119). This type of failure, where steel yields before the crushing of concrete with cracks widening extensively, gives warning before structure collapses (Hassoun & Al-Manaseer, 2008:70). Thus contrary to FRP re-bars failure, tension failure governs the design philosophy of steel reinforced concrete as tension failure shows more ductile curvature than crushing concrete.

Egyptian FRP code (2005:5-4), CNR-DT (203/2006, 2007) and Pilakoutas et al. (2007:32) evaluated the two modes of failure considering variation of strength reduction coefficient γ_f, denoted in this study as ρ_{fb}, of FRP with FRP

reinforcement ratio μ_f, denoted here as ρ_f. From observations by Pilakoutas et al (2007:32) in their research, when FRP reinforcement ratio ρ_f is below 0.5%, rupture of the re-bar occurs in the case of the Glass Fibre Reinforced Polymer (GFRP) and Carbon Fibre Reinforced Polymer (CFRP) reinforced sections. Therefore ρ_{f_b}can be considered equal to 0.5%.

According to Egyptian FRP code (2005), when ρ_f is less than ρ_{f_b}, the ultimate concrete strain 0.0035 may not be attained and β_1 (the ratio of the depth of the equivalent rectangular stress block to the depth of the neutral axis) is unknown. The ultimate limit moment in this case can be computed as:

$$M_u = \left(\frac{A_f f_{f_u}}{\gamma_f}\right)\left(d - \frac{\beta_1 d}{2}\right) \text{ [Nm]} \quad (8)$$

In case of steel reinforcement, the curvature increases rapidly until the strain in concrete ε_c reaches an ultimate value equal to 0.0035 at the extreme compressive fibre and thus failure occurs. The stress in concrete is idealized by the rectangular stress block shown in Figure 7(b). However, when FRP bars are used, the corresponding strain ε_c at the extreme compressive fibre will be less than ε_{c_u} (Newhook et al., 2002:126) and can be expressed by Equation 9 (CNR-DT 203/2006, 2007:15). It is necessary to determine the concrete compressive strain ε_c at which FRP rupture occurs.

$$\varepsilon_c = \varepsilon_{f_u}\left(\frac{x}{d-x}\right) \leq \varepsilon_{c_u} \quad (9)$$

Thus the distribution of compressive stress on the concrete can be idealized by a parabolic block shown in Figure 7(a) and Equation 8 has to be reconsidered with the new value of parameter β_1.

From the equilibrium of internal forces:

$$F_C = F_T \quad (10)$$

where: F_C is the compression force in the concrete and F_T is the tensile force acting in the reinforcement, presented in the stress diagram in Figure 7(a).

The ultimate moment can be found by considering the force multiplied by the lever-arm:

$$M_u = (F_c)(y_{CT}) = (F_T)(y_{CT}) \tag{11}$$

With y_{CT} being the distance between the resultant concrete compressive force and the tension reinforcement and $F_c = F_T = bd\xi \frac{\int_0^{\varepsilon} f_c d\varepsilon_c}{\varepsilon_c} = \frac{A_f f_{fk}}{\gamma_f}$ from Pilakoutas et al.(2007:34).

where f_{fk} is the characteristic tensile strength of FRP re-bars; γ_f is the partial safety factor of FRP re-bars; ξ is the equivalent rectangular stress block parameter, denoted here by β_1.

So, the moment can be calculated considering the stress diagram in Figure 7(a), the corresponding curvature is given by:

$$\psi_u = \frac{(\varepsilon_c + \varepsilon_{fu})}{d} \tag{12}$$

where: ψ_u is the corresponding curvature of compression in concrete in Figure 7(a) and d is the depth of reinforcement. The determination of location of the resultant compressive force, y_{CT} was done using numerical integration (Newhook et al., 2002:126).

The strain in the FRP reinforcing will be:

$$\varepsilon_{fu} = \frac{f_{fu}}{E_f} \tag{13}$$

where: f_{fu} is the tensile strength (MPa) and E_f is the modulus of elasticity of the FRP (GPa).

Pilakoutas et al (2007:34) developed a mathematical model for the Fibre Reinforced Polymer Reinforced Concrete (FRP RC). From their research, the ultimate moment for FRP rupture was calculated by the following Equation 14:

$$M_u = \frac{A_f f_{fk}}{\gamma_f}\left(1 - \frac{\xi}{2}\right) \text{ [Nm]} \quad (14)$$

where: M_u is the ultimate moment; A_f is the area of FRP reinforcement (mm^2); f_{fk} is the characteristic tensile strength of FRP (MPa); ξ is the equivalent rectangular stress block parameter, denoted in this study by β_1 and γ_f is the partial factor strength of FRP and FRP reduction factor γ_f is obtained by multiplying the environmental conversion factor by the conversion factor due to long term effects (CNR-DT 203/2006, 2007:11).

Therefore in this study, Equation 14 was used in the design of ultimate moment when FRP rupture governs the behaviour of reinforced concrete.

2.4.2.2 Shear Capacity

A number of tests were carried out to determine the capacity of shear strength of FRP reinforced concrete members. Using the expression developed for steel reinforced concrete, the results showed that the shear strength capacity of the FRP reinforced concrete is lower than the shear strength of steel reinforced concrete members (Goodspeed et al., 1990:593; Yost et al., 2001:268).

In fact, the FRP reinforcement has a lower modulus of elasticity and linear stress-strain diagram up to rupture with no discernible yield point and different bond strength according to the type of FRP product (Wegian and Abdalla, 2005:130). This behaviour affects the shear capacity of FRP reinforced concrete. Nehdi et al (2007:1034) reported that Shehata (1999) noticed a significant reduction in the ultimate capacity of FRP bars when used as stirrups. The reduction was up to 79% of the guaranteed tensile strength parallel to fibres and that failure of FRP stirrups was more likely to occur at bends.

Using the genetic algorithms approach for the proposed shear design equations for FRP – Reinforced Concrete beams, Nehdi et al (2007:1039) concluded that the actual shear design equations proposed by ACI 440 (2006:106) guidelines is adequate for the FRP materials having low modulus of elasticity. However, the guidelines overestimate the capacity of FRP stirrups with high modulus of elasticity.

2.5 Cost Evaluation

Today, FRPs are more expensive than the conventional construction materials on an initial cost basis. There are a number of factors contributing to the high cost of composite materials including; high cost of raw materials and processing, the use of imported materials, the general acceptance of high prices in markets such as marine and aerospace and occasional low availability of materials (Goldstein, 1996:47). However, different low cost techniques are currently under development by many manufacturers (Alsayed et al., 2000: 555). For many researchers and composites commentators, it is likely that production volume increases resulting from the use of fibre composites in civil engineering applications will lead to decreased cost of materials (Humphreys, 2003:2-12).

Actually, the process of manufacturing of Fibre Reinforced Polymer was developed for aircraft, marine and/or car industries. Most recently, advantages of strengthening existing concretes structures emphasized applications of FRP in civil engineering. Aircraft, marine or car industries are vastly different to those as civil and structural industries. Civil and structural engineers are concerned with the design and construction of rather large – scale structures. This implies that the manufacturing industries need a new method of production for civil engineering (Humphreys, 2003:2-12) in order to bring down the cost of FRP re-bars.

2.6 Summary

The literature study outlined the deterioration of reinforced concrete and the corrosion process of steel re-bars and presented FRP materials as an alternative solution to corrosion. The FRP materials can be used as external and internal reinforcement.

The FRP materials are used as external reinforcement for strengthening reinforced concrete members such as beams, slabs and columns or masonry walls. The reason for using FRP materials as external reinforcement was to upgrade or repair existing structures.

As internal reinforcement, FRP reinforced concrete was governed by two modes of failure namely, FRP ruptures and concrete crushing. However, if one had to happen concrete crushing failure was more desirable than FRP ruptures as it showed some ductility.

CHAPTER 3: RESEARCH METHODOLOGY

3.1 Introduction

This chapter outlines research materials, test methods and samples preparations, experimental set up including equipment and tools used in this research.

3.2 Research Material

a) Concrete

Three materials were used in the concrete mix design namely, cement, coarse aggregates and fine aggregates. The type of cement used was Portland cement type II CEM complying with SABS 50197-1 and of class strength 32.5R. The coarse aggregates were crushed dolomite aggregate type from Gauteng province with a modulus of elasticity K_o between 24 – 25 GPa. For the purpose of good concrete, coarse aggregates had two sizes namely 15 and 19 mm. Fine aggregates used in this study had an average of 96.69 percent passing the sieve of 0.600 mm size that corresponded to grading zone IV according to British standard of grading requirements for fine aggregate (Krishna, 2007:16).

b) Reinforcing Bars

Two types of reinforcing bars were used in this study namely Fibre Reinforced Polymer (FRP) re-bars and steel re-bars. In addition, two types of FRP rebars were used namely, Glass Fibre Reinforced Polymer (GFRP) and Carbon Fibre Reinforced Polymer (CFRP). These types of FRP re-bars were chosen for their availability on the local market. The FRP re-bars were sourced from Industrial Composites of South Africa and Pultrall Company of Canada.

Steel re-bar used was high tensile strength bars produced locally in South Africa. They were of a nominal tensile strength of 450 MPa and modulus of Elasticity of 200 GPa.

3.3 Tests Methods and Foundation Samples Preparations

3.3.1 Tests Methods

a) Concrete

The concrete used in this research was designed according to British method known as the Department of Environment, DoE, (Dewar 2008:1/32). This method takes into account workability, water/cement ratio (proportion between the quantity of water to that of cement) related to the quantities of finer particles in the mix concrete and proportion of aggregates in the design process such as the percentage of fine aggregates passing through a 0.600 sieve size.

Before the concrete mix design, raw materials such as Coarse and Fine Aggregates were analysed for grading according to the method described in South African Bureau of Standard (SABS) method 829-B4 (1994). From SABS method 829 – B13 (1994), the Fineness Modulus (FM) was calculated for Fine Aggregates. By definition, FM is equal to the sum of cumulative percentage of material retained on each of the standard sieves 0.15 mm and coarser, all divided by 100.

There are two phases in concrete namely: fresh concrete (the state of concrete when concrete is handled, transported, placed and compacted) and hardened concrete (the state of concrete, when it is hard and tested for strength). In the first step, the consistence of fresh concrete was measured by the slump test carried out in accordance with SABS method 862-1 (1994): concrete test – consistence of freshly mixed concrete – slump test. However in the second step, different concrete cubes were made and cured in the laboratory as prescribed in the following methods:

SABS method 861-1: Concrete test – Mixing fresh concrete in the laboratory;

SABS method 861-2: Concrete test – Sampling of freshly mixed concrete and

SABS method 861-3: Concrete test – Making and curing of test specimens.

The cube specimens of 150 mm size were tested on the 7^{th} and 28^{th} day in accordance with SABS method 863: concrete test – Compressive strength of hardened concrete.

b) Fibre Reinforced Polymer Re-bars

The most recent guide test method for FRP re-bars was developed by American Concrete Institute (ACI 440.3R-04, 2004) and used in this study. In this research, two tests were performed on FRP, namely cross –sectional properties of FRP re-bars (ACI 440.3R-04: Part 2, 2004:3-9) and tensile properties of FRP re-bars (ACI 440.3R-04: Part 3, 2004:9-12) in purpose to compare the local products to the imported products.

(i) Cross-sectional Testing

The cross-sectional test method was used to determine the equivalent diameter of FRP re-bars. According to the procedure described in ACI 440.3R-04 (2004:7), five specimens of 200 mm length were tested. The specimens were conditioned in the laboratory for 24 hours before the test, where the temperature in the laboratory was 23 ± 3^{o} Celsius and 50 ± 10 percent relative humidity. A graduated cylinder filled with water was used and specimen was inserted into the cylinder as shown in Figure 8.

Figure 8 FRP immersed in graduated cylinder.

The length of each specimen was measured three times by rotating the specimen through 120 degrees for each measurement. The average of the three measurements was used as the specimen length. The volume of water was measured before and after the specimen was immersed into the cylinder, therefore the variation of the water volume was determined and used to calculate the cross-sectional area.

The cross-sectional area A_f of FRP re-bars was calculated as:

$$A_f = \frac{Variation\ of\ volume\ \Delta V}{length\ of\ specimen\ L}(1000)\ [\text{mm}^2] \quad (15)$$

Then, the equivalent diameter of specimens was obtained from Equation 16.

$$d_b = 2\sqrt{\frac{A_f}{\pi}} \quad [\text{mm}] \quad (16)$$

where: d_b is the equivalent diameter; A_f is the cross-sectional area of FRP.

(ii) Tensile Testing

From the tensile test method described in ACI 440.3R-04 guideline, tensile strength, modulus of elasticity and ultimate elongation of FRP re-bars were determined. FRP rebar anchorage was excluded as this test method focused on the failure of FRP re-bar itself. Pull out at anchoring section was disregarded as it assumed that there is a perfect bond between the anchors and the re-bars. According to ACI 440.3R-04 (2004:8), all test specimens were protected against any deformation, heating, outdoor exposure to ultraviolet light subjected to cause changes to the material properties of FRP during the sampling and preparation of the test. An extensometer was used to record strain measurements until load reached at least 50% of the guaranteed tensile capacity.

Tensile strength was calculated as:

$$f_{fu} = \frac{F_u}{A_f} \quad (17)$$

Tensile modulus of elasticity, E_f, was taken as a linear regression of the data points from 20 to 50 percent of the tensile strength of the bar and computed as:

$$E_f = \frac{F_1 - F_2}{(\varepsilon_1 - \varepsilon_2)A_f} \text{ [MPa]} \quad (18)$$

where F_1 is the tensile force in FRP re-bars at 20 percent of tensile strength; F_2 is the tensile force in FRP re-bars at 50 percent of tensile strength; ε_1 is the strain in FRP rebars at 20 percent of tensile strength; ε_2 is the strain in FRP rebars at 50 percent of tensile strength

The ultimate strain was calculated from the ultimate tensile capacity and modulus of elasticity as:

$$\varepsilon_u = \frac{F_u}{E_f A_f} \text{ [\%]} \quad (19)$$

c) Steel Reinforcing Bars

The test method used for Steel re-bars is described in ASTM D638: Tensile test method. The ductility of Steel re-bars was determined using this method and the tensile strength was computed as:

$$f_s = E_s \varepsilon_s \quad (20)$$

3.3.2 Foundation Samples Preparation

All foundations bases tested in this investigation had the dimensions of 1000 mm length by 500 mm width by 150 mm depth (see Figures 9 and 10). These dimensions were chosen considering the width of Universal Testing Machine. Thirty- six reinforced concrete specimens were cast in total on the same day and cured in a bath where the temperature was between 22^{o}Celsius to 25^{o}Celsius.

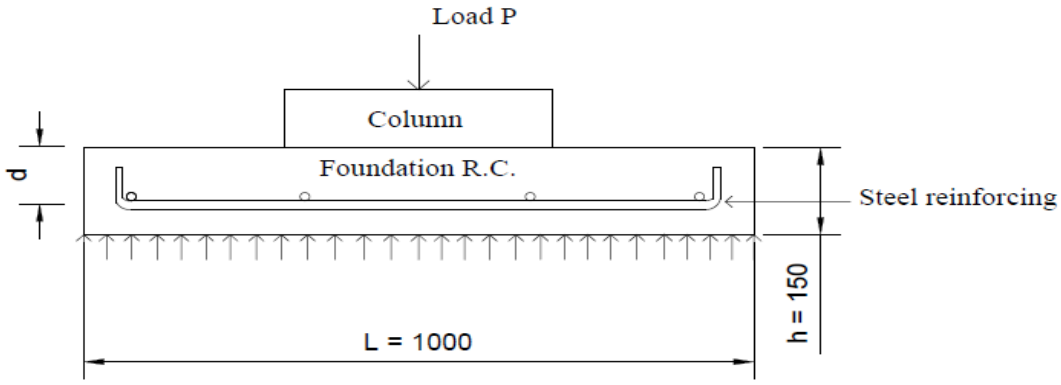

Figure 9 Typical dimensions for steel reinforced concrete bases.

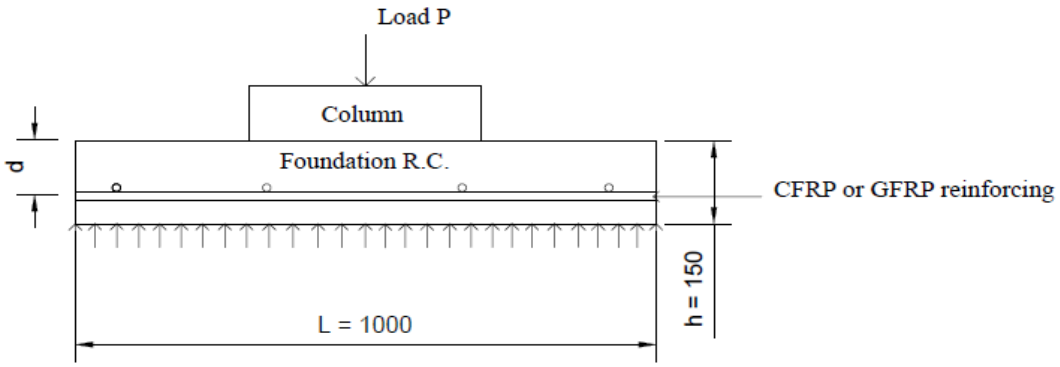

Figure 10 Typical dimensions of FRP reinforced concrete bases.

The specimens were removed from the bath one day before the test date and placed in the laboratory environment for test preparation. The 36 specimens used comprised of 12 samples of steel reinforced concrete bases, 12 samples of CFRP reinforced concrete bases, and 12 samples of GFRP reinforced concrete bases. They were all tested according to the frame – time presented in Table 5.

Table 5 Frame – time of tests.

Items	Days				Total
	7	14	21	28	
GFRP R.C.	3	3	3	3	12
CFRP R.C.	3	3	3	3	12
Steel R.C.	3	3	3	3	12
Total	9	9	9	9	**36**

In case of GFRP and CFRP reinforced concrete bases, the re-bars were cut in short spans by 50 mm length to achieve a perfect bond between concrete and FRP reinforcement as FRP could not be bent in the laboratory. In the long span, FRPs were cut exactly the same length of 1 m. A typical specimen of FRP reinforced concrete base is shown in Figure 10.

To achieve a good simulation of the deformation of base foundation under loading, Soil Bearing Pressure was represented by wooden plank of 5 mm thick placed on top of several series of 31 mm by 59 mm by 83 mm timber to act as an Elastic Foundation. Reinforced concrete column was simulated through use of square steel plate of 200 mm by 200 mm.

3.4 Experimental Set Up

3.4.1 Equipment and Tools

In this research, the following equipment and tools were used:

(i) A compressive machine of 3000 kN of load was used for compressive test;
(ii) A Universal Testing Machine with a capacity load of 2000 kN;
(iii) A Flexural Testing Machine with a capacity load of 1000 kN;
(iv) Graphtec device for strain recording and strain gauges;
(v) Cubes mould and tamping rod for cube test;
(vi) Sieves of sizes: 75 mm; 53 mm; 37.50 mm; 26.50 mm; 19.0 mm; 13.20 mm; 9.50 mm; 6.70 mm; 4.75 mm; 3.35 mm; 2.36 mm; 1.18 mm; 0.60 mm; 0.425 mm; 0.30 mm; 0.15 mm; 0.075 mm and Pan;
(vii) Slump mould, base plate and tamping rod for slump test.

3.4.2 Simulation of Foundation

The simulation set up of the foundation for the experiment is as shown in Figure 11, where the column was represented by the 200 x 200 mm (thickness) square steel plate; the simulation of soil bearing pressure was done using two plates of timber and pieces of timber between them. Each piece of timber had the dimension of 31 mm width of 59 mm height and 83 mm length.

200 x 200 mm (thickness) square steel plate.

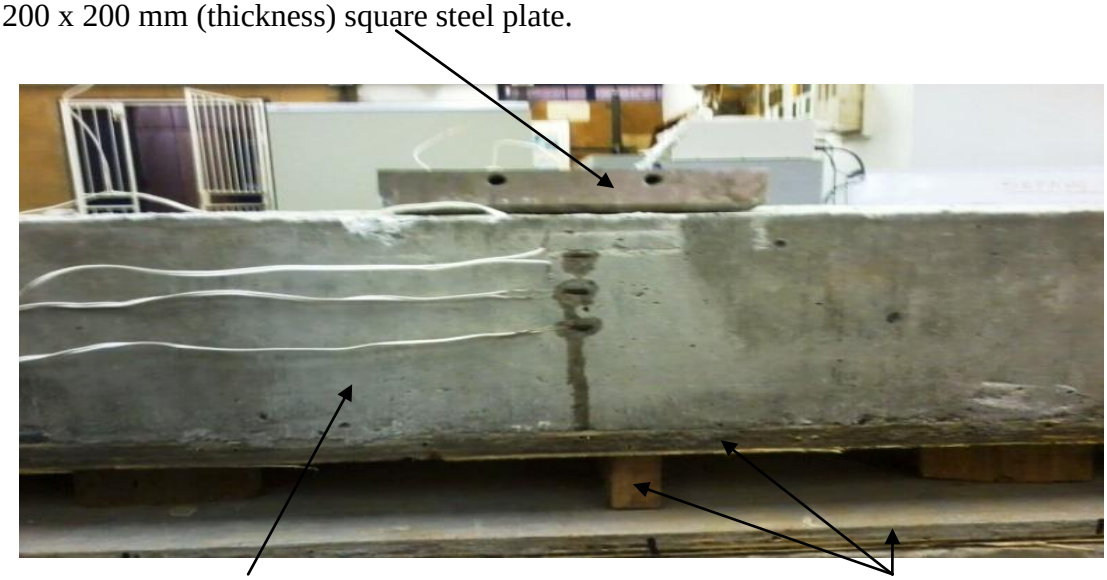

Figure 11 Typical simulation of foundation base soil bearing pressure

Three different types of data were collected namely, strain on the re-bars; strain on the concrete; and ultimate loads. Strain data which constituted a variation of voltage on the strain gauges and these were recorded using Graphtec device and interfaced with computer. The strain device as connected to the sample specimen is shown in Figure 12.

(a) (b)

Figure 12 Strain device connections

The capturing of loading data was recorded manually by reading values off the digital display of the equipment as shown in Figure 13.

Figure 13 Digital display of flexural strength testing equipment

3.4.3 Strain Gauges Connection

The investigation of foundation strain behaviour was done using the experimental set up, shown in Figures 14 and 15. In Figure 14, the strain gauges were placed on the reinforcement and in Figure 15, they were placed on the compression area of concrete. One hundred and eighty strain gauges, manufactured by Kyowa Company, were used in the study.

a. FRP rods b. Steel bars

Figure 14 Strain gauge placed on the reinforcement

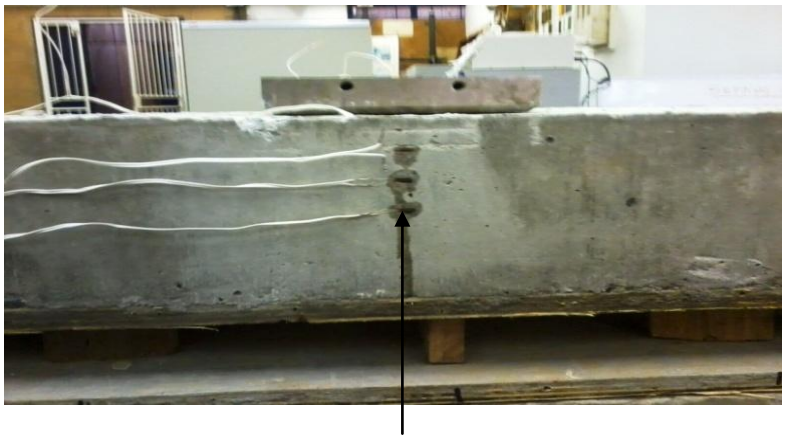

Strain gauge placed on the concrete

Figure 15 Strain placed on concrete

Five strain gauges were used for each base specimen; three on the compressive area of concrete and two on the longitudinal reinforcing bars. Each strain gauge was connected to a full bridge constituted of four resistances as shown in Figure 16. The full bridge was supplied with five volts and connected to the device as channel. Thus, five channels were recording the variation of voltage in the strain gauges.

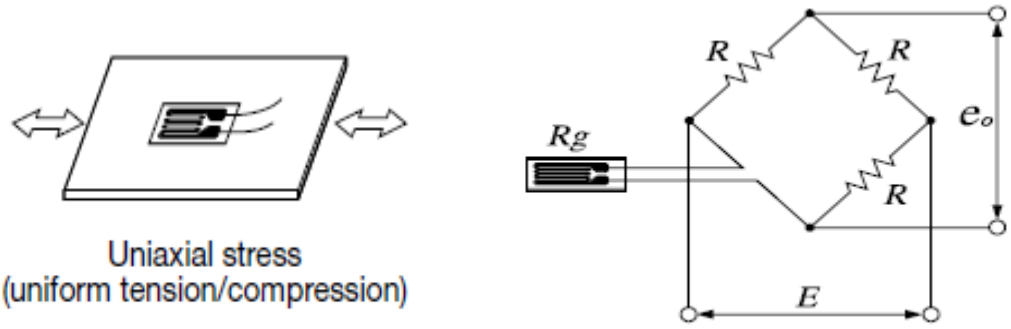

(a) (b)

Figure 16 Full bridge for strain gauge: (a) Strain gauge on the material and (b)

Construction of full bridge.

To ascertain the polarity of strain, i.e. tensile strain or compressive strain, Kyowa (2005:3) recommended positive sign (+) for tensile strain (elongation) and negative sign for compressive strain (contraction).

3.4.4 Data Acquisition

During the tests, load and strain were recorded. All data recorded on the test dates were presented in different graphs using Exploratory Data Analysis for investigation and comparison between values obtained from FRP reinforced concrete foundation – bases to steel reinforced concrete foundation – bases. The values plotted in graphs were: Strain – Age, Load – Age and Stress – Strain.

3.5 Summary

The methodology presented in this chapter was based on procedures described in different guidelines and standards. The necessary equipment and tools were prepared and the experimental set up was done to meet the required specifications while tests were conducted.

In the fourth chapter, the design philosophy and approach to collect and analyse samples are presented.

CHAPTER 4: MODELLING APPROACH

4.1 Introduction

In this section, the approach used to analyse the theoretical moment capacity of foundation and simulate the soil bearing capacity are presented.

4.2 Assumptions

The FRP concrete design philosophy described in different design codes such as CNR-DT 203/2006 (2007), ACI. 440.1R06 (2006) and Egyptian FRP code (2005) are similar. According to the three design codes mentioned above, the design equations for ultimate limit state analysis of FRP reinforced concrete sections are derived on the basis of the following assumptions:

a. A plane section before loading remains plane after loading;
b. Perfect bond exists between concrete and FRP re-bars;
c. The tensile behaviour of the FRP re-bars is linearly elastic until failure;
d. Tensile stresses in concrete are neglected;
e. Contribution in compression of the FRP re-bars to the flexural capacity is neglected and
f. The ultimate concrete compressive strain, ε_{cu}, is assumed to be 0.0035 mm/mm.

4.3 Stress-Strain Relationship Model

a) Concrete

The stress distribution in the concrete in composite material such as FRP reinforced concrete can be represented by either rectangular stress block or parabolic stress block shown in Figure 17 (a) or (b), respectively.

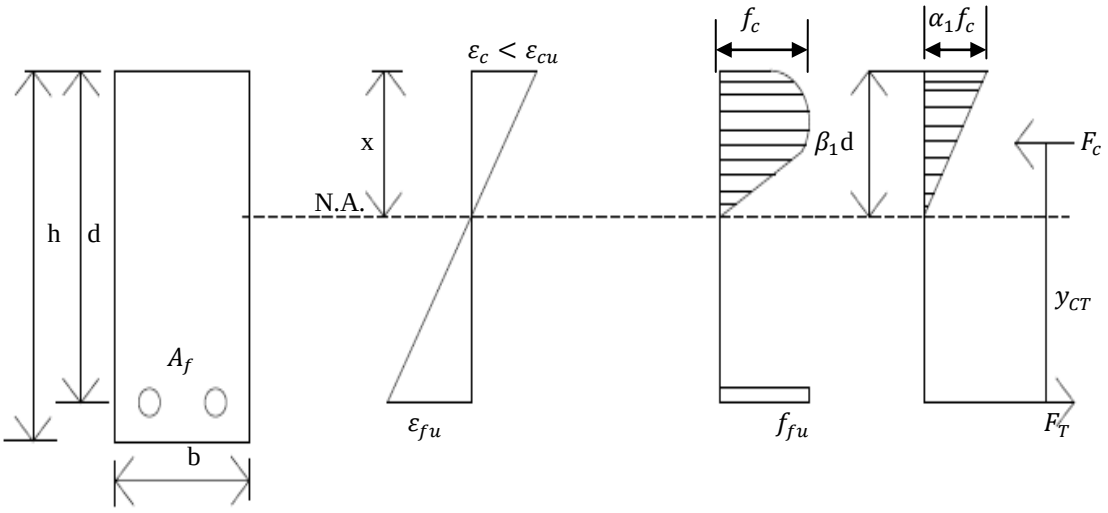

Figure 17(a) Stress-strain distribution in flexure: Failure by rupture of FRP.

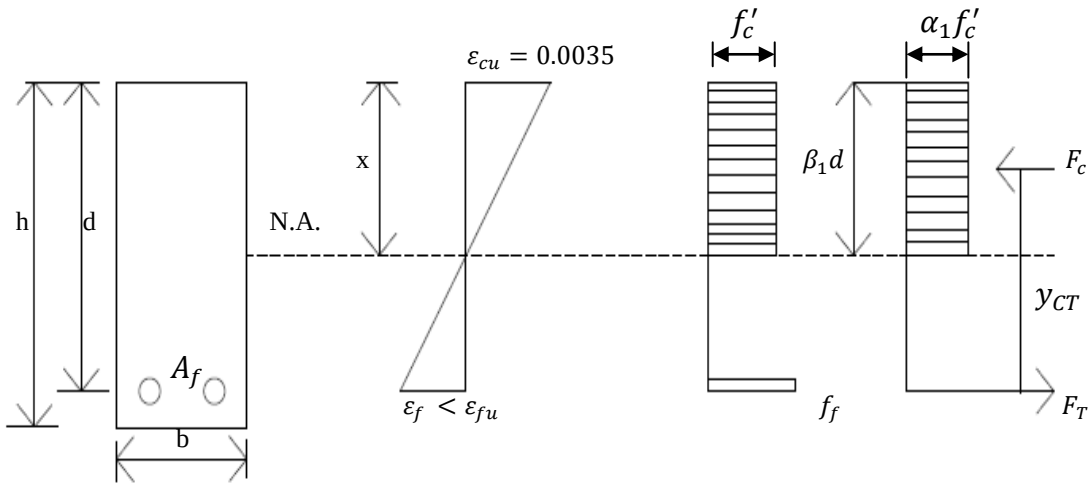

Figure 17 (b) Stress-strain distribution in flexure: Failure by concrete crush

Figure 17 Strain distribution, stress distribution and internal forces at ultimate conditions (Newhook et al., 2002:126).

The rectangular stress block is preferable to be used in compression failure of reinforced concrete when ultimate strain ε_{cu} is reached. MacGrecor and James (2006:113-114) provided values for α_1 and β_1. They proposed that α_1 should be taken to 0.85 and β_1 should be taken to 0.85 for concrete strength, f_c', up to and

including 30 MPa. However, when f_c' varies between 30 and 55 MPa, β_1 is calculated as follows:

$$\beta_1 = 1.09 + 0.008 f_c' \tag{21}$$

In case f_c' is greater than 55 MPa, β_1 is taken as 0.65. However, when the failure mode is governed by FRP ruptures, the stress distribution is idealised as parabolic and therefore the rectangular stress block factors α_1 and β_1 are unknown. The factor, α_1, is the ratio of the average concrete stress to the concrete strength. β_1 is an equivalent rectangular stress block parameter. The stress-strain curve for concrete is simulated using a constitutive model proposed by Todeschinic et al. (1964) and adjusted by MacGregor (1997) and is illustrated in Figure 18 (Kulkarni, 2006:32).

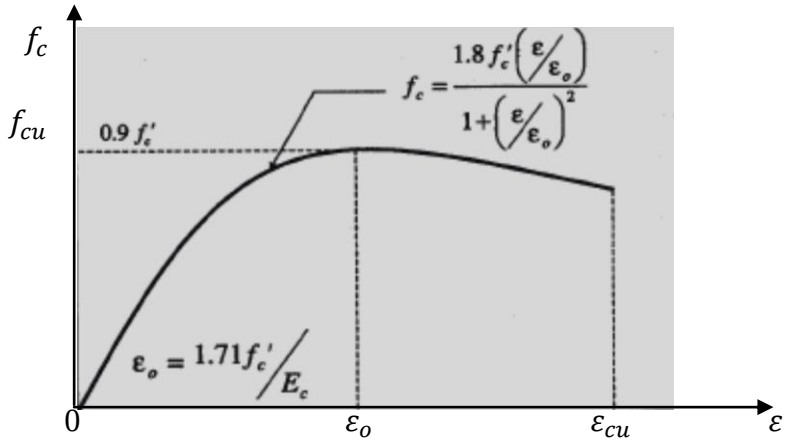

Figure 18 Stress – Strain curve for concrete

Where: f_c is the compressive strength of concrete; f_{cu} is the ultimate cube compressive strength; f_c' is the cylinder compressive strength of concrete; ε is the strain in the concrete; ε_o is the initial strain in concrete; ε_{cu} is the ultimate strain in concrete; E_c is the modulus of elasticity of concrete.

The stress-strain relationship can be represented by the following Equation:

$$f_c = \frac{1.8 f_c' \left(\frac{\varepsilon}{\varepsilon_0}\right)}{1+\left(\frac{\varepsilon}{\varepsilon_0}\right)^2} \tag{22}$$

(i) Computation of factor α_1

α_1 is obtained by equating the integral of the area under the stress-strain curve in Figure 18.

$$\int_0^{\varepsilon} f_c d\varepsilon = \alpha_1 f_c^{'} \varepsilon \tag{23}$$

$$\alpha_1 = \frac{\int_0^{\varepsilon} f_c d\varepsilon}{f_c^{'} \varepsilon} \tag{24}$$

$$\alpha_1 = \frac{0.9 f_c^{'} \varepsilon_0 ln\left[1+\left(\frac{\varepsilon}{\varepsilon_0}\right)^2\right]}{f_c^{'} \varepsilon} \tag{25}$$

Therefore the factor, α_1, can be computed as:

$$\alpha_1 = \frac{0.9 ln\left[1+\left(\frac{\varepsilon}{\varepsilon_0}\right)^2\right]}{\left(\frac{\varepsilon}{\varepsilon_0}\right)} \tag{26}$$

(ii) Computation of parameter β_1

The equivalent rectangular stress block parameter, β_1, can be obtained by assuming that the centroid of area under the concrete stress-strain curve is the same as the centroid of the area of the rectangular stress block since the concrete compressive force (C) acts at the centroid of the compression zone (Kulkarni, 2006:33).

The first moment of the area, M_0, under concrete stress-strain curve is:

$M_0 =$ (Area under the curve) x (Strain at the centroid of the area under the curve)

$$M_0 = \left\{\int_0^{\varepsilon} f_c d\varepsilon\right\}\left(1 - \frac{\beta_1}{2}\right)\varepsilon \tag{27}$$

The first moment of area of the equivalent rectangular stress block is:

$$M_0 = \int_0^{\varepsilon} f_c \varepsilon \, d\varepsilon \tag{28}$$

Equating Equations 27 and 28, β_1 can be calculated as:

$$\beta_1 = 2\left[1 - \frac{\int_0^{\varepsilon} f_c \varepsilon d\varepsilon}{\varepsilon \int_0^{\varepsilon} f_c d\varepsilon}\right] = 2\left[1 - \frac{\int_0^{\varepsilon} \frac{1.8 f_c'\left(\frac{\varepsilon}{\varepsilon_0}\right)}{1+\left(\frac{\varepsilon}{\varepsilon_0}\right)} \varepsilon d\varepsilon}{0.9 f_c' \varepsilon_0 ln\left[1+\left(\frac{\varepsilon}{\varepsilon_0}\right)^2\right]\varepsilon}\right] \quad (29)$$

$$\beta_1 = 2\left[1 - \frac{1.8 f_c' \varepsilon_0 \int_0^{\varepsilon}\left(\frac{\varepsilon}{\varepsilon_0+\varepsilon}\right)^2 d\varepsilon}{0.9 f_c' \varepsilon_0 ln\left[1+\left(\frac{\varepsilon}{\varepsilon_0}\right)^2\right]\varepsilon}\right] \quad (30)$$

$$\beta_1 = 2\left[1 - 2\frac{\int_0^{\varepsilon}\left(\frac{\varepsilon}{\varepsilon_0+\varepsilon}\right)^2 d\varepsilon}{ln\left[1+\left(\frac{\varepsilon}{\varepsilon_0}\right)^2\right]\varepsilon}\right] \quad (31)$$

$$\beta_1 = 2 - 4\frac{\left[\left(\frac{\varepsilon}{\varepsilon_0}\right) - tan^{-1}\left(\frac{\varepsilon}{\varepsilon_0}\right)\right]}{\left[\left(\frac{\varepsilon}{\varepsilon_0}\right) ln\left(1+\frac{\varepsilon^2}{\varepsilon_0^2}\right)\right]} \quad (32)$$

b) Fibre Reinforced Polymer

The mechanical behaviour of FRP materials is fundamentally linear-elastic up to failure with no post peak. As failure is not preceded by yielding or plastic elongation observed in steel bars, FRP re-bars are not ductile. The tensile strength depends on the properties of fibres which represent the main carrying component and diameter of FRP re-bars has an effect on its tensile strength, due to the non-uniform stress distribution on the rebar cross-section (Egyptian FRP code, 2005:2-25). Failure in FRP re-bars is reached when the tensile stress reaches, f_{fu} at corresponding failure tensile strain, ε_{fu}, as represented in Figure 19.

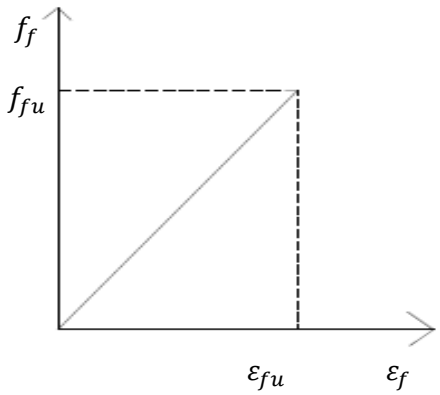

Figure 19 Stress-strain curve for FRP re-bars

The tensile strength can be computed from Equation 17 on page 34 (ACI 440.3R, 2004:9):

$$f_{fu} = \frac{F_u}{A_f} \quad \text{[MPa]}$$

The ultimate tensile strain ε_{fu} of FRP re-bars is calculated from Equation 33.

$$\varepsilon_{fu} = 0.9(\eta_a)\left(\frac{\varepsilon_{fk}}{\gamma_f}\right) \quad \text{[mm/mm]} \qquad (33)$$

where: the coefficient 0.9 accounts for the lower ultimate strain of re-bars subjected to flexure as compared to re-bars subjected to standard tensile tests; ε_{fk} is the characteristic tensile strain of FRP re-bars; η_a is the environmental conversion factor and its values are shown in Table 6; and γ_f is the partial factor of FRP re-bars.

Table 6 Environmental conversion factor η_a for different FRP re-bars (CNR-DT 203/2006, 2007:45)

Exposure Conditions	**Type of Fibre**	η_a
Concrete not exposed to moisture	Carbon	1.0
	Glass	0.8
	Aramid	0.9
Concrete exposed to moisture	Carbon	0.9
	Glass	0.7
	Aramid	0.8

c) Steel Reinforcing Bars

There is no definite yield point in the stress-strain curve for high strength tensile rebar as shown in Figure 20. High strength tensile rebar has a gradual change from elastic to plastic behaviour as opposed to mild steel (Mosley et al., 2007:6). However, high strength tensile steel has a high modulus of elasticity and good ductility behaviour compared to FRP composites.

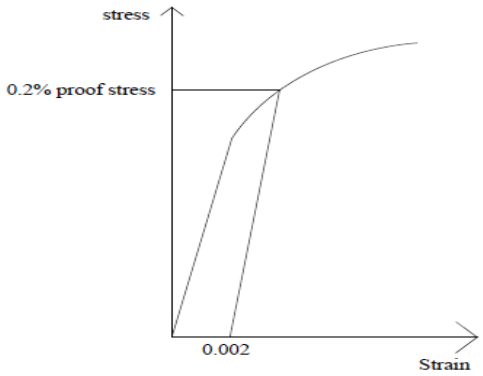

Figure 20 Stress - Strain curve for high strength steel re-bars

The behaviours of tensile strength and ultimate strain presented in Figure 20 are obtained through experimentation and governed by Equations 34 and 35, respectively.

$$f_{su} = \frac{F_u}{A_s} \tag{34}$$

$$\varepsilon_{su} = \frac{f_{su}}{\gamma_s E_s} \quad \text{[mm/mm]} \tag{35}$$

where: f_{su} is the ultimate tensile strength of high tensile rebar [MPa]; F_u is the ultimate tensile capacity [N]; A_s is the cross-sectional area of steel re-bars [mm^2]; ε_{su} is the ultimate strain for steel re-bars [mm/mm]; E_S is modulus of Elasticity of Steel re-bars and equals to 200 GPa; γ_s is the partial safety factor of steel re-bars as provided in SABS 0100-1.

4.4 Ultimate Flexural Behaviour

4.4.1 Failure Modes

Due to the nonductile behaviour of both FRP re-bars and concrete, flexural failure modes of concrete sections reinforced with FRP are brittle in nature (Egyptian FRP code, 2005:5-3). This implies that new design philosophy should be considered from that adopted in steel reinforced concrete.

Two modes of failure can govern the ultimate flexural behaviour of FRP reinforced concrete. One is compression failure due to crushing of concrete and other is rupture of FRP re-bars.

The two failure modes can be determined by comparing the FRP re-bars ratio, ρ_f, to the balanced reinforcement ratio ρ_{fb} and ρ_f is calculated from the following relationship:

$$\rho_f = \frac{A_f}{bd} \tag{36}$$

The balanced reinforcement ratio can be determined as: (ACI.440.1R.06 2006:18)

$$\rho_{fb} = 0.85\beta_1 \left(\frac{f_c'}{f_{fu}}\right)\left(\frac{E_f \varepsilon_{cu}}{E_f \varepsilon_{cu} + f_{fu}}\right) \tag{37}$$

where: $E_f$is the modulus of elasticity of FRP re-bars.

Therefore, when $\rho_f \leq \rho_{fb}$; FRP rupture failure mode governs and when $\rho_f > \rho_{fb}$; concrete crushing governs. However, the concrete crushing failure mode is more desirable for a flexural member reinforced with FRP re-bars (Pilakoutas et al., 2007:32; Egyptian FRP code 2005:5-3).

a) Concrete compression failure mode

CNR-DT 203/2006 (2007) reported that the ultimate strain in the FRP re-bars cannot be attained in this type of failure. However, in the compression zone, the maximum concrete compressive strain ε_{cu} is reached. Strain in FRP bars can be determined from Figure 17(b) strain diagram and given by: (Pilakoutas et al., 2007:33)

$$\varepsilon_f = \frac{-\varepsilon_{cu} + \sqrt{\varepsilon_{cu}^2 + \frac{4(\eta)(\alpha_{cc})(f_{ck})(\lambda)(\varepsilon_{cu})}{(\gamma_c)(\rho_f)(E_f)}}}{2} \tag{38}$$

The distribution of compressive stress in the concrete can be idealized by the rectangular block analogy. Therefore the ultimate moment can be evaluated by

adopting the framework of Eurocode-2 (EC2) and calculated by: (Pilakoutas et al, 2007:33):

$$M_u = \eta f_{cd} b d^2 (\lambda\xi)\left(1 - \frac{\lambda\xi}{2}\right) \text{ [Nm]} \quad (39)$$

where f_{cd}: the compressive strength of concrete is calculated from Equation 40; η, λ are factors; ξ is the equivalent rectangular stress block parameter, denoted in this study by β_1; η equals to 1 and λ equals to 0.8, when f_c is less or equals to 50 MPa.

$$f_{cd} = \frac{\alpha_{cc} f_c}{\gamma_c} \quad \text{[MPa]} \quad (40)$$

where the factor α_{cc} is equal to unity.

b) FRP ruptures failure mode

The ultimate strain ε_{fu} in FRP re-bars is reached when this type of failure mode occurs. However, in the compression zone, the ultimate concrete strain ε_{cu} may not be attained. This implies that the preferable rectangular stress block for concrete is not applicable and the stress block can be represented by a parabolic, constitutive model discussed in section 4.3(a) and shown in Figure 17(a) (Kulkarni, 2006:32; Egyptian FRP code, 2005:5-6).

Therefore the ultimate moment of resistance can be determined by the mathematical model developed by Pilakoutas et al (2007:34) given in Equation 41.

$$M_u = \frac{A_f f_{fk}}{\gamma_f}\left(1 - \frac{\beta_1}{2}\right) \text{ [Nm]} \quad (41)$$

The ultimate moment is obtained after determination of β_1 from Equation 32 and the current value of concrete compressive strain ε_c obtained from Equation 42 when FRP rupture occurs (CNR-DT 203/2006, 2007:15).

$$\varepsilon_c = \varepsilon_{fu}\left(\frac{x}{d-x}\right) \leq \varepsilon_{cu} \text{ [mm/mm]} \quad (42)$$

where, α_1 and β_1, as discussed in Equations 25 and 31, are used to calculate the centroid of the parabolic area where the compressive force is acting.

4.5 Soil Bearing Pressure Simulation

The following approach was used to simulate the soil bearing pressure; where the foundation base was treated as a beam while the soil was treated as an elastic foundation. This analysis is based on the assumption that elastic foundation is modelled by different springs. Thus vertical deformation characteristics of the foundation are defined by means of identical, independent, closely spaced, discrete and linearly elastic springs (Teodoru, 2009:38).

The method of analysis of beam on elastic foundation is well documented (Den Hartog, 1952:159; Timoshensko, 1976:15). The investigation of this problem led (about 1880) to the theory of interaction between a beam of moderate bending stiffness and an elastic foundation which imposes reaction forces on the beam that are proportional to the deflection of the foundation (Den Hartog, 1952:141). Two cases were studied such as infinite beam and beam of finite length on elastic foundation. In this study, the beam of finite length was considered (Figure 21) and the mathematical model of deflection of specimen is expressed as (Den Hartog, 1952:160; Timoshensko, 1976:18):

$$y_{centre} = \frac{P\beta_e}{2k}\left(\frac{2+\cos\beta_e L+\cosh\beta_e L}{\sin\beta_e L+\sinh\beta_e L}\right) \text{ [mm]} \quad (43)$$

$$y_{end} = \frac{2P\beta_e}{k}\left[\frac{\cos\left(\frac{\beta_e L}{2}\right)\cosh\left(\frac{\beta_e L}{2}\right)}{\sin\beta_e L+\sinh\beta_e L}\right] \text{ [mm]} \quad (44)$$

where P is the load applied on the beam, denoted by P_o; L is the length of the beam, denoted by l; k is the modulus of foundation (or the elastic foundation stiffness) and β_e is the characteristic of beam on elastic foundation, denoted by β, computed using Equation 45.

$$\beta_e = \sqrt[4]{\frac{k}{4EI}} \quad (45)$$

And the elastic foundation stiffness can be determined using Equation 46 (Andersson and Bergendahl, 2009:33):

$$k = \frac{4E_T(D_w)(h_T)^3}{bl^3} \quad [\text{N/mm}^2] \tag{46}$$

where k is the elastic foundation stiffness, denoted by S; E_T is the modulus of elasticity of timber (In this study, grade 10 of timber is considered from SABS 0163-2, 2001:62), denoted by E; D_w is the width of timber element; h_T is the height of timber element, denoted by h; l is the length of the timber element and b is the width of the beam, denoted by w.

The bending moment is obtained by:

$$M_{centre} = \frac{P}{4\beta_e}\left(\frac{\cosh\beta_e L - \cos\beta_e L}{\sinh\beta_e L + \sin\beta_e L}\right) \text{[Nm]} \tag{47}$$

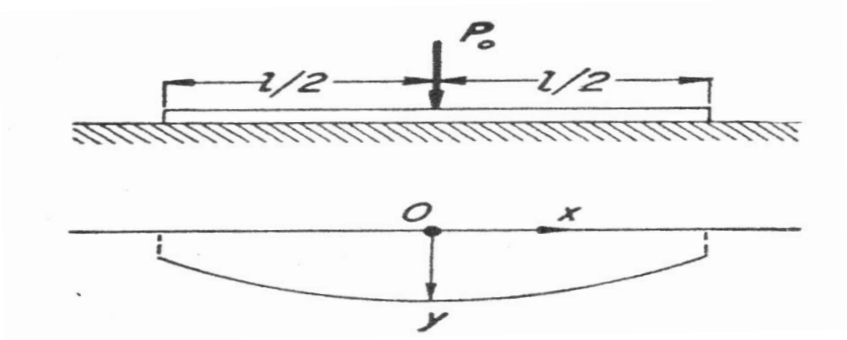

Figure 21 Beam resting on two-parameter elastic foundation.

In this figure, P_o is the concentrated load; O is the centre point of beam; y is the deflection of beam; l is the length of beam.

In this study, the soil bearing pressure was simulated by using an elastic plate that can deform only in bending and supported by independent spring element (Kerr, 1964:494).

4.6 Summary

It has been shown that FRP re-bars have a different failure mode and approach in tensile strength test from steel re-bars. New philosophy is considered for flexural

analysis of FRP reinforced concrete where concrete crushing is more desirable than FRP ruptures. The soil bearing pressure and elastic foundation are simulated by using timber as flexural elements and springs.

CHAPTER 5

PRESENTATION AND DISCUSSION OF RESULTS

5.1 Introduction

This chapter deals with presentation and discussion of results of the research. The chapter is divided into three parts. Part one deals with mix design and mechanical properties of reinforcement; part two deals with the theoretical design of foundations, while the third part focuses on experimental results conducted on the foundation bases in the laboratory.

5.2 Concrete

5.2.1 Sieve Analysis

The fine and coarse aggregates were analysed for grading. The coarse aggregates constituted 15 mm and 19 mm sizes. Typical results of fine aggregates as well as 15 mm and 19 mm coarse aggregates are presented in Table 7. The rest of the sieve analysis results are presented in Appendix A.

Table 7 Sieve Analysis results of Fine and Coarse Aggregates

	Fine Aggregates (FA)			15 mm Coarse Aggregates (CA)			19 mm Coarse Aggregates (CA)		
Sieve Size (mm)	**Mass Retained (grams)**	**Percentage Retained**	**Percentage Passing**	**Mass Retained (grams)**	**Percentage Retained**	**Percentage Passing**	**Mass Retained (grams)**	**Percentage Retained**	**Percentage Passing**
75.0	0	0	100	0.2	0.02	99.98	0.1	0.01	99.99
53.0	0	0	100	0.1	0.01	99.97	0.1	0.01	99.98
37.5	0	0	100	0.4	0.04	99.93	0.1	0.01	99.97
26.5	0	0	100	0.1	0.01	99.92	0.2	0.02	99.95
19.0	0	0	100	5.6	0.56	99.36	200.1	20.01	79.94
13.2	0	0	100	433.5	43.35	56.01	740.0	74.00	5.94
9.5	0	0	100	488.5	48.85	7.16	49.1	4.91	1.03
6.7	0	0	100	54.4	5.44	1.72	5.5	0.55	0.48
4.75	0.8	0.08	99.92	7.8	0.78	0.94	1.1	0.11	0.37
3.35	-	-	-	2.4	0.24	0.70	0.7	0.07	0.30
2.36	0.2	0.02	99.90	0.8	0.08	0.62	0.3	0.03	0.27
1.18	0.3	0.03	99.87	0.3	0.03	0.59	0.3	0.03	0.24
0.600	25.9	2.59	97.28	0.3	0.03	0.56	0.2	0.02	0.22
0.425	117.5	11.75	85.53	0.3	0.03	0.53	0.1	0.01	0.21
0.300	355.7	35.57	49.96	0.3	0.03	0.50	0.2	0.02	0.19
0.150	405.1	40.51	9.45	1.0	0.10	0.40	0.6	0.06	0.13
0.075	71.3	7.13	2.32	2.1	0.21	0.19	1.0	0.10	0.03
TOTAL	**976.8**	**97.68**		**998.1**	**99.81**		**999.7**	**99.96**	

The data in Table 7 was used to plot the curves of aggregates presented in Figure 22.

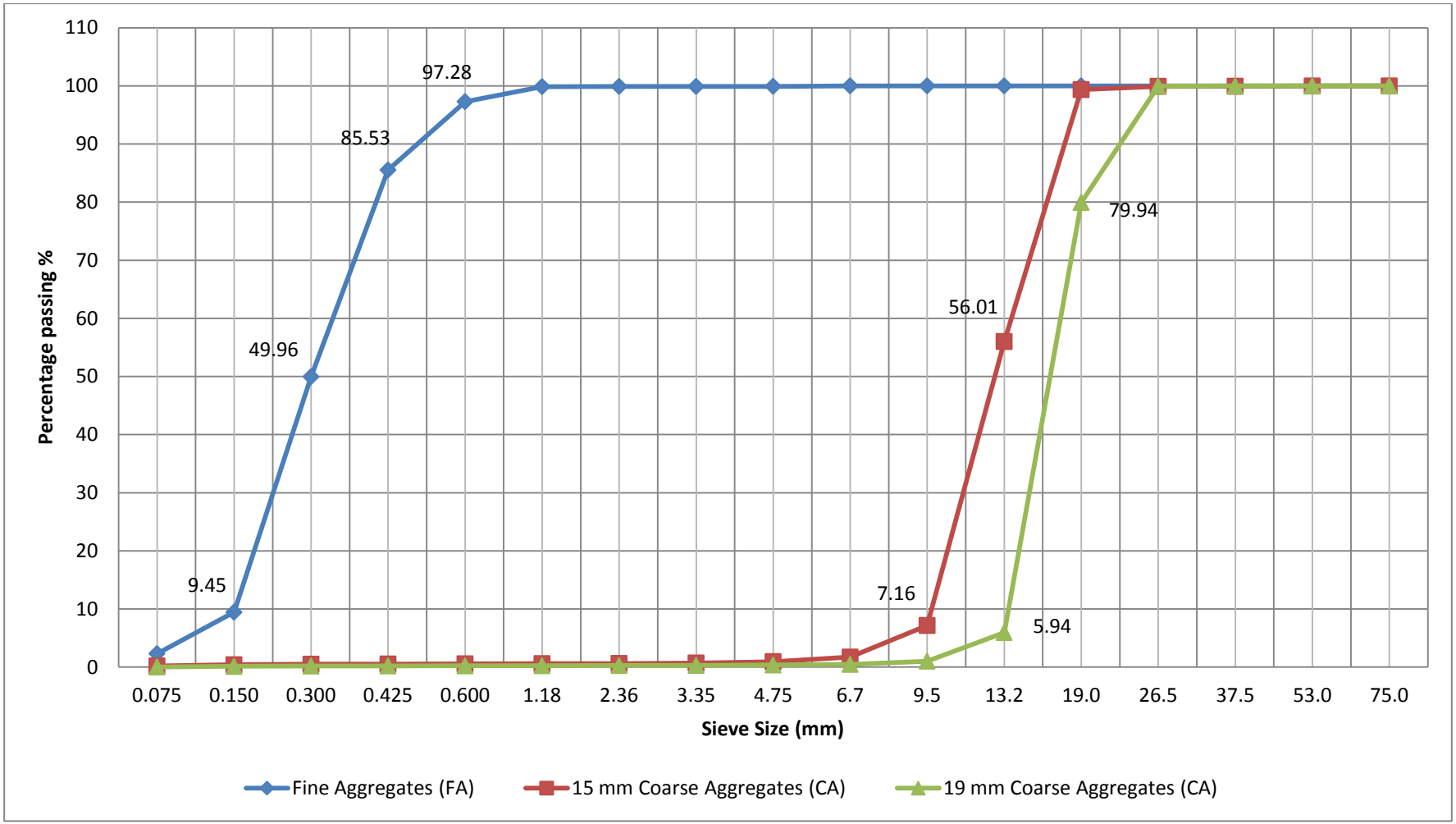

Figure 22 Grading curves of fine and coarse aggregates.

It is known that concrete is a mixture of cement, water, coarse aggregates and fine aggregates. Considering the microscopic aspect of concrete, the space between the coarse aggregates often referred to as the "void volume" should be filled completely by the volume of fine aggregates. The small spaces between the fine aggregates grains in turn should be filled by the very much smaller particles of the cement (the later mixed with water, undergoes the chemical process which changes it into rock-hard concrete) (Robertson, 2000:1). Therefore, little sand would result in a very harsh mix and would require cement to be used as voids filler and too much sand captures the cement paste to coat the individual grains resulting in the increased cement demand. This underscores the importance of having the correct quantities of each constituent material so as to produce concrete of the desired properties.

It appears in Figure 22 that 97.28 percent of fine aggregates were passing through sieve of a 0.600 mm size. That constituted too much fine particles in the fine aggregates. This implies higher cement demand as the cement paste coated fine elements and will enhance the flow and mobility of concrete. Therefore, the sieve analysis results for fine aggregates presented in Table 7 and in Figure 22 had an influence on the fresh concrete and the hardened concrete which is discussed later in this chapter. The cement costs more than aggregate and the cement paste requirement for concrete increases with increasing void content of the combined aggregates, hence it is desirable to keep the void content as low as possible. This implies that too many voids would result in expensive concrete.

In practice, to reduce the cost of concrete, two types of coarse aggregates are used, 15 and 19 mm. Concrete mix in this study was made with these two types of coarse aggregates. The 15 mm aggregate will fill the voids between 19 mm one. Then the fine aggregates will fill those which are between 15 mm coarse aggregates.

In Figure 22, it is seen that 43.99 percent coarse aggregate was retained above 13.2 mm sieve size for 15 mm aggregate. Therefore, this coarse aggregate had enough particles to fill the void between 19 mm coarse aggregates and make the concrete sufficiently dense. The second type of coarse aggregates (19 mm) had 74 percent of particle size which is between 13.5 mm and 19 mm. This large quantity of aggregates

has an influence on the workability of concrete. Therefore an increase in mass per cubic meter of this aggregate in concrete will result in coarser concrete mix. Thus a good balance between quantities of fine aggregates and coarse (15 mm and 19 mm) aggregates has to be attained for a dense concrete with the specific required workability.

5.2.2 Concrete Mix Design

There are three methods used to design concrete mix. These include ACI (1991), the British method and the C & CI design method developed by Cement and Concrete Institute of South Africa. The C & CI design method is based on ACI committee Report 613-54 (Brian, 1998:105) and is similar to the British method. In this research, the British concrete mix design method was used. It was published in 1975 and revised in 1988 by the Department of the Environment and is known as the "DoE" (Dewar, 2003: 1/32). The reason for using this type of concrete mix design was motivated by the high amount of fine aggregates passing 0.600 mm sieve size.

According to the British method of concrete mix design, the determination of quantities of fine aggregates grading takes into consideration the percent passing 0.600 mm sieve size analysis of fine aggregates. Less fine aggregates is required when free Water/Cement ratio is low while the fine aggregate is finer (i.e. higher per cent passing 0.600 mm), maximum aggregate size is higher and the target slump is low.

Dewar (2003:1/35) requires that water demands in the ACI (1991) method are 5 to 10 kg/m^3 higher than the DoE values for uncrushed aggregates. As a large amount of fine aggregates (97.28 percent) was passing 0.600 mm sieve size, it was necessary to consider it in the concrete mix design by keeping the water demands at a lower level. Thus, the mix design on the basis of DoE method is presented in Table 8.

Table 8 Mix design calculations for class 20 concrete.

STEP	ITEM	REFERENCE	CALCULATION AND VALUES
1	Characteristic strength	Specified	Compressive 20 MPa at 28 days
			Proportion defective 5 %
	Degree of control	Table 9.1 (Brian,1998:117)	Good
	Standard deviation	Table 9.1(Brian, 1998:117)	5 MPa
	Margin	Table 9.1 (Brain, 1998:117)	8.5 MPa
	Target mean strength class	C1	20+8.5=28.5 MPa
	Cement strength class	Specified	CEM 32.5 R
	Aggregate type: coarse	Crushed/ Uncrushed	
	Aggregate type: fine		
	Free Water/Cement Ratio	Figure 20.1 (Krishna, 2007:265)	0.68
	Maximum free water/cement ratio	Figure 8.3 (Brian, 1998:108)	0.59 Lower value used (0.59)
2	Slump or Vebe time	Specified	Slump 50 mm or Vebe time 3-6
	Maximum aggregate size	Specified	20 mm
	Free water content	Table 20.2 (Krishna, 2007:265)	210 kg/m^3
3	Cement content	C2	210/0.59=356 kg/m^3
	Maximum cement content	Specified	-
	Minimum cement content	Specified	290 kg/m^3
4	Relative density of aggregate (SSD)		2.6
	Concrete density	Figure 20.2	2,329 kg/m^3
	Total aggregate content	C3	2, 329-210-356=1,763 kg/m^3
5	Grading of fine aggregates	SABS 829,1994:1	Average % Passing 600 sieve=96.69 %
	Proportion of fine aggregate	Figure20.4 (Krishna, 2007:268)	27 %
	Fine aggregate content	C4	1,763(0.27)=476.01 kg/m^3
	Coarse aggregate content	C5	1,763-476.01=1,286.99 kg/m^3

5.2.3 Tests on Fresh Concrete

Slump test was done to determine the workability of concrete. From the mix design, the required slump taken into account was 50 mm. For a given workability, there exists a unique aggregate-cement ratio which gives the desired workability. Workability is affected by the properties of aggregates such as the maximum size, grading type, shape and texture. Therefore, slump tests were conducted on the three trial mixes summarized in Table 9.

Trial one was based on the mix design, trial two had the same cement and water contents as trial one but the proportions of 15 mm coarse aggregates vis – à – vis 19 mm coarse aggregates and the ratio of fine aggregates and coarse aggregates were modified by increasing fine aggregates and 15 mm coarse aggregates and decreasing 19 mm coarse aggregates. Trial three had different quantities of proportions compared to the other two. On the basis of steps 2, 3 and 5 in Table 8 the batch weights of the designed concrete mix obtained are presented in Table 9.

Table 9 Batch weight of the concrete mixes

Items	**Cement (kg/m^3)**	**Water (l/m^3)**	**Fine aggregates F.A. (kg/m^3)**	**Coarse aggregates C.A.(kg/m^3)**		**Concrete mix ratio**
				15 mm	19 mm	Cement : F.A.: C.A.
Trial 1	356.00	210	476.01	643.50	643.50	1 : 1.34 : 3.62
Trial 2	356.00	210	676.01	723.94	361.97	1 : 1.90 : 3.05
Trial 3	379.66	224	676.01	782.63	304.36	1 : 1.78 : 2.86

The slump test conducted on the first trial mix (as shown in Figure 23(a)) gave zero slump. This might have been due to the high amount of coarse aggregates in the mix and to the higher fine aggregates/coarse aggregates ratio of 63.01 percent. To improve on the workability, the proportions of fine and coarse aggregates were adjusted in the second trial mix shown in Table 9. In the second trial mix, the adjustment on the fine aggregates/ coarse aggregates ratio was needed to make the

concrete mix less coarser and increase the workability. Normally the fine aggregates/ coarse aggregates ratio has an influence on the result of slump test (Santhakumar, 2007:35). This adjustment had an impact on the second slump test, where the result achieved was a slump of 40 mm as shown in Figure 23(b). However, the required slump of 50 mm was not achieved and a second adjustment was necessary to improve the workability of the mix.

Progressive modifications were made until the required slump was obtained. Those adjustments on the quantities of materials were made to improve the workability, before doing the third slump test. In the first adjustment, the quantity of water was increased by 6.67 percent from the initial quantity. The Water/Cement ratio was maintained constant, i.e. 6.65 percent of cement was added as second adjustment. Two other adjustments were made on coarse aggregates. The 19 mm coarse aggregates was decreased by 15.92 percent and 15 mm coarse aggregates was increased by 8.11 percent. This resulted in the third trial mix.

(a) No slump (b) 40 mm Slump

(c) 50 mm Slump

Figure 23 Results of slump tests

This third trial mix gave the target 50 mm slump shown in Figure 23(c).

5.2.4 Tests on Hardened Concrete

Three different trial mixes were tested on fresh concrete (slump test) and four different trial mixes were made from the third sample of fresh concrete (50 mm slump) which were tested on the hardened concrete for compressive strength as indicated in step 1 of Table 8. A typical cube test is shown in Figure 24. The results of tests conducted on the four trial mixes made and the ready-mixed concrete supplied are presented in Table 10 and plotted in Figure 25.

As (a practical assumption) concrete at 28 days is 1.5 times as strong as at 7 days: the range was varied between 1.3 and 1.7, the British code of practice accepts concrete if the strength at 7 days is not less than two-thirds of the required 28 day strength (Hassoun and Al-Manaseer, 2008:26). Therefore, the compressive strength projected at 28 days is calculated as:

$$f_{cu28} = \frac{3}{2} f_{cu7} \tag{48}$$

where: f_{cu28} is the cube compressive strength at 28 days, denoted by σ_{28} and f_{cu7} is the cube compressive strength at 7 days, denoted by σ_7.

Figure 24 Typical cube test

From Table 10 and Figure 25 it is observed that the compressive strength of concrete mix trial one at 28 day was 20.56 percent lower than target strength. Hence concrete trial mix one was rejected as it could not yield the desired target concrete strength.

This decrease can be attributed to the presence of large amount of Fine Aggregates in the mix, where the particles captured the cement paste. Consequently, three other trial mixes were made with an increased cement content as shown in Table 10 to improve the strength of concrete.

Table 10 Compressive strength of concrete cubes.

Items	**Cement content (kg/m^3)**	**Water/Cement ratio**	**Proportions of materials to cement Aggregates**		**Compressive strength (MPa) Days**		
			Fine	**Coarse**	**7**	**28**	**28 projected**
Concrete trial mix 1	379.66	0.590	1.78	2.86	17.33	22.64	25.99
Concrete trial mix 2	384.41	0.583	1.76	2.86	19.79	23.08	29.69
Concrete trial mix 3	385.36	0.581	1.75	2.82	21.40	27.78	32.10
Concrete trial mix 4	413.00	0.542	1.64	2.63	23.50	27.18	35.25
Ready-mixed concrete supplied by JPFC Construction	-	-	-	-	20.15	27.84	30.23
Compressive strength targeted	379.66	0.590	1.78	2.86	19.00	28.50	28.50

Concrete trial mix 3 had a compressive strength that was 12.63 percent higher at 7 days than the targeted strength and 2.53 percent higher at 28 days than the targeted value. This mix formed the desired concrete mix for this research. It is also observed from Table 10 that a decrease of Water/Cement ratio increased the strength of concrete. However, the compressive strength of ready-mixed concrete was referred to that of concrete trial mix 3.

Figure 25 emphasizes the influence of Fine Aggregates on the concrete strength when the behaviours of concrete trial mix 2 and concrete trial mix 4 are compared to ready-mixed concrete supplied. Concrete trial mix 2 had a lower difference of 1.82 percent at the 7 day strength and 20.62 percent lower after 28 days to ready-mixed concrete supplied.

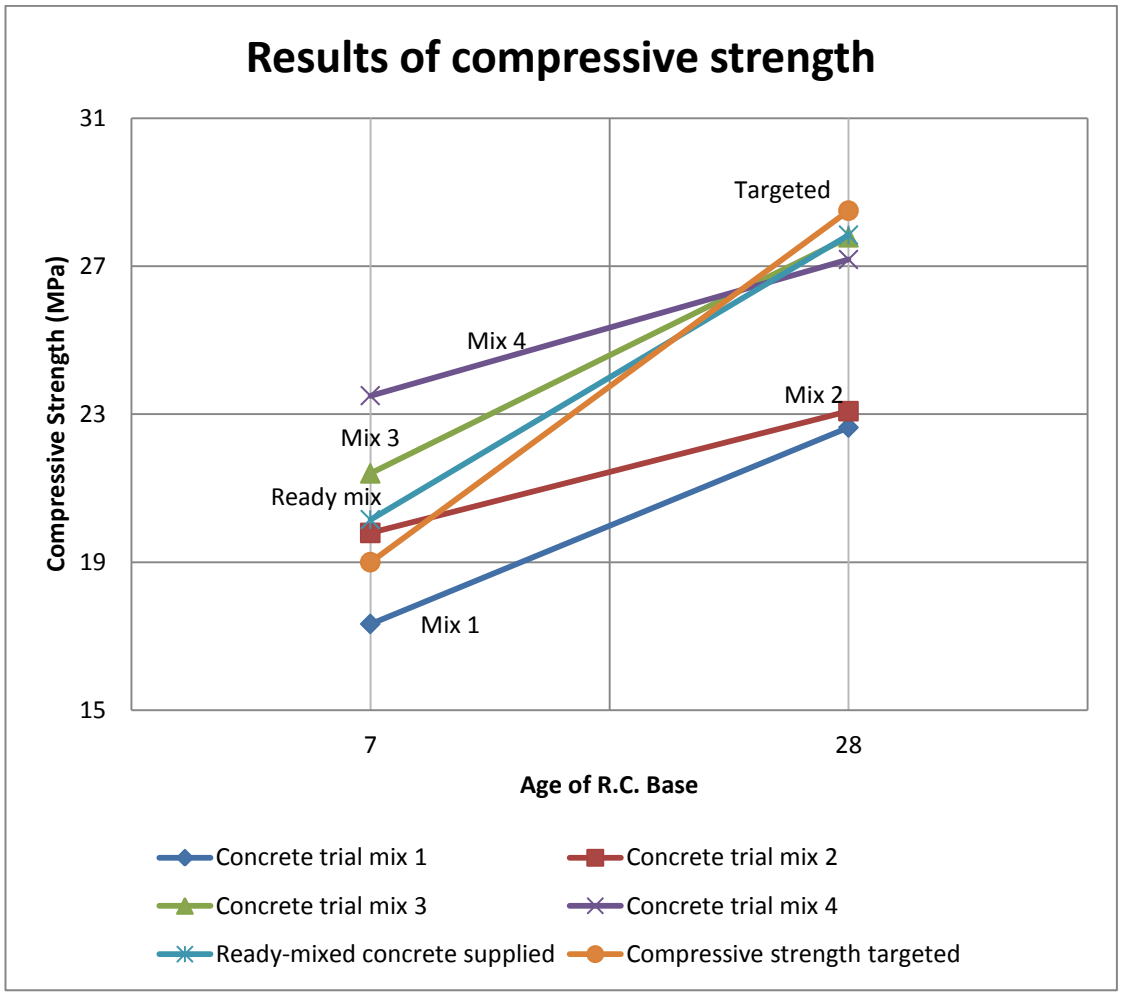

Figure 25 Compressive strength of concrete mixes

Compared to the ready-mixed concrete supplied, concrete trial mix 4 had higher strength by 16.63 percent and lower strength by 2.37 percent at 7 and 28 days, respectively.

In most of the equations used in this study (concrete), the cylinder compressive strength was mentioned. Therefore, the cube compressive strength was converted to cylinder compressive strength. From experimental consideration, Equation 49 links the ultimate compressive strength of concrete in compressive zone of the beam to the ultimate compressive strength obtained from cube and cylinder tests (Alexander and Beushausen, 2010:44):

The ultimate compressive strength of concrete in the compressive zone of the beam equals to $0.85f_c' = 0.67\ f_{cu}$ (49)

where f_c' is the ultimate compressive strength obtained from the cylinder test and f_{cu} is the ultimate compressive strength obtained from the cube test.

The ultimate compressive strength obtained by cylinder test is close to being the same as the ultimate compressive strength of the beam as the coefficient of 0.85 is almost equal to unity.

Equation 49 can be rewritten to yield Equation 50, where cylinder compressive strength cylinder is calculated from cube compressive strength:

$$f_c' = \frac{0.67}{0.85} f_{cu}$$

$$f_c' = 0.79\ f_{cu} \quad (50)$$

Therefore, the compressive strength of cylinder, f_c', can be obtained from Equation 50. From the compressive strength values presented in Table 10, the correspondent cylinder compressive strength of the ready mix concrete was calculated as:

$$f_c' = 0.79(27.84)$$

$$f_c' = 21.99 \text{ MPa.} \quad (51)$$

With the cylinder compressive strength, the short term modulus of concrete used in this study was determined. The short term modulus of elasticity, E_c, was calculated from Equation 52 given in ACI design code (MacGregor and Wight, 2005:23) as

$$E_c = 0.043(w^{1.5})\sqrt{f_c'} \quad (52)$$

where w is the density of the concrete in kg/m^3 and f_c' is the compressive strength from the cylinder test in MPa. In the case of normal-weight concrete with a density of 2 300kg/m^3 (the weight of concrete used in this project was a normal-weight concrete) Equation 53 becomes (MacGregor and Wight, 2005:23):

$$E_c = 4700\sqrt{f_c'} \quad (53)$$

Thus the elasticity of modulus of concrete was found to be:

$$E_c = 4700\sqrt{21.99}$$

E_c = 22.04 GPa. (54)

However, SABS 0100 (2000:189) recommend the short term modulus of elasticity of concrete to be calculated from:

$$E_{c_{28}} = K_o + \alpha f_{cu,28} \quad (55)$$

where K_o is a constant closely related to the modulus of elasticity of the aggregate and α is the ratio of the modulus of elasticity to tensile strength of the aggregate. It is clear that K_o and α depend on the type of aggregates used in the concrete mix. Alexander & Beushausen (2010:23) proposed a Table (Table 11) where parameters K_o and α are determined according to the type of aggregates available in South Africa.

Table 11 Design values for estimating modulus of concrete for ages of 3 to 28 days. (Alexander & Beushausen, 2010:23)

Aggregate type	Range of design values 3 to 28 days	
	K_o (GPa)	α (GPa/MPa)
Western Cape		
Granite	21	0.25
Greywacke (Malmesbury shale)	24	0.25
TM quartzite (Mossel Bay area)	23	0.25
KwaZulu-Natal		
Dolerite	15 – 22	0.40
TM quartzite	17 – 21	0.25
Tillite	20	0.35
Siltstone (KwaZulu-Natal Midland)	21	0.15
Gauteng and surrounding areas		
Andesite	25 – 26	0.30
Dolomite	24 – 25	0.45
Felsite	18 – 21	0.35
Granite	17 – 18	0.25
Quartzite: Ferro	17	0.40
Daspoort	14	0.30
Reef quartzite	18 – 20	0.25

Since the type of aggregate used in this study is dolomite from Gauteng province, the average value of K_o of 24.5 and a value of α of 0.45 were used in the calculation of short term modulus of elasticity for concrete as follows from Equation 55:

$$E_{c_{28}} = 24.5 + 0.45(27.84) = 37.028 \text{ GPa} \quad (56)$$

However, the standard values of K_o and α are 20 and 0.2 respectively. Thus the short term modulus of elasticity of concrete was SABS 0100 (2000:189):

$$E_{c_{28}} = 20 + 0.2(27.84)$$

$$E_{c_{28}} = 25.568 \text{ GPa} \quad (57)$$

The short term modulus of elasticity of concrete obtained from equation 54 was 40.48 percent lower compared to that obtained in equation 56 while that to the last equation was 44.82 percent higher than that obtained from the South African standard code. This difference is attributed to the fact that in equation 57, the characteristics of aggregate were not considered and the average characteristic of

aggregates available in South Africa was taken into account in equation 56. Thus the short term modulus of elasticity of concrete used in this research was 37.028 GPa.

In Table 12, shows the short term modulus of elasticity and the compressive strength of concrete of the four trial mixes. In this table, the ready mix concrete was not considered due to the fact that Water/Cement ratio was not given by the supplier (JPFC construction).

Table 12 Comparison between short term modulus of elasticity and compressive strength of the trial mixes

Item	Water/Cement ratio (%)	Cement content (kg/m^3)	Proportions of material to cement Aggregates		Compressive Strength of cube at 28 Days (MPa)	Short term modulus of Elasticity (GPa)
			Fine	Coarse		
Concrete trial mix 1	0.590	379.66	1.78	2.86	22.64	34.688
Concrete trial mix 2	0.583	384.41	1.76	2.86	23.08	34.886
Concrete trial mix 3	0.581	385.36	1.75	2.82	27.78	37.001
Concrete trial mix 4	0.542	413.00	1.64	2.63	27.18	36.731

It appears from Table 12 that short term modulus of elasticity and compressive strength are affected by water/cement ratio. The water/cement ratio increases the porosity of the paste and the workability of concrete. When concrete is workable, then compressive strength is less and modulus of elasticity is lower. Therefore, the short term modulus of elasticity depends on water/cement ratio (cement paste) and type of coarse aggregates as shown in equation 53 where concrete trial mix 1 had the biggest water/cement ratio with lowest short term modulus of elasticity. It is clear that quality of coarse aggregates affects the performance of concrete and the density of concrete as coarse aggregate weighs more than other materials such as fine aggregates, water and cement. Therefore, it is necessary to do a good selection of materials and mix design for better performance of concrete.

5.3 Reinforcing Bars

5.3.1 Fibre Reinforced Polymers Re-bars

In this study, Carbon Fibre Reinforced Polymer (CFRP) and Glass Fibre Reinforced Polymer (GFRP) re-bars were used. The two different rebar products cited above were considered: one manufactured locally by Industrial Composite C.C. (South Africa) and the other one by Pultrall Company of Canada. Two tests were performed on the FRP; namely cross-sectional properties and longitudinal tensile properties. The procedures described in ACI 440. 3R-04: Part 2, B-1 and B-2, respectively were followed for the tests as discussed in Section 3.3.1 (b).

a) Cross-sectional dimensions of FRP Re-bars

The cross-sectional dimensions test was conducted on CFRP and GFRP from the two manufacturers. Five specimens of 200 mm length of CFRP and GFRP were tested and the results are presented in Table 13.

Table 13 Cross-sectional dimensions test results of FRP re-bars

Material	**Manufacturer**	**Level of Water**		**Area** A	**Equivalent Diameter** d_b	**Equivalent Circumference** c_b
		Before (ml)	After (ml)	(mm^2)	(mm)	(mm)
GFRP	Industrial Composites cc	700	716.4	82.00	10.22	32.09
	Pultrall Company	700	715.5	77.50	9.94	31.20
CFRP	Industrial Composites cc	700	716.8	84.00	10.34	32.48
	Pultrall Company	700	715.6	78.00	9.97	31.30

The local products were found to have bigger diameter than the imported ones with a difference of 0.89 mm (2.82 percent) and 1.18 mm (3.71 percent) for GFRP and CFRP re-bars respectively. This difference is attributed to the adhesive added on the surface of the local re-bar. The purpose of the adhesive on the re-bar was to improve the bond between the FRP re-bar and the concrete. This difference has an implication

on the structural performance of the FRP re-bars such as the modulus of elasticity, the FRP reinforcement ratio and the mode of failure of FRP reinforced concrete.

b) Longitudinal Tensile Properties of FRP Re-bars

Five specimens of 1000 mm length each of CFRP and GFRP were tested using the Universal Testing Machine. The mean results are presented in Table 14. Typical graphs of tensile test of FRP re-bars are presented in Figure 26 and the ruptured typical samples are shown in Figure 27.

Table 14 Longitudinal tensile test results of FRP re-bars

Material	Manufacturer	Ultimate Tensile Strength f_{fu} (MPa)	Modulus of Elasticity E_f (GPa)	Ultimate Tensile Strain ε_{fu} (%)
GFRP	Industrial Composites cc	641.88	43.67	1.47
	Pultrall Company	558.40	28.35	1.97
CFRP	Industrial Composites cc	701.65	60.49	1.16
	Pultrall Company	866.80	76.04	1.54

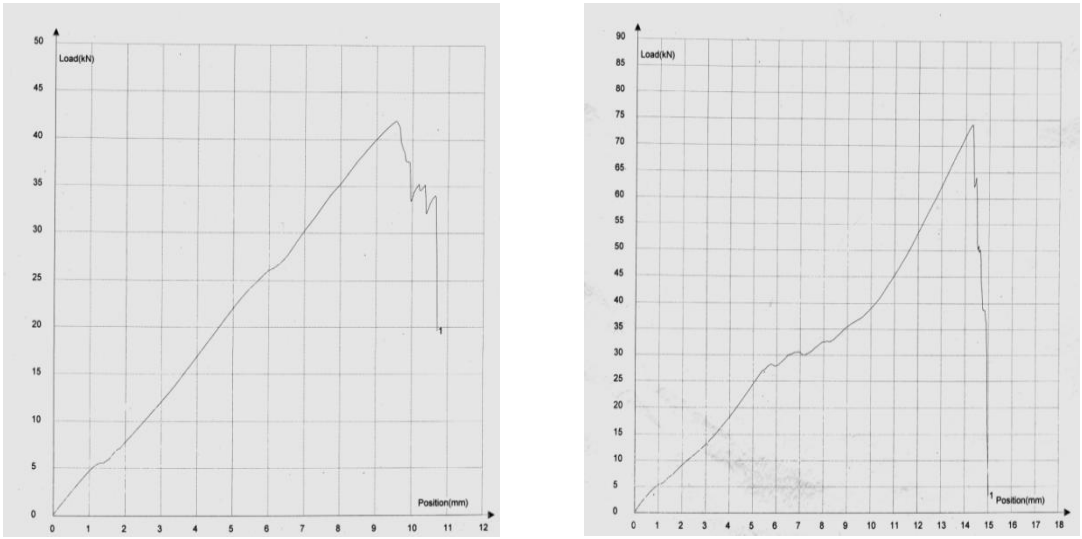

(a) Glass FRP (b) Carbon FRP

Figure 26 Tensile test curves of FRP samples.

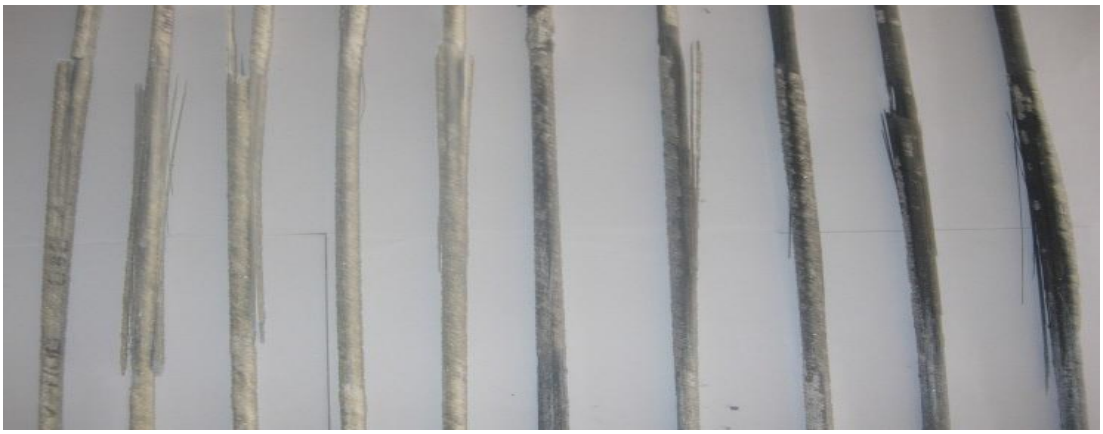

Figure 27 Ruptured samples of GFRP and CFRP re-bars.

As shown in Table 14, the local products made by Industrial Composites did not have the same tensile strength as materials sold overseas by Pultrall Company. The tensile strength of Pultrall CFRP product was 23.54 percent higher than the Industrial Composites product. Considering the GFRP re-bars, the Industrial Composite products did have a higher tensile strength than Pultrall product by 14.95 percent. It is observed from Figure 26 that the load on the re-bar was linearly distributed on fibres and rupture occurred suddenly without warning; this emphasized the non-ductility of FRP.

These differences could be caused by the five major factors described in chapter two namely, volume and type of fibre and resin; fibre orientation; dimension and quality control during manufacturing; loading history; duration, temperature and moisture. The last three factors i.e. duration, temperature and moisture were related to the conservation of materials before they could be used.

The results for modulus of elasticity tabulated in Table 15 were determined as described in Section 4.3(b).

The modulus of elasticity of Industrial Composites products of GFRP re-bars was found to be 15.32 MPa or 25.71 percent higher than that of Pultrall Company while the modulus of elasticity of CFRP (from Pultrall) was found to be 15.55 MPa or 35.08 percent higher than that from Industrial composites. However, the ultimate

tensile strain of CFRP and GFRP re-bars were found to be higher than those of Industrial Composites by 32.76 percent and 34.01 percent respectively.

Now consider the theoretical properties given in the technical sheet of Pultrall Company presented in Table 15.

Table 15 Theoretical properties of FRP re-bars from the technical sheet.

Material	Ultimate Tensile Strength f_{fu} (MPa)	Modulus of Elasticity E_f (GPa)	Ultimate Tensile Strain ε_{fu} (%)
GFRP	856	45.4	1.89
CFRP	1,596	120.0	1.33

There is a difference between the values in technical sheet (Table 15) and the values presented in Table 14. According to CNR-DT 203/2006 (2007:7), the material partial factors γ_m to be used in case of ultimate limit should be 1.5 for all types of FRP re-bars. This is subject that the characteristic strength of FRP re-bars provided are not less than 400 MPa, and the average value of Young's modulus of elasticity in the longitudinal direction is not less than 100 GPa for CFRP re-bars and 35 GPa for GFRP re-bars.

To explain deviation between the experimental and technical sheet values, take the partial safety factor of γ_f to be 1.5 and denoted by γ_m, the conversion factor of η_f to be 1.0, denoted by η, for CFRP and GFRP re-bars in Equation 58 as recommended in CNR-DT 203/2006 (2007:11).

$$X_k = \gamma_f \frac{X_d}{\eta} \tag{58}$$

where X_k is the characteristic value of property being considered from the technical sheet supplied by the manufacturer and X_d is the experimental value. The calculated values are presented in Table 16.

Table 16 Longitudinal tensile test results of FRP re-bars

Material	Manufacturer	Ultimate Tensile Strength f_{fu} (MPa)	Modulus of Elasticity E_f (GPa)
GFRP	Industrial Composites cc	962.82	65.51 > 35
	Pultrall Company	837.60	42.53 > 35
CFRP	Industrial Composites cc	1,052.48	90.74 < 100
	Pultrall Company	1,300.20	114.06 > 100

From Table 16 the CFRP re-bars manufactured by Industrial Composites had modulus of elasticity less than 100 GPa. Therefore, it is necessary for the local manufacturer to review its manufacturing process and quality control standards of CFRP re-bars. It is clear that properties of FRP changed with time and environment (as the conversion factor of FRP is related to the environmental conversion factor and conversion factor due to long-term effects) unlike that of steel which loses its characteristics only when exposed to corrosion. A decision was made to use products from Pultrall Company due to the good test results of its re-bars.

5.3.2 Steel Re-bars

The mechanical properties of three samples of the high tensile strength bars are presented in Table 17 and a ruptured typical sample is presented in Figure 28. A typical graph of tensile test is shown in Figure 29. Theoretical ultimate tensile strength, modulus of elasticity and ultimate tensile strain for high tensile strength bars given in standard (SABS 0100-1, 2000:11,17) are 450 MPa, 200 GPa and 0.225% respectively.

Table 17 Mechanical properties of high strength steel bars

Materials	Ultimate Tensile Strength σ_u (MPa)	Modulus of Elasticity E (GPa)	Ultimate Tensile Strain ε_{su} (%)
STEEL SAMPLE 1	588.62	245.26	0.24
STEEL SAMPLE 2	603.40	167.61	0.36
STEEL SAMPLE 3	588.78	226.39	0.26
MEAN	593.60 > 450	213.09 > 200	0.28 > 0.225

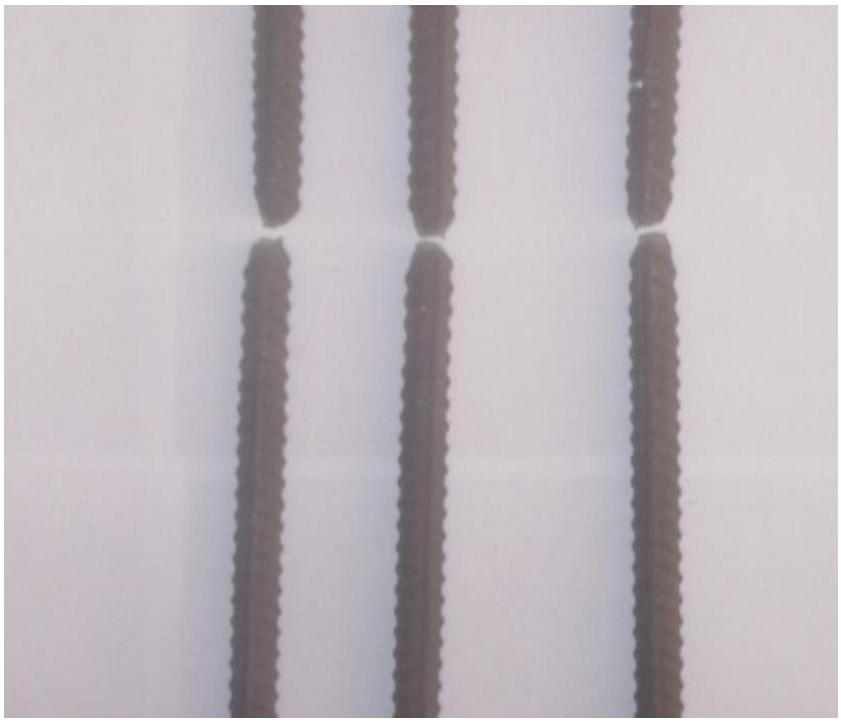

Figure 28 Ruptured samples of Steel re-bars

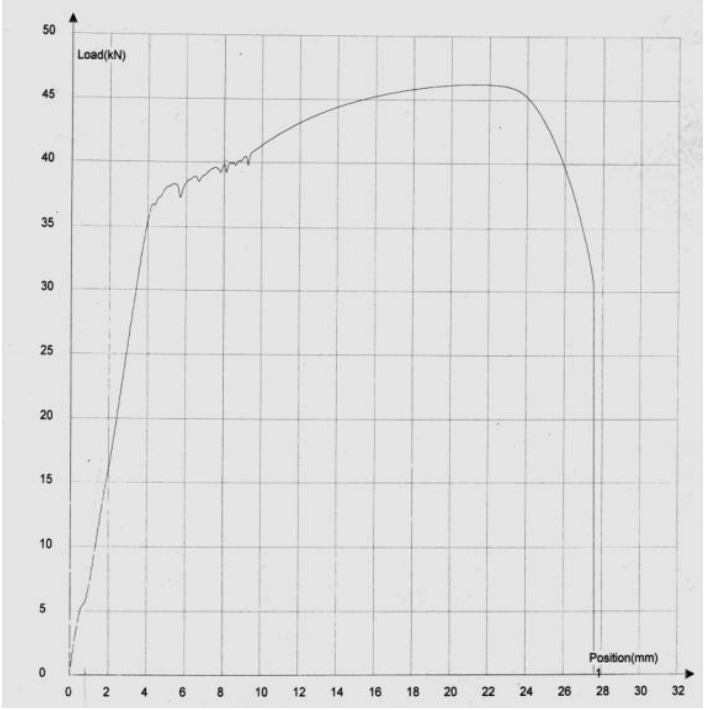

Figure 29 Tensile test curve for the steel sample.

It was observed from Figures 27 and 28 that the two types of reinforcing bars had two different modes of fracture. The fibres are the main carrying component of FRP re-bars; figure 27 shows the longitudinal rupture of fibres without developing a plastic hinge which is important for redistribution of moment in the reinforced concrete member and for compression in the reinforced concrete columns.

As the modulus of elasticity is the tangent of the curve of stress-strain, it appeared from Figures 26 and 29 that there is a big difference of the angle and this explains the difference in values. This implies that large stress was developed for a small strain in the steel re-bars while the opposite occurred in FRP re-bars. The stress was well redistributed along the area of steel re-bar as shown by the parabola resulting in a plastic hinge rather than by the linear curve for FRP re-bar.

The mean tensile strength of high strength steel bar, obtained from the experiment, was 1.32 times higher than the theoretical tensile strength. This difference is considered to be the safety margin of Steel bars. There is no big gap between the mean modulus of elasticity obtained and the theoretical modulus of elasticity (6.55 percent deviation only).

5.3.3 Comparison between Steel and FRP Re-bars

Results of the mechanical properties of the three types of reinforcing bars, namely Steel, GFRP and CFRP re-bars that were used in this study are presented in Table 18.

Table 18 Mechanical properties of the GFRP, CFRP and steel reinforcing bars.

Type of rebar	Ultimate Tensile Strength (MPa)	Modulus of Elasticity (GPa)	Ultimate Tensile Strain (%)
GFRP	558.40	28.35	1.97
CFRP	866.80	76.04	1.54
STEEL	593.60	213.09	0.28

CFRP had the highest tensile strength compared to the other re-bars. Its value was 273.20 MPa or 46.02 percent higher than that of steel while the steel value was 308.40 MPa or 6.30 percent higher than that of GFRP's. Steel had the highest

modulus of elasticity while GFRP had the lowest value. Although the FRP re-bars had lower value of modulus of elasticity than that of steel (they had higher tensile strain than steel re-bars), it can then be concluded that they have good resistance to deformation.

It is clear from the results obtained that the material partial factor, γ_f of 1.5 for FRP re-bars is higher than that of the steel rebar, γ_s of 1.32. Considering the mode of failure of re-bars shown in Figures 27 and 28, the FRP materials are more brittle compared to steel re-bars, and this implies that a higher safety factor than 1.5 need to be considered in the theoretical design process of FRP for internal reinforcement.

5.4 Foundation Specimens

All foundation-base specimens were reinforced with the same number of reinforcement of the same diameter in this research. Twelve samples reinforced with steel re-bars of 10 mm diameter; twelve samples reinforced with Carbon FRP re-bars of 9.97 mm diameter; and twelve samples reinforced with Glass FRP re-bars of 9.94 mm diameter were used.

The main reason for using the same size of reinforcement, in the three types of Reinforced Concretes bases, was to obtain a reasonable comparison as the diameter of reinforcing rebar has an influence on the anchorage in the Reinforced Concrete and on the behaviour of FRP Reinforced Concrete. This is because the ultimate tensile strength of FRP re-bars decreases with diseasing bar diameter. Besides, the mechanical properties of FRP materials differ from one diameter to another (as shown in technical sheets from manufacturers of FRP, Table 15) unlike the steel re-bars.

The above resulting properties of concrete and FRP re-bars were used to determine the moments as well as modes of failure.

5.4.1 Determination of Mode of Failure of FRP Reinforced Concrete

a) Physical Properties and Parameters

Precautions were taken to ensure that a cover for 50 mm was same for all reinforcing re-bars and the dimensions of foundation specimen were as required. These precautions were essential so as to meet the specifications of the specimen.

The depth of reinforcement was determined as shown by equation 59.

$$y = h - c - \frac{1}{2} d_b \ \text{[mm]} \quad (59)$$

where y is the depth of reinforcement; h is the depth of sample; c is the cover to reinforcement and d_b is the nominal diameter.

Therefore, depth of CFRP was:

$y = 150 - 50 - \frac{1}{2}(9.97)$

$y = 95.02$ mm

And the depth of GFRP was:

$y = 150 - 50 - \frac{1}{2}(9.94)$

$y = 95.03$ mm

The value of parameter β_1 was as 0.85 since f_c' was 21.99 MPa (Equation 51) and being less than 30 MPa as discussed in section 4.3.a.

$$\beta_1 = 0.85 \quad (60)$$

In Table 19, physical properties and longitudinal tensile properties of FRP extracted from Tables 13 and 16, depth of reinforcement and parameter, β_1, are presented.

Table 19 Physical properties and parameters for FRP re-bars

Items	Diameter obtained ø (mm)	Area of rebar A_f (mm^2)	Area of reinforcement (mm^2)	Depth of reinforcement y (mm) obtained from Equation 59	Modulus of Elasticity E_f (GPa) from Table 16	Ultimate Tensile strength f_{fu} (MPa) from Table 16	β_1 obtained in Equation 60
GFRP	9.94	77.50	77.5(2) = 155	95.02	42.53	837.60	0.85
CFRP	9.97	78.00	78.0(2) = 156	95.03	114.06	1,300.20	0.85

In chapter four of this study, some assumptions were made. The ultimate strain in concrete was assumed to be 0.0035. In this section, the ultimate strain in concrete is the theoretical value and it will be compared with the experimental value later in this chapter. The physical properties and parameters for concrete are presented in Table 20 below.

Table 20 Physical properties and parameters for concrete

Material	Breadth b (mm)	Ultimate strain ε_{cu} (SABS 0100-1, 2000:13)	Compressive strength f_c' (MPa) obtained in Equation 51 on page 65
CONCRETE	500	0.0035	21.99

The parameters shown in Tables 19 and 20, were used to determine the mode of failure of FRP reinforced concrete as discussed in section (b) below.

b) Comparison of the Modes of Failure

The mode of failure was determined by comparing the FRP reinforcement ratio, ρ_f, to the balanced reinforcement ratio, ρ_{fb}. The results of modes of failure and the balanced reinforcement ratios, calculated using equations 36 and 37 discussed in section 4.4.1, are presented in Table 21.

Table 21 Determination of modes of failure

Items	Parameters	Calculations	Results (%)
GFRP	ρ_f from equation 35	$\frac{155}{500(95{,}02)}$	0.3263
	ρ_{fb} from equation 36	$(0{,}85)(0{,}85)\left[\frac{21.99(10^6)}{837.60(10^6)}\right]\left\{\frac{[42.53(10^9)](0.0035)}{[[42.53(10^9)](0.0035)]+837.60(10^6)}\right\}$	0.2867
CFRP	ρ_f	$\frac{156}{500(95{,}03)}$	0.3283
	ρ_{fb}	$(0{,}85)(0{,}60)\left[\frac{21.99(10^6)}{1{,}300.20(10^6)}\right]\left\{\frac{[114.06(10^9)](0.0035)}{[[114.06(10^9)](0.0035)+1{,}300.20(10^6)]}\right\}$	0.2868

The results from these calculations show that ρ_f is greater than ρ_{fb} for FRP re-bars. Hence concrete crushing governs the failure mode for the FRP reinforced concrete bases. These results further show that strain in the compressive zone of concrete reached the ultimate value while strain in the FRP re-bars was still below the ultimate value. Thus, the FRP reinforced concretes sections were considered to be over-reinforced. Therefore, the FRP reinforced concrete foundations presented some pseudo-plastic behaviour and their failure would not be sudden.

This agrees with the results of Nanni and Faza (2002:4) who pointed out that concrete crushing failure mode is marginally more desirable for flexural members reinforced with FRP re-bars since the member does exhibit some pseudo-plastic behaviour before failure.

5.4.2 Design Consideration

In this section, the calculated fracture failure strain ε_f in FRP re-bars and the corresponding ultimate moments, when the concrete crushes, are reported. Detailed calculations are presented in Appendix B.

The soil bearing pressure of the foundation was simulated but no numerical value could be determined for the maximum and minimum soil pressure. In addition, no ultimate value was determined for the imposed load acting on the column as experiment was conducted up to failure for all the specimens (i.e. a destructive test). Therefore, the ultimate moment for steel reinforced concrete bases could not be calculated.

a) Calculated Strains in FRP Re-bars.

The failure strains in the FRP re-bars at the moment when the concrete crushes are 1.269 percent and 2.188 percent for the CFRP and GFRP respectively. The strain in GFRP was 72.42 percent higher than the strain in CFRP re-bars. Comparison between the ultimate tensile strains of both composite materials extracted from Table 14 and the strains calculated are presented in Table 22.

Table 22 Comparison of GFRP and CFRP re-bars of strain values

Material	Strain in %	
	Strain extracted from Table 14	Strain calculated
GFRP rebar	Ultimate strains 1.97	2.188
CFRP rebar	Ultimate strains 1.54	1.269

It was evident that the calculated ε_{fCFRP} strain was lower by 17.60 percent compared that from Table 14 and the calculated ε_{fGFRP} 11.07 percent higher than ε_{fGFRP} shown in the Table 22. The strain in CFRP re-bars did not exceed the ultimate strain, but the strain in GFRP re-bars did exceed the ultimate strain. Therefore, the mode of failure in CFRP reinforced concrete foundation – base was governed by concrete crushing. However, the mode of failure in GFRP reinforced concrete foundation – bases as described in Section 5.4.1.b, were contradicted by the results obtained above. That is the GFRP reinforced concrete foundation – base failure should have been governed by FRP failure and not concrete crushing.

In the case of GFRP reinforced concrete bases, the approach currently adopted is to accept that FRP reinforced concrete sections is over-reinforced (to prevent sudden rupture of reinforcement) and that the ultimate failure was by concrete crushing rather than by the reinforcement failure as the latter does not show some pseudo-ductility. This observation concurs with that observed by Pilakoutas et al (2007:32). A section of FRP reinforced concrete is considered to be over-reinforced when the reinforcement ratio, ρ_f remains above 0.5 percent as shown in Figure 30. Results presented in Table 22, indicate that GFRP and CFRP re-bars had a reinforcement ratio of 0.326 and 0.328, respectively being below the 0.5 percent threshold.

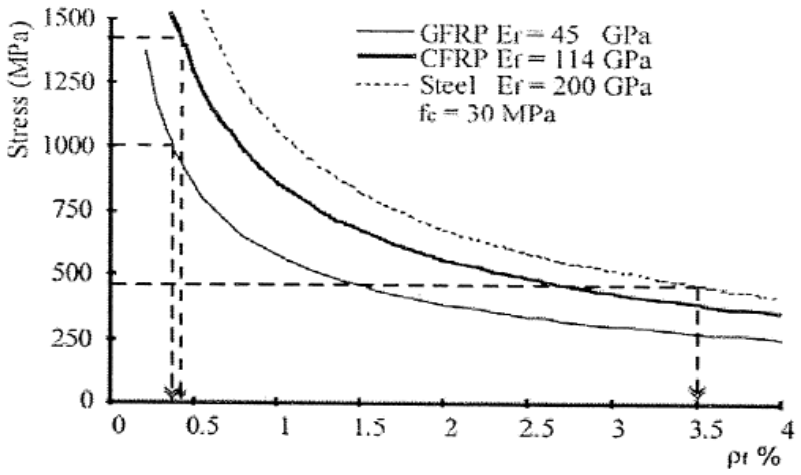

Figure 30 Stress in reinforcement at concrete failure versus percentage amount of reinforcement (Pilakoutas et al., 2007:32).

The ultimate strain in CFRP rebar contradicted the hypothesis of under-reinforced section. Therefore, Concrete crushing failure was considered as the mode of failure for GFRP reinforced concrete bases.

As the mode of failure was governed by concrete crushing, it was preferable in the stress distribution of reinforced concrete to consider the stress block similar to the rectangular stress block.

b) Calculated ultimate moments of Fibre Reinforced Polymer reinforced concrete foundation – bases

The ultimate moments M_u of CFRP and GFRP reinforced concrete foundation – bases were 30.193 kNm and 30.187 kNm, respectively as shown in Appendix B. These calculated moments are compared to those obtained from the experimental results later in the chapter.

5.5 Presentation and Discussion of Tests Results for the Foundation Bases

5.5.1 Strain Behaviour

Typical data recording of strain readings are shown in Figure 31, where the X – axis represents the time in seconds and the Y – axis represents the variation of output voltage in Volts. More data recording are shown in Appendix C. Five colours were used to represent the five channels: red and blue for strain in reinforcement; and green, orange and violet for the strain gauges on concrete. In Figure 31 (a) and (b), only two colours were represented i.e. red for strain in reinforcement and green for strain gauges on concrete. In Figure 31 (c), four colours namely red for reinforcement and green, orange and violet for concrete were shown.

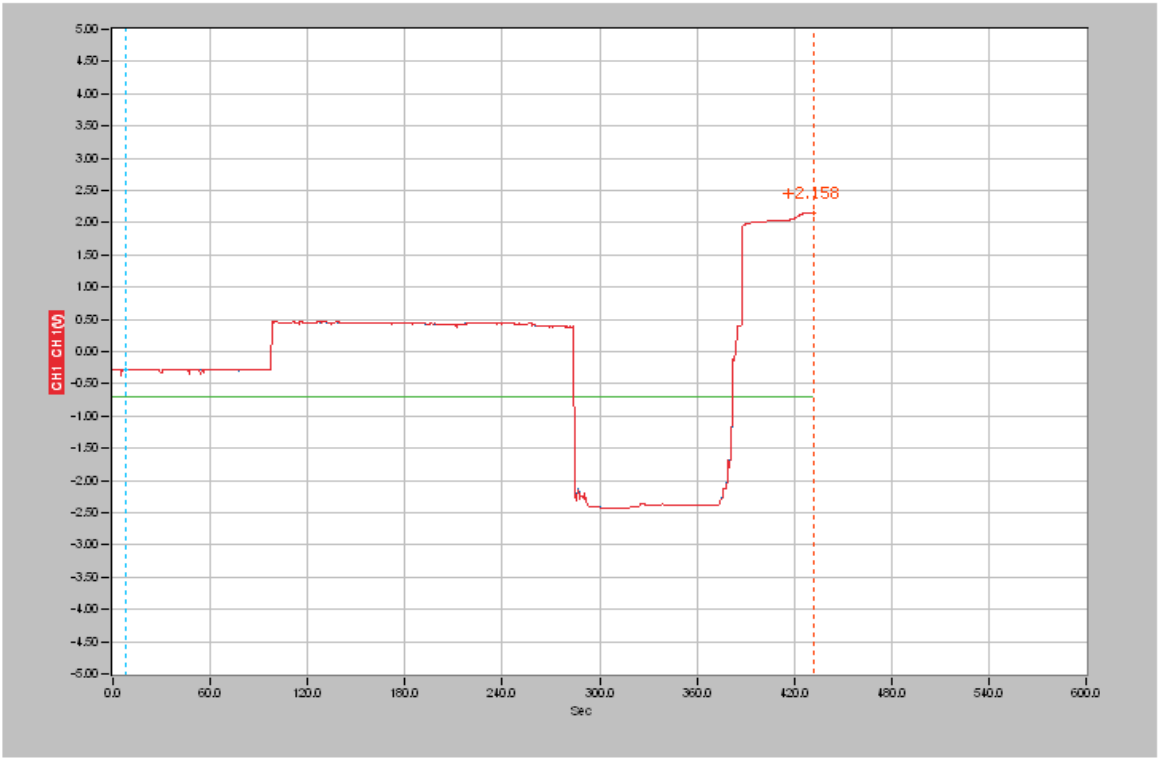

Figure 31(a) Steel reinforcement

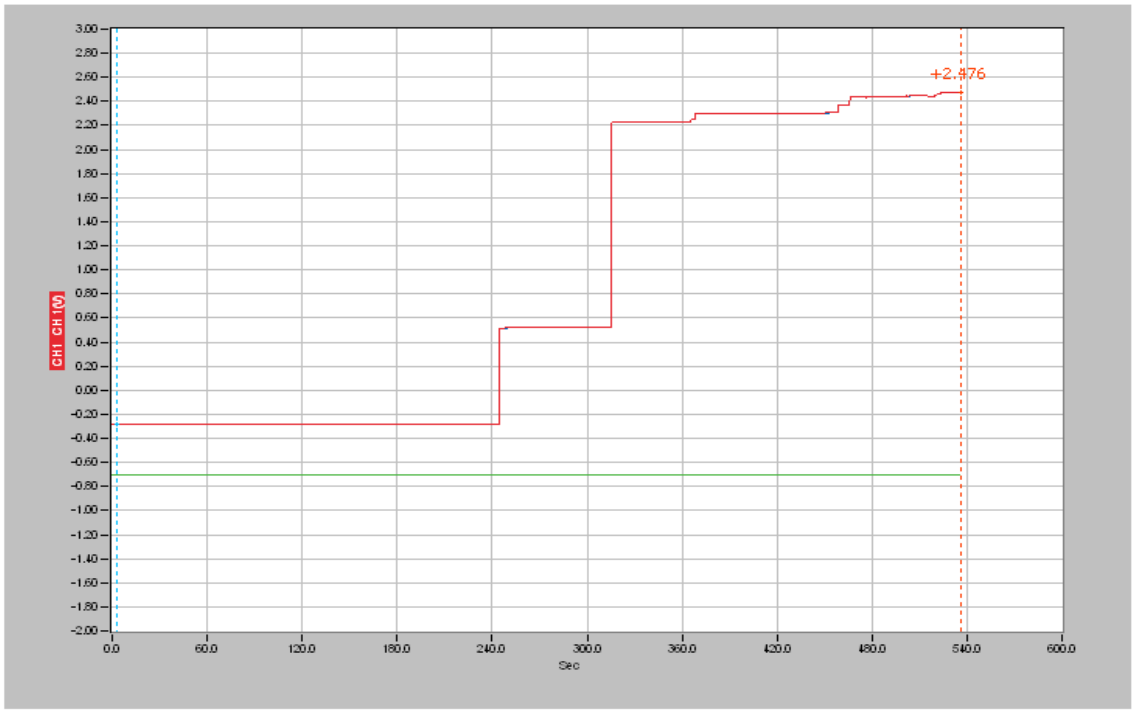

Figure 31(b) CFRP reinforcement

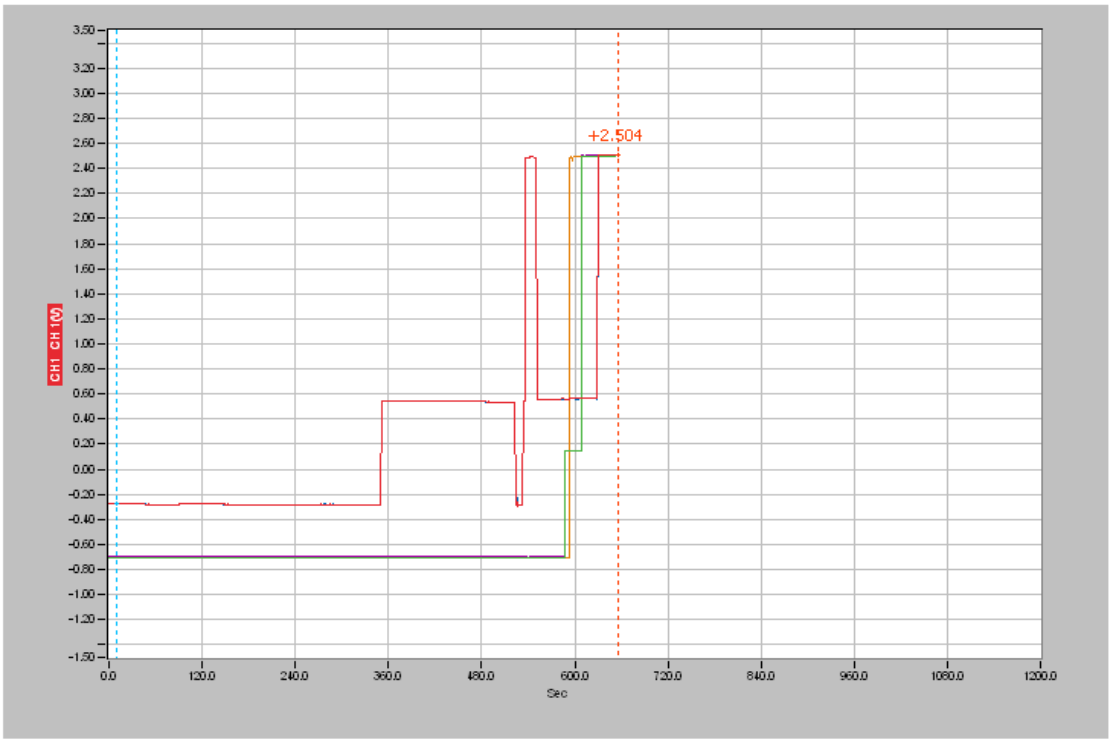

Figure 31(c) GFRP reinforcement

Figure 31 Strain curves recorded at 28 days test.

In Figure 31, the blue and red colours had the same variation of voltage. They responded to tension in the same manner. In cases where one gauge was placed to measure compressive strains and other tensile strains; variation of voltage output was expected to be totally different in both gauges as they would measure opposite displacements.

A small variation of voltage in steel was likely to be recorded as opposed to FRP; therefore, strain gauges on steel re-bars were more sensitive to variation of voltage than the strain gauges on FRP re-bars. This behaviour indicated that FRP re-bars had good electrical resistance compared to steel re-bars. It can be concluded that FRP reinforced concrete provided a better electrical insulation than steel reinforced concrete. Steel strain failure values were lower than those observed on the FRP re-bars. This can be attributed to the lack of anchorage as the FRP re-bars were more curved than the steel ones as tensile stress increased in the fibres.

As seen from Figure 31, values recorded by the strain gauges on concrete were constant except where strain gauges ruptured by cracking in the concrete. According to the polarity of strain and the sign convention discussed earlier, positive values were recorded on concrete instead of negative ones. This was due to tensile forces on the gauges due to cracks. When reinforced concrete is stressed small cracks are not visible in some cases. The results have shown that the re-bars are already under high stress when cracks are more visible and this situation serves as warning of possible failure.

Figure 31 (b) shows a positive variation of strain in the CFRP re-bars up to failure, but in the case of steel and GFRP re-bars, strains increased and decreased during the experiment and ended with higher values compared to the initial ones. This behaviour indicated that the CFRP was in tension from the beginning to the end of experiment while the steel and GFRP re-bars experienced some compression; this behaviour is due to the higher tensile strength of CFRP re-bars.

According to the sign convention adopted earlier, the strain gauges on reinforcing bars in Figures 31 (a) and (c), displayed an alternating behaviour between tension and compression. This behaviour is explained by the temporary loss of bond between

the two materials namely (concrete and reinforcing bar). Strain values recorded in volt on the reinforcement and on the concrete are presented in Tables 23 and 24.

Table 23 Strain values recorded on reinforcing bars

MATERIALS	STRAIN IN VOLT (+) Tension and (-) Compression															
	7 DAYS				14 DAYS				21 DAYS				28 DAYS			
	1st	2nd	3rd	Aver.	1st	2nd	3rd	Aver.	1st	2nd	3rd	Aver.	1st	2nd	3rd	Aver.
GFRP	2.627	2.777	2.702	2.702	2.769	2.778	2.788	2.778	2.658	2.778	2.898	2.778	2.783	2.779	2.775	2.779
CFRP	2.313	1.836	2.790	2.313	2.627	2.777	1.576	2.327	2.758	2.724	2.792	2.758	2.785	2.756	2.757	2.766
STEEL	2.328	2.163	2.793	2.428	2.768	2.781	2.754	2.768	2.771	2.793	2.782	2.782	2.932	2.783	2.634	2.783

Table 24 Strain values recorded on concrete

MATERIALS	STRAIN IN VOLT (+) Tension and (-) Compression															
	7 DAYS				14 DAYS				21 DAYS				28 DAYS			
	1st	2nd	3rd	Aver.	1st	2nd	3rd	Aver.	1st	2nd	3rd	Aver.	1st	2nd	3rd	Aver.
GFRP R.C.	-0.001	-0.001	-0.001	-0.001	-0.001	-0.946	-0.001	-0.316	-0.001	-0.002	-0.001	-0.001	-0.000	-0.000	-0.000	-0.000
CFRP R.C.	-0.001	-0.001	-0.002	-0.001	-0.001	-0.000	-3.203	-1.068	-3.205	-0.001	-0.000	-1.069	-1.767	-3.203	-0.845	-1.938
STEEL R.C.	-0.003	-0.003	-0.003	-0.003	-0.001	-0.006	-0.844	-0.284	-0.002	-0.001	-0.001	-0.001	-0.001	-0.002	-0.001	-0.001

The average strain in volts presented in Table 24 is summarized in Table 25 below.

Table 25 Average strain values on the concrete

MATERIALS	STRAIN IN VOLT (e_o: output voltage) (+) Tension and (-) Compression			
	7 DAYS	14 DAYS	21 DAYS	28 DAYS
GFRP Reinforced Concrete (R.C.)	-0.001	-1.068	-1.069	-1.938
CFRP Reinforced Concrete (R.C.)	-0.001	-0.316	-0.001	-0.000
STEEL Reinforced Concrete (R.C.)	-0.003	-0.284	-0.001	-0.001

It is observed from the values in Table 25 that the strains on the reinforced concrete are significantly small in magnitude. The higher variation in magnitude of strain values on concrete corresponds to the rupture of strain gauges due to cracks passing through. Results for strains recorded on concrete and on reinforcing bars at different ages are presented in Table 26.

Table 26 Strain values on reinforcement and on the concrete at different ages

MATERIALS	STRAIN IN VOLT (e_o: output voltage) (+) Tension and (-) Compression			
	7 DAYS	14 DAYS	21 DAYS	28 DAYS
GFRP	2.702	2.778	2.778	2.779
CFRP	2.313	2.327	2.758	2.766
STEEL	2.428	2.768	2.782	2.783
CONCRETE	-0.002	-0.556	-0.357	-0.646

The strain values in Table 26 are expressed as output voltage (mV/V or μV/V) against the bridge voltage. In many publications, the output of strain-gauge bridge is expressed as a strain quantity ($\mu\varepsilon$) as opposed to output voltage (mV/V or μV/V). The strain quantity and the output voltage have the following relation (Kyowa, 2005:6):

$$e_0 = \frac{E}{4} K_s \varepsilon_{0S} \quad (61)$$

where $e_o$is the Output voltage; E is the Bridge voltage; K_s is the Gauge factor; ε_{OS} is the ouput strain.

Assume that the voltage E in the bridge is equals to 1 voltage and the gauge strain factor K_s equals to 2.00, then ε_{OS} is equals to 2 e_0 (Kyowa, 2005:6). Thus, a strain output is always two times larger than a bridge output voltage.

A full bridge has:

1 mV/V = 2000$\mu\varepsilon$. (62)

Equation 61 can be expressed as follows:

$$\varepsilon_{OS} = \frac{4e_o}{E(K_S)} \quad (63)$$

The bridge voltage E considered in this study was up to 5 V and the gauge factor K_s equal to 2.10 (Kyowa, 2005:1). Thus Table 27 results are obtained by applying Equation 63 to Table 26 results.

Table 27 Strain values computed from output voltage ($\mu\varepsilon$)

Materials	**Parameters**	**Days of Tests (+) Tension and (-) Compression**			
		7	**14**	**21**	**28**
GFRP	e_0 (mV)	2.702	2.778	2.778	2.779
	ε_0 ($\mu\varepsilon$)	1,029.33	1,058.29	1,058.29	1,058.67
CFRP	e_0 (mV)	2.313	2.327	2.758	2.766
	ε_0 ($\mu\varepsilon$)	881.14	886.48	1,050.67	1,053.71
STEEL	e_0 (mV)	2.428	2.768	2.782	2.783
	ε_0 ($\mu\varepsilon$)	924.95	1,054.48	1,059.81	1,060.19
CONCRETE	e_0 (mV)	-2.0(10^{-3})	-5.56(10^{-1})	-3.57(10^{-1})	-6.46(10^{-1})
	ε_0 ($\mu\varepsilon$)	-7.619(10^{-1})	-211.81	-136.00	-246.10

Figure 32 presents the strain values plotted from Table 27.

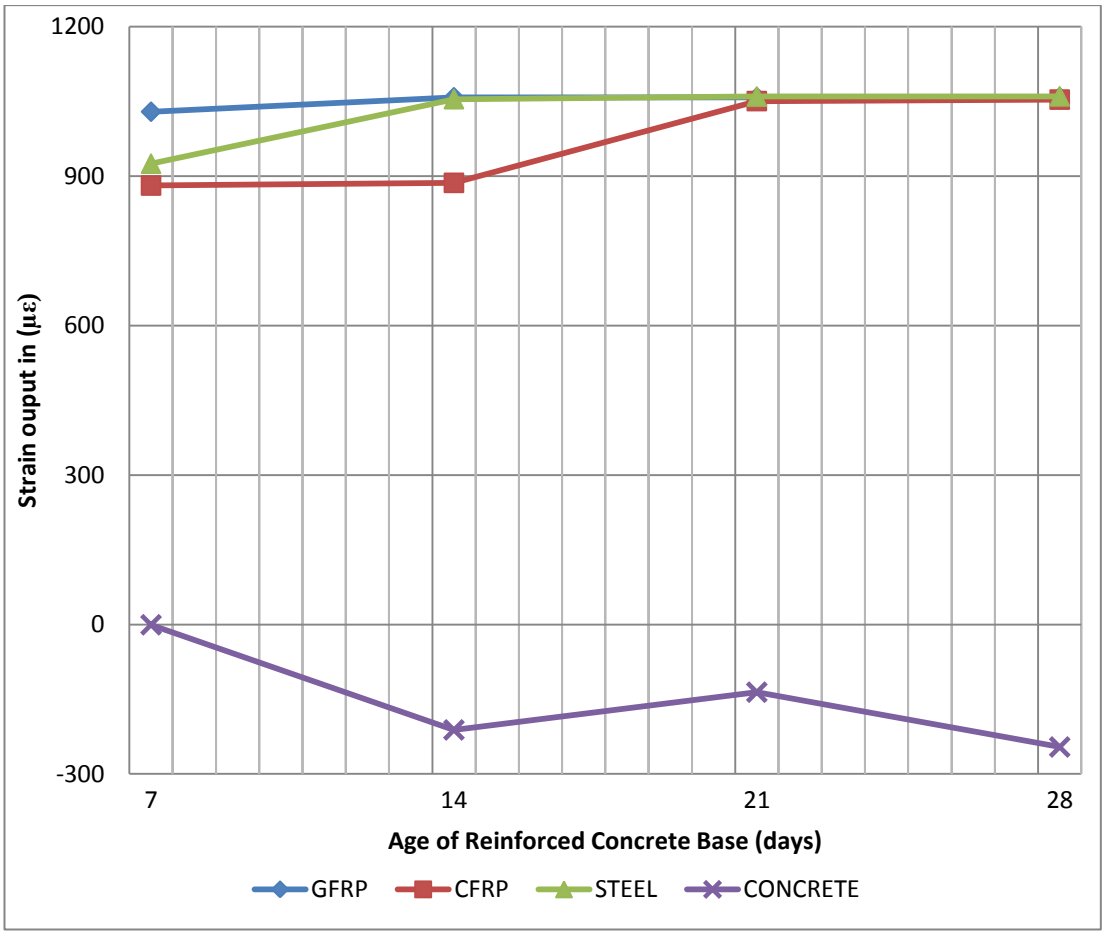

Figure 32 Strain curves: Output voltage

It is observed that the strain values at the 7th day for CFRP re-bars had the lowest magnitude in all the three bars. The CFRP was 4.74 percent lower than the steel re-bars and 14.40 percent lower than the GFRP re-bars.

Between 14 days and 21 days, the strain in CFRP increased significantly compared to those of other reinforcing bars. But all reinforcing bars had an output voltage close to each other on the 28th day. Furthermore, from Figure 32, the GFRP and steel strain curves seemed to remain constant from the seventh day and fourteenth day respectively compared to the rest. This implied that the variations of strain in GFRP and steel decreased. The strain output was converted to strain (in percentage) using Equation 64 and strain values from Table 27 are summarized in Table 28.

$$\varepsilon_{OS} = 1{,}029.33\mu\varepsilon$$

$$\varepsilon_{OS} = 1.029\varepsilon \text{ or } \varepsilon_{OS} = 1.029\% \quad (64)$$

Table 28 Strain values in percentage form

MATERIALS	STRAIN (%) (+) Tension and (-) Compression			
	7 DAYS	**14 DAYS**	**21 DAYS**	**28 DAYS**
GFRP	1.029	1.058	1.058	1.059
CFRP	0.881	0.887	1.051	1.054
STEEL	0.925	1.055	1.060	1.060
CONCRETE	-7.62(10^{-4})	-0.212	-0.136	-0.246

From literature review and assumptions made in standard codes for design SABS 0100-1(2000:13) or BS 8110 (2001:6), the theoretical ultimate strain in the concrete is considered to be equal to 3.5 x 10^{-3}. The results obtained in Table 28 are higher than the assumed values (59.57 percent at 14 days; 37.86 percent at 21 days and 69.29 percent at 28 days). The 7 day value for concrete is 78.23 percent lower than theoretical value as seen in Figure 33 and it can be concluded that the ultimate strain was not exceeded then. However, failure of the samples was governed by concrete crushing and not yielding of reinforcement as the re-bars were not fractured.

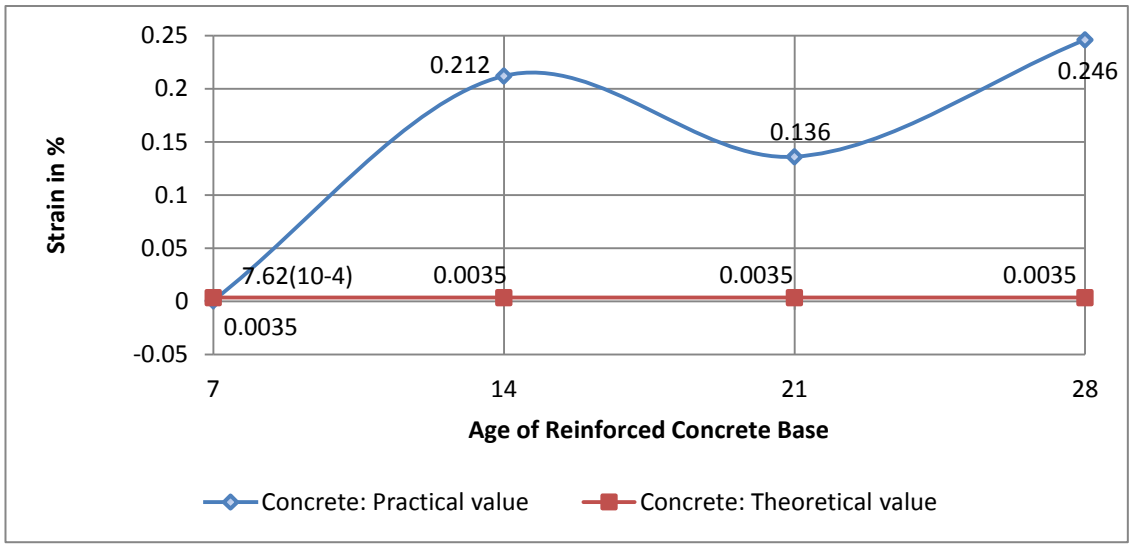

Figure 33 Comparison between practical and theoretical values of strain on concrete.

Plates of failure of reinforced concrete bases at 7 days (Figure 34) contradict the latter statement as cracks were developed from the bottom up to the top of the specimens and correspond to concrete failure type. This phenomenon is also seen from behaviours of strain curves in Figure 31, where strains gauges not damaged by the cracks did not record a larger variation of voltage than those destroyed.

Figure 34 Foundation – base failure.

MacGregor and Wight (2006:64) pointed out that failure for a simply supported reinforced concrete beam subjected to flexural behaviour occurs when further deformations occur at decreasing loads. During the experiment, failure of samples of reinforced concrete occurred when loads decreased. Strictly speaking, there is no such a thing as limiting concrete compressive strain in practice. However, concrete compressive strain is limited to the theoretical value of 0.0035 for design purpose.

The values in Table 28 are plotted in Figure 35. Three observations are made from this figure. The first observation is that the strains in the CFRP and GFRP reinforcement did not exceed the ultimate strain presented in Table 29, while strain in the steel reinforcement exceeded the ultimate strain from the tensile strength test.

Table 29 Comparison of strain values of reinforcing bars.

Material	Strain in %					
	Strain obtained from the tensile strength test (Table 18)	Strain calculated in section 5.4.2(a) (Table 22)	Strain extracted from Table 28			
			7 Days	14 Days	21 Days	28 Days
GFRP rebar	1.97	2.188	1.029	1.058	1.058	1.059
CFRP rebar	1.54	1.269	0.881	0.887	1.051	1.054
STEEL rebar	0.28	-	0.925	1.055	1.060	1.060

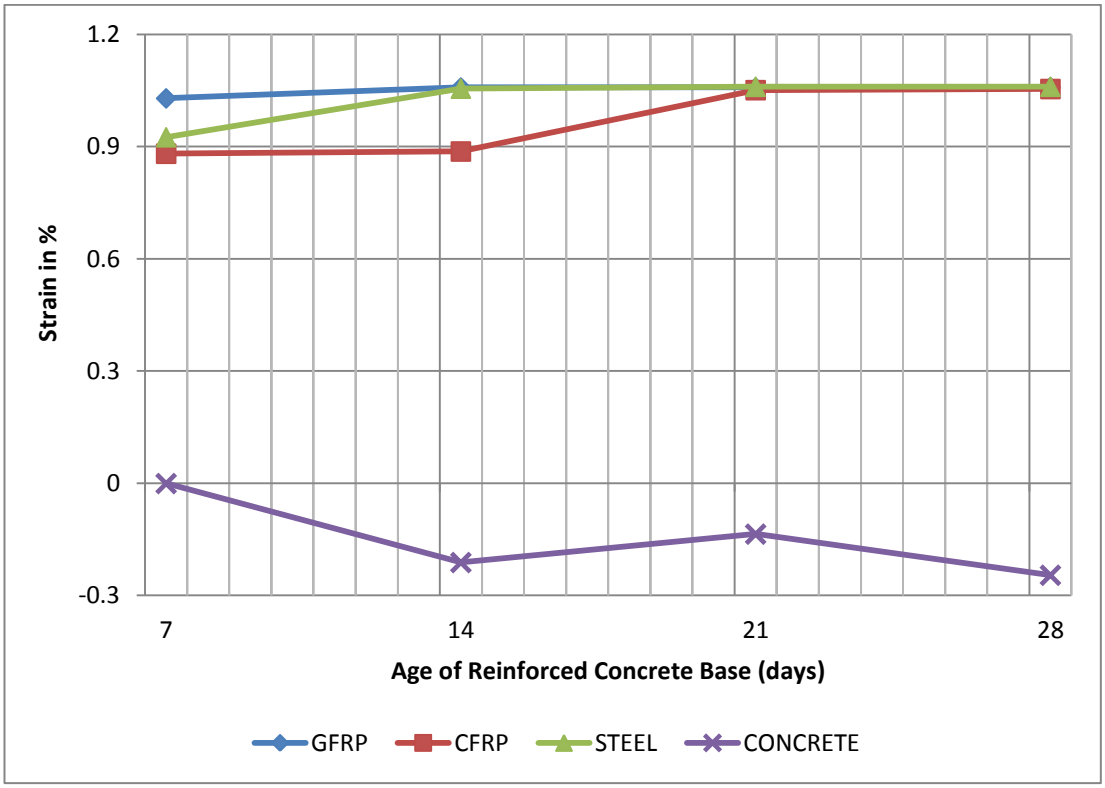

Figure 35 Strain age curves expressed as percentage.

These results confirm that the mode of failure in CFRP reinforced concrete foundation is governed by concrete crushing. Regarding the GFRP reinforced concrete foundation – bases, results show that concrete crushing was the mode of failure and contradict the findings in Section 5.4.2(b) of FRP rupture. This result showed that foundation reinforced with GFRP re-bars had the same behaviour as the CFRP reinforced concrete foundation – bases despite the fact that the reinforcement ratio was less than 0.5 percent.

The strains in FRP reinforcing bars at 28 days from Table 29, were found to be 51.60 and 16.94 percent lower compared to strains calculated in section 5.4.2 (a), respectively. It appears that the strains calculated were overestimated and this was attributed to the fact that soil pressure was not considered in the calculation of strain in the reinforcement. Therefore, soil pressure is a critical parameter in the design of foundation as this would modify the behaviour of the reinforced concrete base.

The second observation is that CFRP displayed the lowest strain of the three types of reinforcement. However, after two weeks CFRP attained the same strain as the other two. Considering the progression of the three curves with age of reinforced concrete as third observation, the strain in the GFRP started at higher level and remained constant earlier than strains in Steel and CFRP.

The fourth observation is based on the behaviour of steel bar. When strain value progressed to the ultimate value, the steel became plastic. As strain in steel re-bars exceeded the ultimate limit and no rupture of steel re-bars was observed, it is clear that the steel deformed plastically up to the point where concrete crushing took place.

Comparing the strains of steel bars obtained at each age of reinforced concrete base to the ultimate strain obtained from the tensile strength test (see Table 29); it is clear that the experimental results deviated from the theoretical values by 69.73 percent at 7 days, 73.46 percent at 14 days, 73.59 percent at 21 days and 28 days. However, Steel bars did not present a sudden rupture as the ultimate strain of steel was exceeded already from the 7^{th} day as the strain continued to increase considering the three others test days. It can be concluded that steel bars exhibited a plastic behaviour up to the failure. The steel reinforced concrete displayed a tensile failure and a ductile moment-curvature response; this type of failure is known as tension controlled sections where steel yields before the crushing of concrete. Consequently, widening cracks appeared on concrete giving warning before structure collapsed.

In a situation where the ultimate strain in FRP re-bars is reached, the mode of failure in FRP reinforced concrete would be FRP rupture. This would result in a sudden rupture of reinforced concrete. This implied that FRP re-bars are not ductile and hence have no plastic elongation.

5.5.2 Loads Capacity Results

Investigation was conducted on the structural performance of three types of reinforced concrete foundation – bases. All specimens were tested up to failure and the ultimate loads applied on the reinforced concrete were recorded as shown in Tables 30 and 31 and plotted in Figure 36.

Table 30 Ultimate loads obtained from experiments

MATERIALS	ULTIMATE LOADS (kN)															
	7 DAYS				14 DAYS				21 DAYS				28 DAYS			
	1st	2nd	3rd	Aver.	1st	2nd	3rd	Aver.	1st	2nd	3rd	Aver.	1st	2nd	3rd	Aver.
GFRP R.C.	321.0	345.3	333.0	333.2	410.1	330.0	370.0	370.0	425.4	383.8	467.0	425.4	447.0	438.0	426.0	437.0
CFRP R.C.	380.0	360.0	330.0	356.7	389.0	375.6	402.0	388.8	430.0	475.0	385.0	430.0	428.7	440.2	451.7	440.2
STEEL R.C.	345.0	350.0	325.0	340.0	397.0	391.8	402.4	397.1	435.8	449.0	470.0	451.6	439.3	458.6	477.9	458.6

Table 31 Average ultimate loads obtained from experiments

MATERIALS	ULTIMATE LOADS (kN)			
	7 DAYS	14 DAYS	21 DAYS	28 DAYS
GFRP R.C.	333.20	370.00	425.40	437.00
CFRP R.C.	356.70	388.80	430.00	440.20
STEEL R.C.	340.00	397.10	451.60	458.60

a) Loads –Age Diagram

The data in Table 31 are plotted on the load-age diagram as shown in Figure 36.

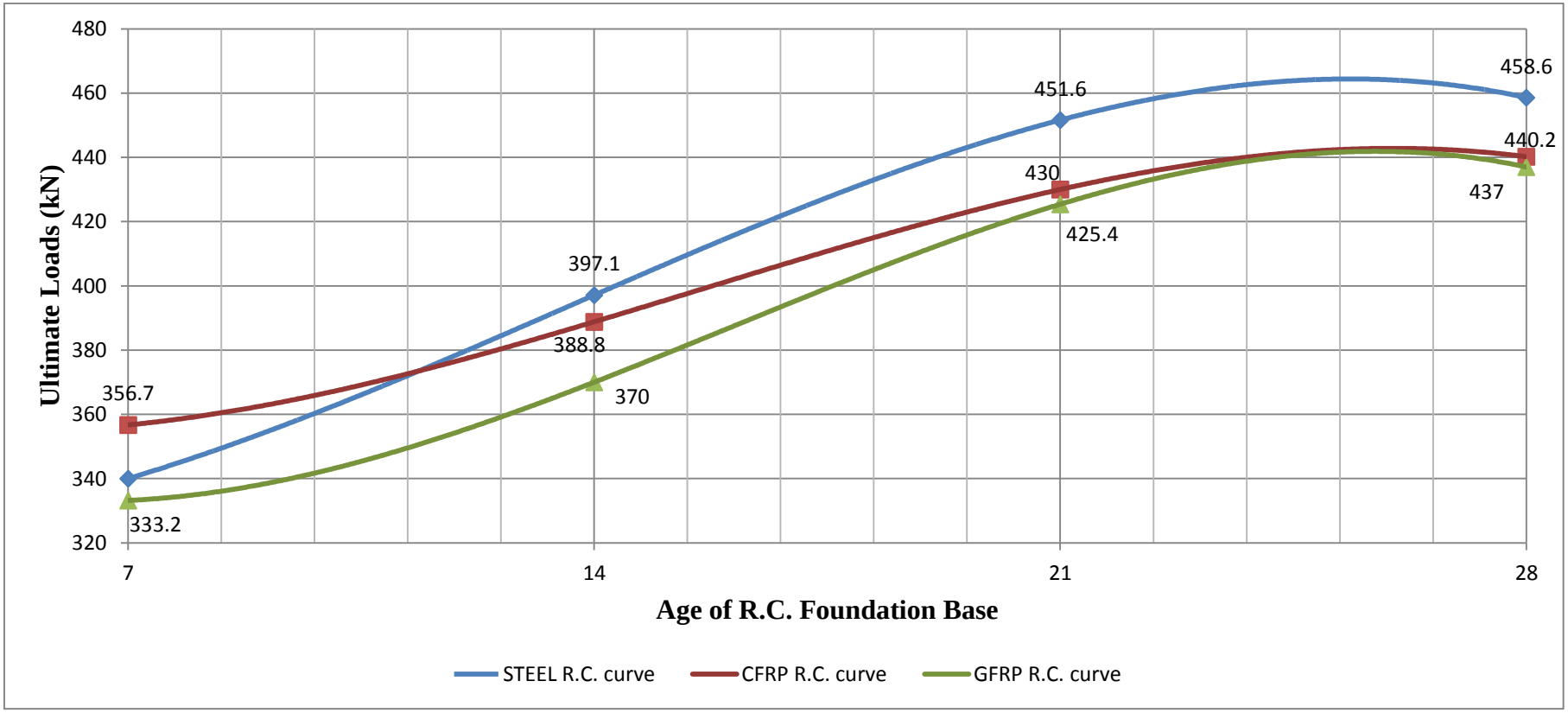

Figure 36 Load – Age diagram

The following three equations are obtained from best fit of load – age curves in Figure 36 for the foundation bases.

For GFRP reinforced concrete foundation – bases:

$$y = -0.0303x_1^3 + 1.4633x_1^2 - 15.071x_1 + 377.4 \quad (65)$$

For CFRP reinforced concrete foundation – bases:

$$y = -0.0195x_1^3 + 0.9112x_1^2 - 7.8667x_1 + 373.8 \quad (66)$$

For steel reinforced concrete foundation – bases:

$$y = -0.0218x_1^3 + 0.8898x_1^2 - 3.0452x_1 + 325.2 \quad (67)$$

where y is the ultimate loads [kN] while x_1 [days] is the age of reinforced concrete bases.

It is observed from Figure 36 that Steel Reinforced Concretes bases had the largest load carrying capacity of 4.18 and 4.94 percent higher than the CFRP and GFRP reinforced concrete bases, respectively at 28 days. At higher strain values, GFRP reinforced concrete had a close load carrying capacity to CFRP reinforced concrete (about 2 percent and 6.59 percent) compared to Steel at 7 days. Due to the higher modulus of elasticity, CFRP performed better.

Steel reinforced concrete bases when compared to CFRP reinforced concrete bases, exhibited lower load carrying capacity at 7 days and a higher carrying capacity at 28 days. This phenomenon can be explained by the bonding strength between concrete and the reinforcements. The effect of bond was to increase the transfer of stress between concrete and the reinforcements.

Figure 37 shows that FRP re-bars slid in the concrete. This can be attributed to the lack of anchorage in FRP reinforced concrete foundation – bases. However, enough anchorage in steel reinforced concrete foundation – bases is attributed to steel bend. This situation was observed on all FRP reinforced concretes bases except those tested at 7 days. This is attributed to the fact that concrete at 7 days did not have enough strength to resist compression.

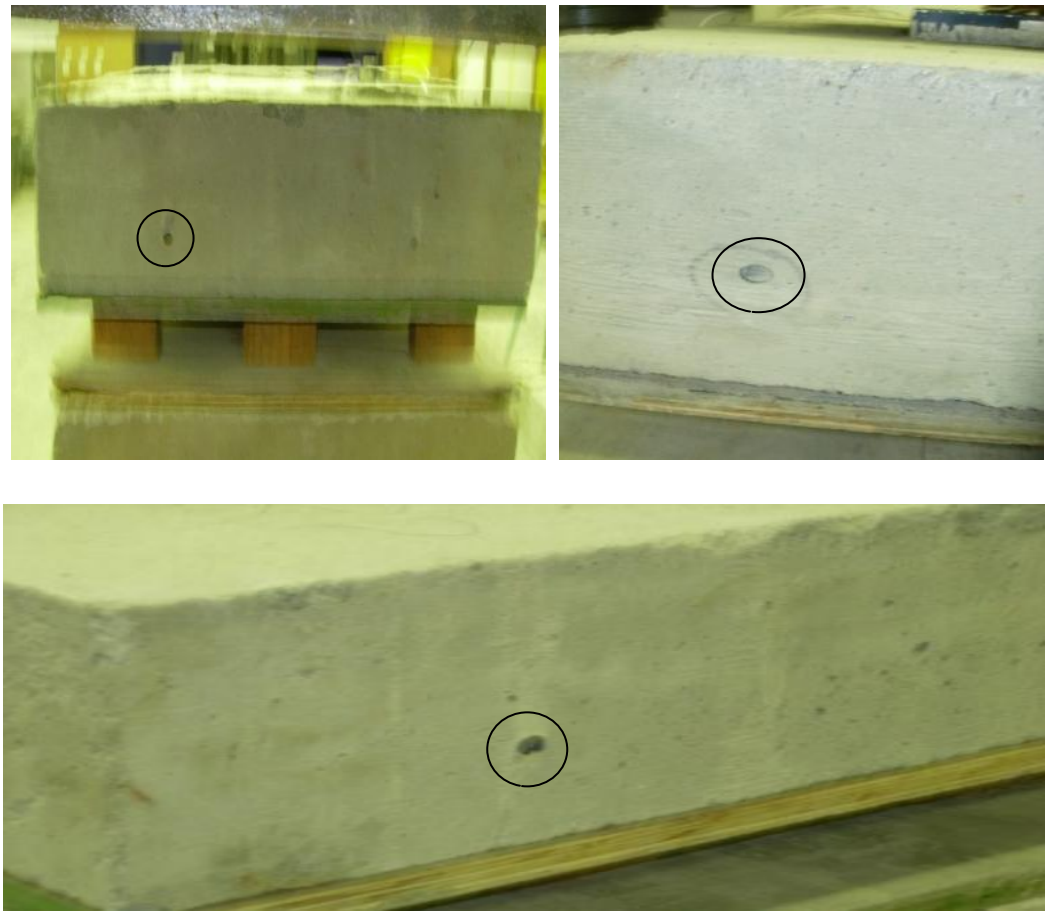

Figure 37 FRP bond

b) Stress – Strain Diagram

The samples of reinforced concrete bases tested in this study were composite system loaded in a flexural manner; hence the equation used to convert the ultimate loads to obtain the stress values in the reinforcing bars was derived from the basic principal of theory of stresses in composite beams (Megson, 2005:305).

Megson (2005:305) studied the case of steel reinforced concrete beam subdued to a flexural deformation and the corresponding stress in each reinforcing bar was found to be obey the following relationship:

$$\sigma_x = \frac{mM}{I_c}(d - x) \qquad (68)$$

Where m is the modular ratio; d is the effective depth of the beam, denoted by d_1; x is the depth of neutral axis, denoted by n; M is the bending moment calculated using

Equation 47 (page 52); I_c is the second moment of area of concrete section computed as:

$$I_c = \frac{bx^3}{3} + mA(d-x)^2 \quad (69)$$

Where b is the breadth of reinforced concrete specimen; A is the area of reinforcement, denoted by A_s. The modular ratio is given by Equation 70:

$$m = \frac{E_c}{E_r} \quad (70)$$

where E_c is the modulus of elasticity of concrete and E_r is the modulus of elasticity of reinforcement, denoted by E_s. However, the depth of neutral axis is computed as:

$$x = \frac{mA}{b}\left(\sqrt{1+\frac{2bd}{mA}}-1\right) \quad (71)$$

The depth of reinforcement of FRP re-bars is given in Table 19 (page 76). However, the depth of reinforcement of steel re-bars was:

d = (150 – 50 – $\frac{10}{2}$) = 95.00 mm.

The second moments of area of reinforced concrete foundation - bases calculated from equation 69 are presented in Table 32. Detailed computations are found in appendix B.

Table 32 Values of parameters used in Equation 68.

Items	**Modular Ratio, m, from Equation 70**	**Depth of neutral axis, x, (mm) from Equation 71**	**Depth of reinforcement, d, (mm)**	**Moment of inertia, I_c, (mm^4) from Equation 69 (10^6)**
GFRP R.C.	0.766	6.499	95.02	0.9761
CFRP R.C.	2.054	10.417	95.03	2.482
STEEL R.C.	5.755	16.814	95.00	6.318

The stresses in the reinforcing bars from Equation 68, are presented in Table 33. Detailed calculations are found in appendix B.

Table 33 Stresses in the reinforcing bars as calculated from Equation 68

MATERIALS	STRESS in (MPa) (10^3)			
	7 Days	**14 Days**	**21 Days**	**28 Days**
GFRP	2.845	3.160	3.633	3.732
CFRP	3.070	3.346	3.701	3.789
STEEL	2.977	3.477	3.954	4.016

From Table 33, GFRP had the lowest stress compared with CFRP and steel. At 7 days, the highest strain obtained in GFRP re-bars corresponds to the lowest stress (its value was lower by 7.33 percent and 4.44 percent compared to value of CFRP and Steel re-bars, respectively). After three weeks, GFRP re-bars still had stress 1.50 percent lower compared to CFRP re-bars and 7.07 percent lower compared to steel re-bars. This result showed that GFRP re-bars will have the same stress to CFRP re-bars after 28 days as the strain in CFRP re-bars was the same as that of GFRP re-bars. It is clear that the behaviour of strain in GFRP re-bars is the inverse of stress in CFRP re-bars.

CFRP re-bars behaved differently compared to Steel re-bars. CFRP re-bars had higher stress of 3.12 percent at 7 days and lower stress of 5.65 percent at 28 days. It is obvious that steel re-bars resisted higher stress due to its higher modulus of elasticity.

From these results, it is clear that stresses in re-bars increased with time. This was attributed to the fact that compressive strength of concrete increased significantly with time and it increased the transfer of stress to the reinforcing bars. The stresses and strains data obtained in the reinforcing bars are summarized in Table 34.

Table 34 Stress and Strain data from Tables 28 and 33

MATERIALS	STRESS (MPa) (10^3)				STRAIN (%)			
	7 Days	14 Days	21 Days	28 Days	7 Days	14 Days	21 Days	28 Days
GFRP	2.845	3.160	3.633	3.732	1.029	1.058	1.058	1.059
CFRP	3.070	3.346	3.701	3.789	0.881	0.887	1.051	1.054
STEEL	2.977	3.477	3.954	4.016	0.925	1.055	1.060	1.060

Stress-strain diagrams for reinforcing bars are shown in Figure 38. Two observations are made. First observation from Figure 38 is based on the behaviour of GFRP and steel re-bars. Between the second and third week, stress in GFRP re-bars increased significantly by 14.97 percent without variation of strain for the same period and this behaviour was also similar for steel re-bars were strain was constant between third and fourth week. However, small increase of stress was recorded of 1.57 percent.

Second observation from Figure 38 is made between CFRP and steel re-bars. With difference of 0.001percent of strain between CFRP strain at 28^{th} day and steel strain at 14^{th} day, CFRP re-bars had higher stress of 8.97 percent. However for the same period of 28 days, steel re-bars had 5.99 percent higher stress than CFRP re-bars.

These two observations are attributed to the ability of three re-bars to resist deformation as the variation between strain at 7 and 28 days were 2.92 percent, 19.64 percent and 14.60 percent for GFRP, CFRP and steel re-bars, respectively.

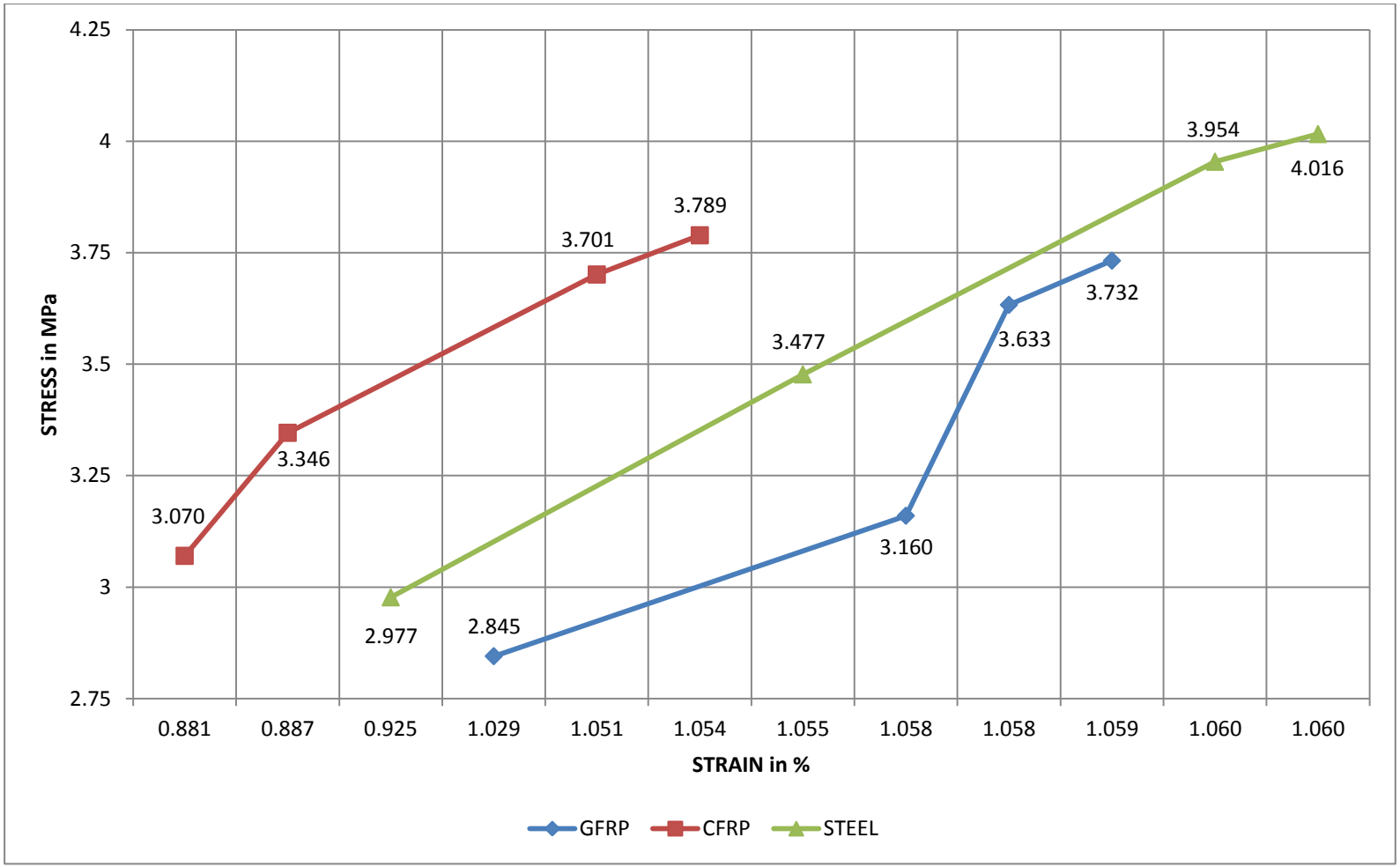

Figure 38 Stress – Strain diagram for reinforcing bars.

5.5.3 Evaluation of Ultimate Moments and Maximum Deflection

In this section, ultimate moments and the deflections of FRP reinforced concretes foundation – bases are compared and discussed. As explained in section 5.4.2, the theoretical ultimate moment of steel reinforced concrete bases were not calculated due to the fact that it was a destructive test experiment. No ultimate value of the imposed load could be given. However, the theoretical ultimate moments for FRP reinforced concrete bases were calculated as the imposed load was not considered in the equation of ultimate moment as shown in Appendix B. The ultimate moments of FRP are shown in Table 35.

Equations 43 and 47 were used to calculate the maximum deflection at the centre of specimen and ultimate moment as shown in Appendix B and reported here.

Table 35 Average ultimate moments computed from Equation 47

Items	Ultimate Moments (kNm)				
	Theoretical ultimate moments	Ultimate moments calculated from Equation 47			
		7 Days	14 Days	21 Days	28 Days
GFRP R.C.	30.187	40.957	45.481	52.291	53.716
CFRP R.C.	30.193	43.846	47.792	52.856	54.110
STEEL R.C.	-	41.793	48.812	55.511	56.372

From Table 35, the experimental ultimate moments for GFRP and CFRP reinforced concrete foundation – bases at 28 days were 23.529 and 23.917 kNm (77.7 and 79.0 percent) higher than the theoretical ultimate moments. This difference is attributed to the fact that characteristic of beam on elastic foundation value was not taken into account in the theoretical ultimate moments.

It is clear from Table 35 that steel reinforced concrete specimens performed better than FRP reinforced concrete specimens with deviations of 4.18 and 4.95 percent (2.262 and 2.656 kNm) compared to CFRP and GFRP, respectively. However, these results showed that FRP reinforced concrete foundation – bases could perform better

than steel reinforced concrete specimens if there was no lack of anchorage in FRP specimens.

The maximum deflection calculated at the centre of reinforced concrete specimens is presented in Table 36.

Table 36 Maximum deflection at the centre of reinforced concrete bases computed from Equation 43

Items	Maximum deflection (mm)			
	7 Days	14 Days	21 Days	28 Days
GFRP R.C. Base	0.671	0.745	0.856	0.880
CFRP R.C. Base	0.718	0.783	0.866	0.886
STEEL R.C. Base	0.684	0.799	0.901	0.923

From table 36, steel reinforced concrete bases had the highest deflection compared to FRP specimens from the second week. However, steel reinforced concrete bases at 7 day had lower deflection than those of CFRP; contrary to those of GFRP. Steel re-bars had the highest modulus of elasticity. Therefore, the higher the modulus of elasticity of reinforcing bars, the higher is the deflection in the reinforced concrete foundation – bases. It is clear that steel reinforced concrete bases gave bigger deflections and they will lead to higher deterioration once they are exposed to aggressive environment as deflection increased with the age of reinforced concrete.

5.6 Summary

As the main reason of substituting steel reinforcing bars by FRP re-bars in reinforced concrete is to prevent deterioration of concrete and corrosion of steel, FRP reinforced concrete foundation – bases can be an environmental solution in the corrosive environment.

For better performance of FRP reinforced concrete, it is clear that the lack of anchorage should be attended to by requiring FRP re-bars to be bent already according to specifications once manufactured.

The gap between the ultimate strains in FRP re-bars when failure occurs and ultimate tensile strains can serve as margin factor to prevent FRP rupture in reinforced concrete foundation – bases.

CHAPTER 6:

CONCLUSIONS AND RECOMMENDATIONS

6.1 Conclusions

In this study, GFRP, CFRP and steel re-bars were used as reinforcement for concrete foundations in order to achieve the following specific objectives:

(a) The strain behaviour of FRP materials and their implications. The re-bars were tested for tensile strength and results showed that:

(i) CFRP had the highest ultimate tensile strength which was 46.02 percent and 55.23 percent higher than the corresponding GFRP and steel values respectively.

(ii) The ultimate tensile strength for the steel re-bars was 6.30 percent higher than that of GFRP.

(iii)The modulus of elasticity of steel was higher than that of the FRP re-bars but the ultimate tensile strain was found to be lower than that of the FRP re-bars.

(iv) From the design calculations made, concrete crushing was found to be the mode of failure for FRP reinforced concrete foundation – bases and the same mode of failure was also observed during the experiments of FRP specimens.

(v) Although the ultimate strains in the FRP re-bars were not exceeded during the experiment, the calculated designed strains resulted in overestimation when compared to the experimental strains obtained by 51.60 and 16.94 percent for the GFRP and CFRP, respectively. The steel re-bars deformed plastically up to the point where concrete crushing took place as the ultimate strain limit of steel was exceeded but no rupture of steel re-bars was observed. However, the experimental strain in concrete was higher than the theoretical value by 69.29 percent.

(b) From the stress-strain behaviour of FRP and steel reinforced concrete foundations, the following was observed that steel reinforced concrete foundation – bases had the highest strain and stress values for the same period of 28 days, whereas the stress in steel re-bars was 5.99 percent and 7.61 percent higher compared to CFRP and GFRP re-bars respectively. However, CFRP re-bars were under higher stress levels than the others at the 7^{th} day.

(c) Concerning, the load carrying and the moment capacity of FRP and steel reinforced concrete foundations, it was found that:

(i) The steel reinforced concrete bases gave the best results of load carrying capacity with 4.18 and 4.94 percent higher than CFRP and GFRP reinforced concrete bases respectively. However, the CFRP was 0.73 percent higher than the GFRP reinforced concrete.

(ii) The experimental ultimate moments of FRP reinforced concrete foundation were found to be higher than the theoretical ones (from the mathematical model used) at the 28^{th} day. The differences in the GFRP and CFRP reinforced concrete foundations were 77.7 percent and 79.0 percent, respectively. When the steel reinforced concrete foundation – bases were compared to those of FRP, the traditional steel reinforced concrete ultimate moment was found to be higher by 4.17 percent than CFRP and 4.91 percent higher than GFRP.

Therefore, it was concluded that steel reinforced concrete foundation – bases performed better than FRP reinforced concrete foundation – bases. However, steel reinforced concrete bases gave higher deflections than those of FRP.

6.2 Recommendations

Five recommendations are made from results of this study:

i. More research is needed in this area of FRP reinforced Concrete foundation – bases to address the influence of non-ductility of FRP re-bars on the behaviour of FRP reinforced concrete in the serviceability limit state.

ii. A more accurate approach should be considered in the design of FRP reinforced concrete foundation – bases as the actual theoretical methods developed for beams and slabs suspended showed that the theoretical strain was overestimated while the theoretical ultimate moment was underestimated.

iii. The lack of anchorage between FRP re-bars and concrete emphasizes the need for more research on the theoretical methods to predict the bond properties of the two materials.

iv. FRP reinforced concrete foundation - bases should not be used where the redistribution of moment is needed.

v. Actual material partial factors recommended by design guidelines for concrete reinforced with FRP should be corrected by taking into account the environmental conversion factor in case of long service life of structures as the mechanical properties of FRP re-bars degrade due to the alkaline environment and moisture.

References

ABDULLA N.A. 2008, Effect of saline environment on the strength of reinforced concrete beams, *Journal of Al-Rafidain Engineering*, 16(2):12-23. [Online]. Available at: <http://alrafidain.engineering-coll-mosul.com/files/2ab30.pdf>. Accessed: 26/10/2009.

ABERDEEN GROUP. 2000, *Calcium chloride: Limit use in residential foundation walls?*, Aberdeen Group a division of Hanley-wood.

ACI 440.XR. 2004, *Guide test methods for Fiber-Reinforced Polymers (FRPs) for reinforcing or strengthening concrete structures*, American Concrete Institute, Michigan.

ACI 440.1R. 2006, *Guide for the design and construction of structural concrete reinforced with FRP bars*, American Concrete Institute, Michigan.

ACI 440.3R. 2004, *Guide test methods for Fiber-Reinforced Polymers (FRPs) for Reinforcing or Strengthening Concrete Structures*, American Concrete Institute, Michigan.

AHMAD, S. 2003, Reinforcement corrosion in concrete structures, its monitoring and service life prediction – a review. *Journal of Cement & Concrete Composites*, 25: 459-471, March. [Online] Available at: <http://isi.kfupm.edu.sa/journals/pdf/R/reinforcement_corrosion_in_concrete_stru_ahmad_isi_000182441600008.pdf>. Accessed: 26/10/2009.

ALEXANDER, M. & MACKECHINE, J. 2003, Concrete mixes for durable marine structures. *Journal of the South African Institution of Civil Engineering*, 45(2): 20-25, Feb.

ALEXANDER, M. & BEUSHAUSEN, H. 2010, Concrete Technology for Structural Engineers: Lecture 2 and 3, University of Cape Town.

ALSAYED, S.H., AL-SALLOUM, Y.A. & ALMUSALLAM, T.H. 2000, Fibre-reinforced polymer repair materials – some facts. *Journal of Civil Engineering*, 138: 131-134, Aug.

ALSAYED, S.H., AL-SALLOUM, Y.A. & ALMUSALLAM, T.H. 2000, Performance of glass fiber reinforced plastic bars as a reinforcing material for concrete structures, *Journal of Composites: Part B*, 31:555-567.

ANDERSSON, E. & BERGENDAHL, J. 2009, Expperimental and numerical investigations on stress laminated timber bridges, M.Sc. Dissertation. Chalmers University of Technology.

APOSTOLOPOULOS, C.A. & PAPADAKIS, V.G. 2008, Consequences of steel corrosion on the ductility properties of reinforcement bar, *Journal of Construction and Building Materials*, 22(10): 2316-2324, Nov.

APOSTOLOPOULOS, Ch.Alk., MICHALOPOULOS, D. & KOUTSOUKOS, P. 2008, The corrosion effects on the structural integrity of reinforcing steel. *Journal of Materials Engineering and Performance*, 17(4):506-516, Aug. [Online] Available at: <http://www.springerlink.com/content/g2473737224v8445/fulltext.pdf>. Accessed: 26/10/2009.

ARYA, C., CLARKE, J.L., KAY, E.A. & O'REGAN, P.D. 2001, TR55: Design guidance for strengthening concrete structures using fibre composite materials – A review, *Journal of Structural Engineering, Mechanics and Computation*, 2: 1243-1250, May.

ARAB REPUBLIC OF EGYPT. 2005, Egyptian code of practice for the use of Fiber Reinforced Polymer (FRP) in the construction fields, Ministry of Housing, Utilities and Urban Utilities, Cairo.

BRIAN, A. 1998, *Fundamentals of Concrete.* Cement and Concrete Institute, Midrand, South Africa.

BRITISH STANDARD, 2001, *Structural use of Concrete – Part 2: Code of practice for special circumstances*, University of Bath.

CNR-DT 203/2006. 2007, *Guide for the design and construction of concrete structures reinforced with Fiber-Reinforced Polymer bars*, National Research Council, Rome.

CERONI, F., COSENZA, E., GAETANO, M. & PECCE, M. 2006, Durability issues of FRP re-bars in reinforced concrete members, *Journal of cement and concrete composites*. 28:857-868, Aug. [online] Available at <http://wpage.unina.it/gamanfre/paper/Durability%20issues%20of%20FRP%20re-bars%20in%20reinforced%20concrete%20members.pdf.> Accessed:16/11/2009.

FIB. 2001. Bulletin 14, *Externally bonded FRP reinforcement for RC structures*, Technical Report, Task Group 9.3 FRP (Fibre Reinforced Polymer) reinforcement for concrete structures, Fédération Internationale du béton, 130.

GAILIUS, A. & KOSIOR-KAZBERUK, M. 2008, Monitoring of Concrete Resistance to Chloride Penetration. *Jounral of Materials Science*, 14(4): 350-355, Jul. [Online]. Available at < http://www.ktu.lt/lt/mokslas/zurnalai/medz/medz0-95/16%20Ceramics...%28pp.350-355%29.pdf > Accessed: 26/10/2009

GOLDSTEIN, H. 1996, *Catching up with composites*, Civil Engineer, March, ASCE, New York.

GOODSPEED, C., SCHMECKPEPER, E., HENRY, R., YOST JR. & GROSS, T. 1990, Fibre reinforced plastic grids for the structural reinforcement of concrete, *In* Proceeding of the 1st materials engineering congress, New York: ASCE, pp. 593-604.

HANNANT, D.J. 2003, Fibre – reinforced concrete. Newman, J & Choo, B. S., Ed. *Advanced Concrete Technology – Processes*, Elsevier, GB, 6/1-17.

DEWAR, J. 2003, Concrete mix design. Newman, J & Choo, B S, Ed. *Advanced Concrete Technology – Processes*, Elsevier, GB, 6/1-17.

DEN HARTOG, J.P. 1952, *Advanced strength of* materials. Mc Graw-Hill.

HUMPHREYS, M.F. 2003, The use of polymer composites in construction. *In* proceedings 2003 International conference on smart and sustainable built environment, Brisbane, pp. 1-9.

HUMPHREYS, M.F. 2003, Development and structural investigation of monocoque fibre composite trusses, Doctoral thesis, Queensland University of Technology. [Online]. Available at <http://eprints.qut.edu.au/15898/1/Matthew_Humphreys_Thesis.pdf>. Accessed: 5/10/2009.

KEAN, R.L. & DAVIES, K.G. 2003, *Cathodic protection*, Department of Trade and Industry. [Online]. Available at <http://www.npl.co.uk/upload/pdf/cathodic_protection.pdf > Accessed: 11/08/2011.

KERR, A.D. 1964, Elastic and Viscoelastic Foundation Models. *Journal of applied Mechanics*, 31(3): 491-498.

KRISHNA, R.N. 2007, *Design of concrete mixes*, 4th ed. New Delhi: CBS Publishers

KULKARNI, S. 2006, Calibration of flexural design of concrete members reinforced with FRP bars. M.Sc. Dissertation, Louisiana State University.

KYOWA ELECTRONIC INSTRUMENTS CO. 2005, What's a strain gauge? : Introduction to Strain Gauges. Tokyo, [Online]. Available at < http://www.kyowa-ei.com> Accessed: 26/08/2010.

LAM, L. & TENG, J.G. 2002. Ultimate axial strain of FRP-confined concrete. *Journal of Advanced in Building* Technology, 1: 789-796. [Online]. Available at < http://jrp.sagepub.com/content/22/13/1149.abstract > Accessed: 26/10/2009

LOVELL, D.R. 1999, Reinforcements, resins and methods of manufacture. *In* Hancox, N. L., ed. *Fibre composite hybrid materials*, Applied Science Publishers. 23-68.

MAADDAWY, T.E. & SOUDKI, K. 2007, Strengthening of Reinforced Concrete slabs with mechanically – anchored unbounded FRP system, *Journal of Construction and Building Materials*, 22(4): 444-455, Jul.

MACGREGOR, J.G. 1997, *Reinforced concrete, mechanics and design*, Upper Saddle River, N.J.: Prentice.

MACGREGOR, J.G. & WIGHT J.K. 2006, *Reinforced concrete: Mechanics and design*, 4th ed. Singapore: Prentice Hall.

MATSUI, T., YAMADA, S., MUTSUYOSHI, H. & NISHIZAKI, I. 2009, Optimizing LCC for Pier Bridges using FRP Members, Proceedings of US-Japan Workshop on Life Cycle Assessment of Sustainable Infrastructure Materials held in Sapporo, Japan on the 21st – 22nd October 2009. Sapporo 1-5, [Online]. Available at <http//www.hucc.hokudai.ac.jp/~m16120/workshop2009/papers/DrYamada.pdf>. Accessed:24/08/2011.

MEGSON, T.H.G. 2005, *Structural and Stress Analysis*, 2nd ed. Elsevier Butter worth.

MOSLEY, W.H., BUNGEY, J.H. & HULSE, R. 2007, *Reinforced Concrete Design*, 6th ed. Hampshire: MacMillan Press.

NADIM HASSOUN, M. & AL-MANASEER, A. 2008, *Structural concrete: Theory and Design*, 4th ed. Hoboken, N.J.: John Wiley &Sons.

NEHDI, M., CHABIB, EL H. & ALY SAÏD, A. 2007, Proposed shear design equations for FRP-Reinforced Concrete beams based on genetic algorithms approach, *Journal of materials in Civil Engineering*, 19 (12): 1033-1042, Dec.

NEWHOOK, J., GHALI, A. & TADROS G. 2002, Concrete flexural members reinforced with fiber reinforced polymer: design for cracking and deformability, *Canadian Journal of Civil Engineering*, 19: 125-134, Feb.

NICOLAE, T., GABRIEL, O., DORINA, I., IOANA, E., VLAD, M. & CĂTĂLIN, B. 2008, Fibre reinforced polymer composites as internal and external reinforcements for building elements, *Buletinul Institutului Politehnic Din Iaşi.*

PILAKOUTAS, K., GUADAGNINI, M., NEOCLEOUS, K. & TAERWE, L. 2007, Design guidelines for FRP reinforced concrete structures, *Journal of Advanced Composites in Construction:* 31-39, 2nd – 4th April.

ROBERTSON, S. 2000. *Concrete: Hard Facts, Durable Structures – Part 1,* [Online]. Available at < http://www.akhupheli.co.za/concrete%20Explained.pdf>. Accessed: 25/10/2010.

SANTHAKUMAR, A.R. 2007, *Concrete Technology*, New Delhi: Oxford University Press.

SABS. 1994, *South African Standard: Method 861: Concrete test,* (South African Bureau of Standards) Pretoria.

SABS. 1994, *South African Standard: Method 862: Concrete test,* (South African Bureau of Standards) Pretoria.

SABS. 1994, *South African Standard: Method 863: Concrete test,* (South African Bureau of Standards) Pretoria.

SABS. 1994, *South African Standard: Method 829 – B,* (South African Bureau of Standards) Pretoria.

SABS 0100-1. 2000, *South African Standard: Code of Practice: The structural use of concrete, Part 1: Design.* Ed. 2.2, (South African Bureau of Standards) Pretoria.

SABS 0163-3. 2001, *South African Standard: Code of Practice: The structural use of timber, Part 2: Allowable stress design,* Ed. 1.1 (South African Bureau of Standards) Pretoria.

SEIBLE, F., PRIESTLEY, M.J.N., HEGEMIER, G.A., INNAMORATO, D. 1997, Seismic retrofit of reinforced concrete conlumns with continuous carbon fiber jackets, *Journal of Composite construction*, 1(2):52-62.

SHANMUGANATHAN, S. 2003, Fibre reinforced polymer composite materials for civil building structures – review of the state – of – the – art. Rowen Travel Awart Report, *Journal of Institution of Structural Engineers*, 26-33, July.

SUGIURA, K., KITANE, Y., KISHIMA, T., NISHIZAKI, I. & YAMADA, S. 2008, FRP Bridges; the State of the Art. *In* Modernizing our infrastructure, Proceedings of the 2nd International Civil Engineering conference on Civil Engineering and Sustainable development held in Mombasa on 23rd – 25th September 2008. Mombasa, 305-314.

TÄLJSTEN, B. 2006, *FRP Strengthening of Existing Concrete Structures: Design Guideline*, 4th ed. Copenhagen: Luleå University of Technology.

TEODORU, I.B. 2009, Beams on Elastic foundation: The simplified continuum approach, *"Gheorghe Asachi" Techn. Univ., Faculty of Civil Engineering*, 37-45, Dec.

TODESCHINI, C.E., BIANCHINI, A.C., & KESLER C.E. 1964, Behaviour of concrete columns reinforced with high strength steels, *Journal of American Concrete Institute (ACI)*, 61(6): 701-716.

TIMOSHENKO, S. 1976, *Strength of Materials: Part II Advanced Theory and Problems*, 3rd ed. Van Nostrand Reinhold.

VAN DEN EINDE, L., ZHAO, L. & SEIBLE, F. 2003, Use of FRP in civil structural applications, *Journal of Construction and Building Materials*, 17: 389-403, Sept.

WEGIAN, F.M. & ABDALLA, H.A. 2005, Shear capacity of concrete beams reinforced with fiber reinforced polymers, *Journal of composite structures*, 71:130-138, Feb.

WILLIAM, F.S. & JAVAD, H. 2006, *Foundation of materials Science and Engineering*, 4th ed. Mc Graw-Hill.

www.spsrepair.com Accessed: 26/10/2009

YOST, JR., GROSS, S.P. & DINEHART, D.W. 2001, Shear strength of normal strength concrete beams reinforced with deformed GFRP bars, *Journal of Composition Construction*, ASCE, 5(4):268-275.

APPENDIX A

Table A1 Sieve Analysis: Fine Aggregates (FA) and Coarse Aggregates (CA)

	Fine Aggregates (FA)			15 mm Coarse Aggregates (CA)			19 mm Coarse Aggregates (CA)		
Sieve Size	**Mass Retained (grams)**	**Percentage Retained**	**Percentage Passing**	**Mass Retained (grams)**	**Percentage Retained**	**Percentage Passing**	**Mass Retained (grams)**	**Percentage Retained**	**Percentage Passing**
75.0	0	0	100	0.2	0.02	99.98	0.1	0.01	99.99
53.0	0	0	100	0.1	0.01	99.97	0.1	0.01	99.98
37.5	0	0	100	0.4	0.04	99.93	0.1	0.01	99.97
26.5	0	0	100	0.1	0.01	99.92	0.2	0.02	99.95
19.0	0	0	100	5.6	0.56	99.36	200.1	20.01	79.94
13.2	0	0	100	433.5	43.35	56.01	740.0	74.00	5.94
9.5	0	0	100	488.5	48.85	7.16	49.1	4.91	1.03
6.7	0	0	100	54.4	5.44	1.72	5.5	0.55	0.48
4.750	0.8	0.08	99.92	7.8	0.78	0.94	1.1	0.11	0.37
3.350	-	-	-	2.4	0.24	0.70	0.7	0.07	0.30
2.360	0.2	0.02	99.90	0.8	0.08	0.62	0.3	0.03	0.27
1.180	0.3	0.03	99.87	0.3	0.03	0.59	0.3	0.03	0.24
0.600	25.9	2.59	97.28	0.3	0.03	0.56	0.2	0.02	0.22
0.425	117.5	11.75	85.53	0.3	0.03	0.53	0.1	0.01	0.21
0.300	355.7	35.57	49.96	0.3	0.03	0.50	0.2	0.02	0.19
0.150	405.1	40.51	9.45	1.0	0.10	0.40	0.6	0.06	0.13
0.075	71.3	7.13	2.32	2.1	0.21	0.19	1.0	0.10	0.03
TOTAL	**976.8**	**97.68**		**998.1**	**99.81**		**999.7**	**99.96**	

Table A2 Sieve Analysis: Fine Aggregates (FA) and Coarse Aggregates (CA)

	Fine Aggregates (FA)			15 mm Coarse Aggregates (CA)			19 mm Coarse Aggregates (CA)		
Sieve Size	**Mass Retained (grams)**	**Percentage Retained**	**Percentage Passing**	**Mass Retained (grams)**	**Percentage Retained**	**Percentage Passing**	**Mass Retained (grams)**	**Percentage Retained**	**Percentage Passing**
75.0	0	0	100	0.1	0.01	99.99	0	0	100
53.0	0	0	100	0.1	0.01	99.98	0.1	0.01	99.99
37.5	0	0	100	0.3	0.03	99.95	0	0	99.99
26.5	0	0	100	0.3	0.03	99.92	0.1	0.01	99.98
19.0	0	0	100	8.4	0.84	99.08	223.5	22.35	77.63
13.2	0	0	100	454.7	45.47	53.61	733.8	73.38	4.25
9.5	0	0	100	472.6	47.26	6.35	36.3	3.63	0.62
6.7	0	0	100	47.7	4.77	1.58	2.1	0.21	0.41
4.750	0.5	0.05	99.95	11.6	1.16	0.42	0.9	0.09	0.32
3.350	-	-	-	1.2	0.12	0.30	0.2	0.02	0.30
2.360	0.3	0.03	99.92	0.2	0.02	0.28	0.2	0.02	0.28
1.180	0.2	0.02	99.90	0.2	0.02	0.26	0.1	0.01	0.27
0.600	43.1	4.31	95.59	0.1	0.01	0.25	0.3	0.03	0.24
0.425	123.4	12.34	83.25	0.1	0.01	0.24	0.2	0.02	0.22
0.300	379.6	37.96	45.29	0.2	0.02	0.22	0.3	0.03	0.19
0.150	375.4	37.54	7.75	0.5	0.05	0.17	0.6	0.06	0.13
0.075	56.8	5.68	2.07	0.8	0.08	0.09	0.8	0.08	0.05
TOTAL	**979.3**	**97.93**		**999.1**	**99.91**		**999.5**	**99.95**	

Table A3 Sieve Analysis: Fine Aggregates (FA) and Coarse Aggregates (CA)

	Fine Aggregates (FA)			15 mm Coarse Aggregates (CA)			19 mm Coarse Aggregates (CA)		
Sieve Size	**Mass Retained (grams)**	**Percentage Retained**	**Percentage Passing**	**Mass Retained (grams)**	**Percentage Retained**	**Percentage Passing**	**Mass Retained (grams)**	**Percentage Retained**	**Percentage Passing**
75.0	0	0	100	0	0	100	0.2	0.02	99.98
53.0	0	0	100	0	0	100	0	0	99.98
37.5	0	0	100	0.1	0.01	99.99	0	0	99.98
26.5	0	0	100	0.1	0.01	99.98	18.0	1.80	98.18
19.0	0	0	100	0	0	99.98	337.3	33.73	64.45
13.2	0	0	100	469.4	46.94	53.04	592.7	59.27	5.18
9.5	0	0	100	494.8	49.48	3.56	42.4	4.24	0.94
6.7	0	0	100	27.6	2.76	0.80	3.8	0.38	0.56
4.750	0.4	0.04	99.96	3.9	0.39	0.41	0.2	0.02	0.54
3.350	-	-	-	0.5	0.05	0.36	0.2	0.02	0.52
2.360	0.3	0.03	99.93	0.2	0.02	0.34	0.4	0.04	0.48
1.180	0.2	0.02	99.91	0.3	0.03	0.31	0.3	0.03	0.45
0.600	31.1	3.11	96.80	0.2	0.02	0.29	0.4	0.04	0.41
0.425	120.9	12.09	84.71	0.2	0.02	0.27	0.2	0.02	0.39
0.300	359.1	35.91	48.80	0.2	0.02	0.25	0.5	0.05	0.34
0.150	406.8	40.68	8.12	0.5	0.05	0.20	1.0	0.10	0.24
0.075	60.4	6.04	2.08	0.9	0.09	0.11	1.3	0.13	0.11
TOTAL	**979.2**	**97.92**		**998.9**	**99.89**		**998.9**	**99.89**	

Table A4 Sieve Analysis: Fine Aggregates (FA) and Coarse Aggregates (CA)

	Fine Aggregates (FA)			**15 mm Coarse Aggregates (CA)**			**19 mm Coarse Aggregates (CA)**		
Sieve Size	**Mass Retained (grams)**	**Percentage Retained**	**Percentage Passing**	**Mass Retained (grams)**	**Percentage Retained**	**Percentage Passing**	**Mass Retained (grams)**	**Percentage Retained**	**Percentage Passing**
75.0	0	0	100	0.3	0.03	99.97	0.3	0.03	99.97
53.0	0	0	100	0.1	0.01	99.96	0	0	99.97
37.5	0	0	100	0.1	0.01	99.95	0	0	99.97
26.5	0	0	100	0.1	0.01	99.94	0.1	0.01	99.96
19.0	0	0	100	17.2	1.72	98.22	203.1	20.31	79.65
13.2	0	0	100	516.7	51.67	46.55	716.1	71.61	8.04
9.5	0	0	100	427.6	42.76	3.79	64.9	6.49	1.55
6.7	0	0	100	27.3	2.73	1.06	8.7	0.87	0.68
4.750	0.4	0.04	99.96	6.0	0.60	0.46	2.4	0.24	0.44
3.350	-	-	-	1.4	0.14	0.32	0.3	0.03	0.41
2.360	0.3	0.03	99.93	0.2	0.02	0.30	0.4	0.04	0.37
1.180	0.3	0.03	99.90	0.3	0.03	0.27	0.2	0.02	0.35
0.600	35.6	3.56	96.34	0.1	0.01	0.26	0.3	0.03	0.32
0.425	144.2	14.42	81.92	0.2	0.02	0.24	0.2	0.02	0.30
0.300	344.9	34.49	47.43	0.2	0.02	0.22	0.4	0.04	0.26
0.150	388.8	38.88	8.55	0.6	0.06	0.16	0.8	0.08	0.18
0.075	60.0	6.00	2.55	0.8	0.08	0.08	1.1	0.11	0.07
TOTAL	**974.5**	**97.45**		**999.2**	**99.92**		**999.3**	**99.93**	

Table A5 Sieve Analysis: Fine Aggregates (FA) and Coarse Aggregates (CA)

	Fine Aggregates (FA)			15 mm Coarse Aggregates (CA)			19 mm Coarse Aggregates (CA)		
Sieve Size	**Mass Retained (grams)**	**Percentage Retained**	**Percentage Passing**	**Mass Retained (grams)**	**Percentage Retained**	**Percentage Passing**	**Mass Retained (grams)**	**Percentage Retained**	**Percentage Passing**
75.0	0	0	100	0.3	0.03	99.97	0.3	0.03	99.97
53.0	0	0	100	0.1	0.01	99.96	0.1	0.01	99.96
37.5	0	0	100	0.1	0.01	99.95	0.1	0.01	99.95
26.5	0	0	100	0.1	0.01	99.94	0	0	99.95
19.0	0	0	100	6.0	0.60	99.34	360.3	36.03	63.92
13.2	0	0	100	497.0	49.70	49.64	578.1	57.81	6.11
9.5	0	0	100	471.2	47.12	2.52	45.1	4.51	1.60
6.7	0	0	100	20.2	2.02	0.50	6.3	0.63	0.97
4.750	0.3	0.03	99.97	2.3	0.23	0.27	2.7	0.27	0.70
3.350	-	-	-	0.2	0.02	0.25	0.8	0.08	0.62
2.360	0.1	0.01	99.96	0.2	0.02	0.23	0.5	0.05	0.57
1.180	0.3	0.03	99.93	0.2	0.02	0.21	0.4	0.04	0.53
0.600	29.6	2.96	96.97	0.1	0.01	0.20	0.5	0.05	0.48
0.425	125.7	12.57	84.40	0.2	0.02	0.18	0.3	0.03	0.45
0.300	367.9	36.79	47.61	0.1	0.01	0.17	0.6	0.06	0.39
0.150	390.0	39.00	8.61	0.4	0.04	0.13	1.1	0.11	0.28
0.075	63.1	6.31	2.30	0.7	0.07	0.06	1.5	0.15	0.13
TOTAL	**977.0**	**97.70**		**999.4**	**99.94**		**998.7**	**99.87**	

Table A6 Sieve Analysis: Fine Aggregates (FA) and Coarse Aggregates (CA)

	Fine Aggregates (FA)			15 mm Coarse Aggregates (CA)			19 mm Coarse Aggregates (CA)		
Sieve Size	**Mass Retained (grams)**	**Percentage Retained**	**Percentage Passing**	**Mass Retained (grams)**	**Percentage Retained**	**Percentage Passing**	**Mass Retained (grams)**	**Percentage Retained**	**Percentage Passing**
75.0	0	0	100	0.2	0.02	99.98	0.3	0.03	99.97
53.0	0	0	100	0.1	0.01	99.97	0	0	99.97
37.5	0	0	100	0.1	0.01	99.96	0	0	99.97
26.5	0	0	100	0.1	0.01	99.95	0	0	99.97
19.0	0	0	100	7.7	0.77	99.18	288.1	28.81	71.16
13.2	0	0	100	414.6	41.46	57.72	658.3	65.83	5.33
9.5	0	0	100	517.1	51.71	6.01	39.9	3.99	1.34
6.7	0	0	100	36.6	3.66	2.35	5.1	0.51	0.83
4.750	0.6	0.06	99.94	11.3	1.13	1.22	1.2	0.12	0.71
3.350	-	-	-	2.9	0.29	0.93	0.6	0.06	0.65
2.360	0.3	0.03	99.91	0.8	0.08	0.85	0.4	0.04	0.61
1.180	0.4	0.04	99.87	0.6	0.06	0.79	0.4	0.04	0.57
0.600	27.0	2.70	97.17	0.4	0.04	0.75	0.4	0.04	0.53
0.425	127.2	12.72	84.45	0.4	0.04	0.71	0.3	0.03	0.50
0.300	359.0	35.90	48.55	0.4	0.04	0.67	0.5	0.05	0.45
0.150	388.9	38.89	9.66	1.4	0.14	0.53	1.3	0.13	0.32
0.075	68.4	6.84	2.82	2.3	0.23	0.30	1.6	0.16	0.16
TOTAL	**971.8**	**97.18**		**997.0**	**99.70**		**998.4**	**99.84**	

APPENDIX B

B.1 Calculation of strains in FRP re-bars

The strain in the reinforcement at the moment of concrete crushing can be computed by:

$$\varepsilon_f = \frac{-\varepsilon_{cu} + \sqrt{\varepsilon_{cu}^2 + \frac{4(\eta)(f_{ck})(\lambda)(\varepsilon_{cu})}{(\gamma_c)(\rho_f)(E_f)}}}{2} \quad \text{(B1)}$$

a) Carbon Fibre Reinforced Polymer Rebar

The strain, calculated from Equation B1, in the CFRP reinforcement at the moment when the concrete crushes is:

$$\varepsilon_{f_{CFRP}} = \frac{-(0.0035) + \sqrt{(0.0035)^2 + \frac{4(1)(1)[21.99(10^6)](0.8)(0.0035)}{(1.2)[3.28(10^{-3})][76.04(10^9)]}}}{2}$$

$$\varepsilon_{f_{CFRP}} = \frac{-(0.0035) + \sqrt{8.352(10^{-4})}}{2}$$

$$\varepsilon_{f_{CFRP}} = 12.69(10^{-3}) = 1.269\ \%$$

b) Glass Fibre Reinforced Polymer Rebar

The strain in the GFRP reinforcement at the moment when concrete crush is:

$$\varepsilon_{f_{GFRP}} = \frac{-(0.0035) + \sqrt{(0.0035)^2 + \frac{4(1)(1)[21.99(10^6)](0.8)(0.0035)}{(1.2)[3.26(10^{-3})][28.35(10^9)]}}}{2}$$

$$\varepsilon_{f_{GFRP}} = \frac{-(0.0035) + \sqrt{2.233(10^{-3})}}{2}$$

$$\varepsilon_{f_{GFRP}} = 21.88(10^{-3}) = 2.188\ \%$$

B.2 Calculation of Ultimate Moments

The theoretical ultimate moment, M_u, of the FRP reinforced concrete base is computed as:

$$M_u = \eta f_{cd} b d^2 (\lambda\beta_1)\left(1 - \frac{\lambda\beta_1}{2}\right) \quad \text{[Nm]} \tag{B2}$$

where $f_{cd} = \frac{\alpha_{cc}\, f_c'}{\gamma_c}$ (B3)

The parameter α_{cc} is 1.0 and γ_c: partial safety factor of concrete equals to 1.2 from SABS 0100-1(2000:8). As the compressive strength of concrete is less than 50 MPa, the parameters η and λ are 1.0 and 0.8 respectively (Pilakoutas et al., 2007:33).

$$f_{cd} = \frac{1\,[21.99(10^6)]}{1.2} = 18.33 \text{ MPa}$$

The ultimate moments M_u of FRP reinforced concrete bases are:

a. GFRP reinforced concrete foundation – bases:

$$M_u = (1.0)[18.33(10^6)](0.5)(0.09502)^2(0.8)(0.6)\left[1 - \frac{(0.8)(0.6)}{2}\right]$$

$$M_u = 30.187 \text{ kNm}$$

b. CFRP reinforced concrete foundation – bases:

$$M_u = (1.0)[18.33(10^6)](0.5)(0.09503)^2(0.8)(0.6)\left[1 - \frac{(0.8)(0.6)}{2}\right]$$

$$M_u = 30.193 \text{ kNm}$$

The practical ultimate moment M_u of the reinforced concrete base is computed by:

$$M_{centre} = \frac{P}{4\beta_e}\left(\frac{\cosh\beta_e L - \cos\beta_e L}{\sinh\beta_e L + \sin\beta_e L}\right) \tag{B4}$$

With L being the length of specimen, 1 meter; P is the ultimate load and β_e is the characteristic of beam on elastic foundation computed using Equation B5.

$$\beta_e = \sqrt[4]{\frac{k}{4EI}} \tag{B5}$$

where k is the foundation modulus (or elastic foundation stiffness) calculated from Equation B6, E is the modulus of elasticity of concrete of 37.028 GPa and I is the moment of inertia was computed from Equation 70 on page 88.

The elastic foundation stiffness can be determined as: (Andersson and Bergendahl, 2009:33)

$$k = \frac{4E_T(D_w)(h_T)^3}{bl^3} \quad [\text{N/mm}^2] \tag{B6}$$

where E_T is the modulus of elasticity of Timber (In this study, grade 10 of timber is considered from SABS 0163-2, 2001:62); D_w is the width of timber element; h_T is the height of timber element; b is the width of the beam and l is the length of the timber element.

$$k = \frac{4(10500)(31)(59)^3}{(500)(83)^3} = 935.313 \text{ N/mm}^2$$

Therefore, β_e are for the three types of reinforced concrete foundation – bases:

$$\beta_e = \sqrt[4]{\frac{935.313}{4[37.028(10^3)][140.625(10^6)]}} = 2.589(10^{-3})$$

Thus, the ultimate moment at the centre of the foundation – base are:

a. GFRP reinforced concrete foundation – base at 28 days:

$$M_{centre} = \frac{437(10^3)}{4[2.589\,(10^{-3})]}\left(\frac{\cosh[2.589(10^{-3})(1)]-\cos[2.589(10^{-3})(1)]}{\sinh[2.589(10^{-3})(1)]+\sin[2.589(10^{-3})(1)]}\right)$$

$$M_{centre} = \frac{437(10^3)}{1.0356(10^{-2})}\left[\frac{3.353(10^{-6})}{2.634(10^{-3})}\right] = 53{,}716.44 \text{ Nm} = 53.716 \text{ kNm}$$

b. CFRP reinforced concrete foundation – base at 28 days:

$$M_{centre} = \frac{440.20(10^3)}{4[2.589\,(10^{-3})]}\left(\frac{\cosh[2.589(10^{-3})(1)]-\cos[2.589(10^{-3})(1)]}{\sinh[2.589(10^{-3})(1)]+\sin[2.589(10^{-3})(1)]}\right)$$

$$M_{centre} = \frac{440.20(10^3)}{1.0356(10^{-2})}\left[\frac{3.353(10^{-6})}{2.634(10^{-3})}\right] = 54{,}109.781 \text{ Nm} = 54.110 \text{ kNm}$$

c. Steel reinforced concrete foundation – base at 28 days:

$$M_{centre} = \frac{458.60(10^3)}{4[2.589(10^{-3})]}\left(\frac{\cosh[2.589(10^{-3})(1)]-\cos[2.589(10^{-3})(1)]}{\sinh[2.589(10^{-3})(1)]+\sin[2.589(10^{-3})(1)]}\right)$$

$$M_{centre} = \frac{458.60(10^3)}{1.0356(10^{-2})}\left[\frac{3.353(10^{-6})}{2.634(10^{-3})}\right] = 56{,}371.526 \text{ Nm} = 56.372 \text{ kNm}$$

Table B1 Average of practical ultimate moments

Items	Ultimate Moments (kNm) Ultimate moments calculated from Equation 7			
	7 Days	**14 Days**	**21 Days**	**28 Days**
GFRP R.C.	40.957	45.481	52.291	53.716
CFRP R.C.	43.846	47.792	52.856	54.110
STEEL R.C.	41.793	48.812	55.511	56.372

B.3 Calculation of Maximum Deflection

In this study, the deflection of reinforced concrete sample was expressed as (Den Hartog, 1952:160; Timoshensko, 1976:18):

$$y_{centre} = \frac{P\beta_e}{2k}\left(\frac{2+\cos\beta_e L+\cosh\beta_e L}{\sin\beta_e L+\sinh\beta_e L}\right) \quad \text{(B7)}$$

where y_{centre} is deflection of beam at the centre of specimen; P is the load applied on the beam; L is the length of the beam of 1 meter; k is the modulus of foundation of 935.313 N/mm^2 and β_e is $2.589(10^{-3})$ for the three types of reinforced concrete foundation – bases.

Therefore, the maximum deflection considered was at the centre of specimens:

a. GFRP reinforced concrete foundation – base at 28 days:

$$y_{centre} = \frac{[437(10^3)][2.589(10^{-3})]}{2[935.313]}\left[\frac{2+\cos[2.589(10^{-3})(1000)]+\cosh[2.589(10^{-3})(1000)]}{\sin[2.589(10^{-3})(1000)]+\sinh[2.589(10^{-3})(1000)]}\right]$$

$$y_{centre} = \frac{1{,}131.393}{1{,}870.626}\left(\frac{9.69475}{6.66585}\right) = 0.880 \text{ mm}$$

b. CFRP reinforced concrete foundation – base at 28 days:

$$y_{centre} = \frac{[440.20(10^3)][2.589(10^{-3})]}{2[935.313]}\left[\frac{2+\cos[2.589(10^{-3})(1000)]+\cosh[2.589(10^{-3})(1000)]}{\sin[2.589(10^{-3})(1000)]+\sinh[2.589(10^{-3})(1000)]}\right]$$

$$y_{centre} = \frac{1{,}139.678}{1{,}870.626}\left(\frac{9.69475}{6.66585}\right) = 0.886 \text{ mm}$$

c. Steel reinforced concrete foundation – base at 28 days:

$$y_{centre} = \frac{[458.60(10^3)][2.589(10^{-3})]}{2[935.313]}\left[\frac{2+\cos[2.589(10^{-3})(1000)]+\cosh[2.589(10^{-3})(1000)]}{\sin[2.589(10^{-3})(1000)]+\sinh[2.589(10^{-3})(1000)]}\right]$$

$$y_{centre} = \frac{1{,}187.315}{1{,}870.626}\left(\frac{9.69475}{6.66585}\right) = 0.923 \text{ mm}$$

Table B2 Maximum deflection in the reinforced concrete bases

Items	Maximum deflection (mm)			
	7 Days	14 Days	21 Days	28 Days
GFRP R.C.	0.671	0.745	0.856	0.880
CFRP R.C.	0.718	0.783	0.866	0.886
STEEL R.C.	0.684	0.799	0.901	0.923

B.4 Modular Ratio, Depth of Neutral Axis, Second Moment of Area of Concrete and Calculation of Stress in Reinforcement

(i) The modular ratio was calculated as:

$$m_{GFRP} = \frac{E_{GFRP}}{E_c} = \frac{28.35GPa}{37.028GPa} = 0.766$$

$$m_{CFRP} = \frac{E_{CFRP}}{E_c} = \frac{76.04GPa}{37.028GPa} = 2.054$$

$$m_{steel} = \frac{E_{steel}}{E_c} = \frac{213.09GPa}{37.028GPa} = 5.755$$

(ii) The depth of neutral axis was calculated as:

$$n_{GFRP} = \frac{(0.766)(155)}{500}\left[\sqrt{1+\left(\frac{2(500)(95.02)}{(0.766)(155)}\right)}-1\right] = 6.499 \text{ mm}$$

$$n_{CFRP} = \frac{(2.054)(156)}{500}\left[\sqrt{1+\left(\frac{2(500)(95.03)}{(2.054)(156)}\right)}-1\right] = 10.417 \text{ mm}$$

$$n_{steel} = \frac{(5.755)(157.08)}{500}\left[\sqrt{1+\left(\frac{2(500)(95)}{(5.755)(157.08)}\right)}-1\right] = 16.814 \text{ mm}$$

(iii) The second moment of area of concrete was computed as:

$$I_{c_{GFRP}} = \frac{(500)(6.499)^3}{3} + (0.766)(155)[95.02-6.499]^2 = 0.976(10^6) \text{ mm}^4$$

$$I_{c_{CFRP}} = \frac{(500)(10.417)^3}{3} + (2.054)(156)[95.03-10.417]^2 = 2.482(10^6) \text{ mm}^4$$

$$I_{c_{steel}} = \frac{(500)(16.814)^3}{3} + (5.755)(157.08)[95.00-16.814]^2 = 6.318(10^6) \text{ mm}^4$$

(iv)The ultimate stress in the reinforcing bars at 28 days was obtained as:

$$\sigma_{GFRP} = \frac{(0.766)[53.716(10^3)]}{9.761(10^{-7})}(0.09502-0.006499) = 3.732(10^3) \text{ MPa}$$

$$\sigma_{CFRP} = \frac{(2.054)[54.110(10^3)]}{2.482(10^{-6})}(0.09503-0.01042) = 3.789(10^3) \text{ MPa}$$

$$\sigma_{steel} = \frac{(5.755)[56.372(10^3)]}{6.318(10^{-6})}(0.095-0.016814) = 4.016(10^3) \text{ MPa}$$

Table B3 Stresses in the reinforcing bars calculated

MATERIALS	**STRESS in (MPa)** $(\mathbf{10^3})$			
	7 Days	**14 Days**	**21 Days**	**28 Days**
GFRP	2.845	3.160	3.633	3.732
CFRP	3.070	3.346	3.701	3.789
STEEL	2.977	3.477	3.954	4.016

B.5 Pictures of Foundation Samples Tested

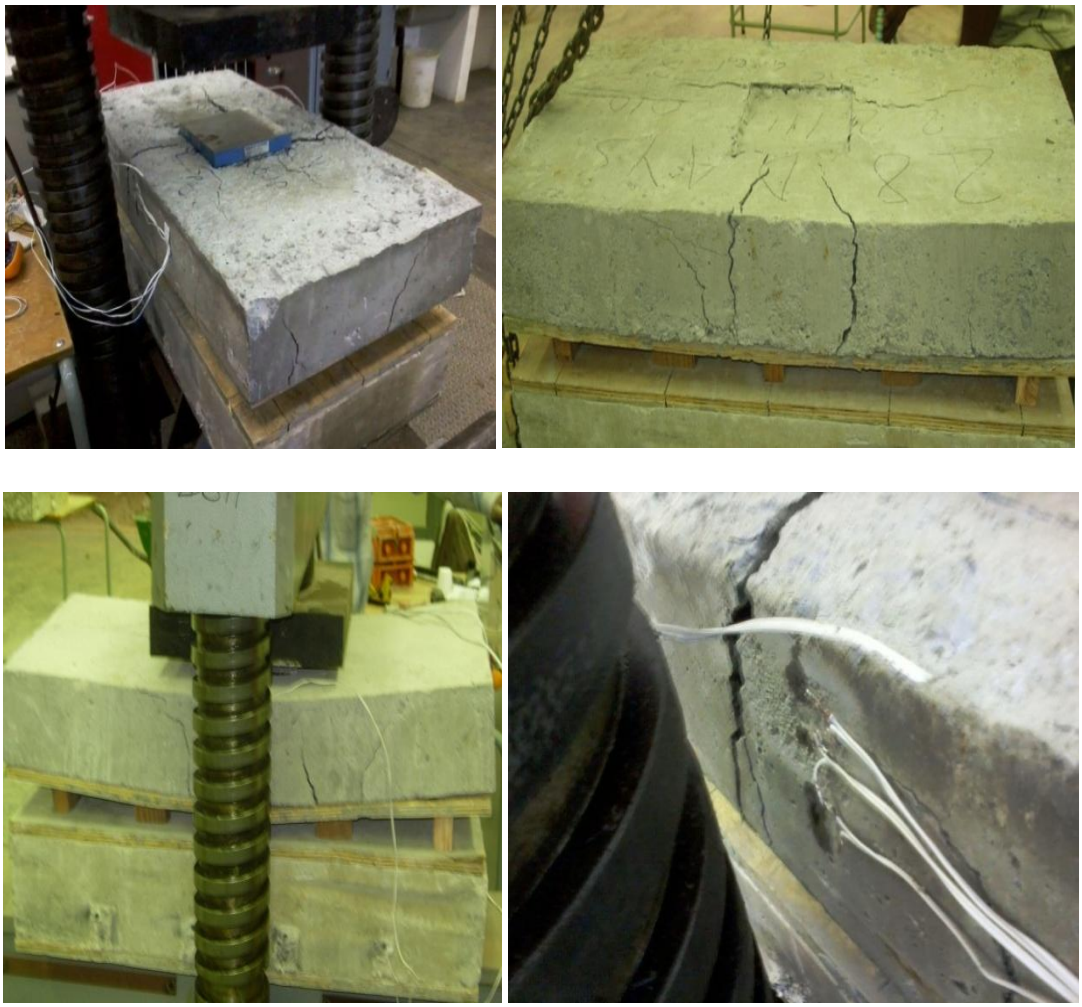

Figure B1 Foundation base failure mode.

APPENDIX C

C.1 Tensile Tests Results of GFRP and CFRP re-bars produced by Industrial Composites C.C. (South Africa).

a) GFRP re-bars:

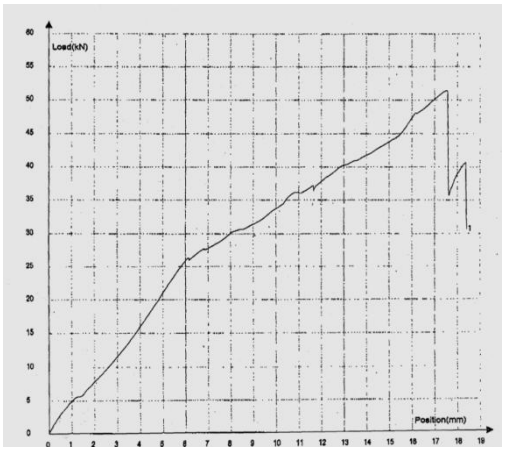

(1)

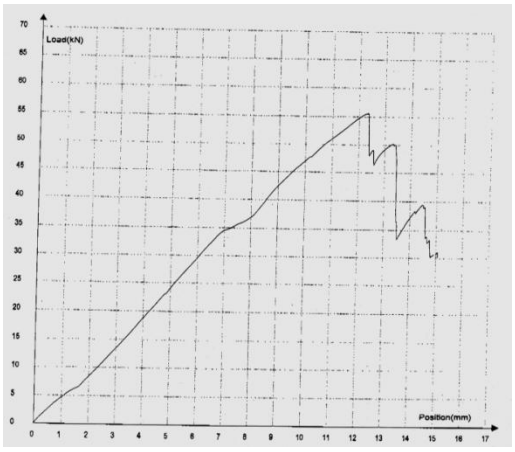

(2)

Table C1 Results values

Items	Maximum Load (kN)	Tensile Strength (MPa)
Sample 1	51.32	539.99
Sample 3	55.58	584.61

b) CFRP re-bars:

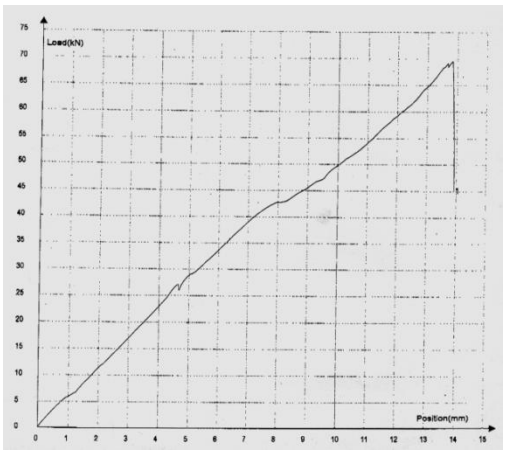

(1)

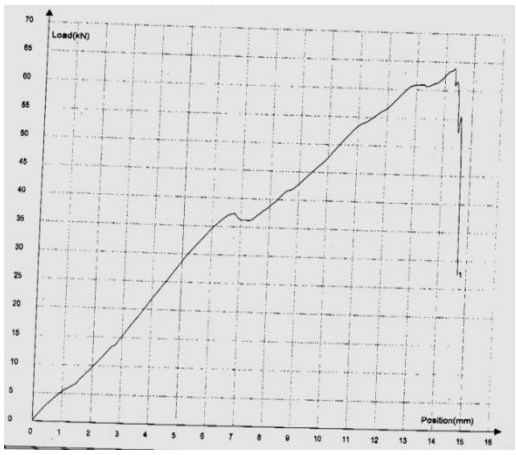

(2)

Table C2 Results values

Items	Maximum Load (kN)	Tensile Strength (MPa)
Sample 1	69.58	732.13
Sample 2	63.85	671.90

C.2 Tensile Tests Results of GFRP and CFRP re-bars produced by Pultrall Company (Canada).

a) GFRP re-bars:

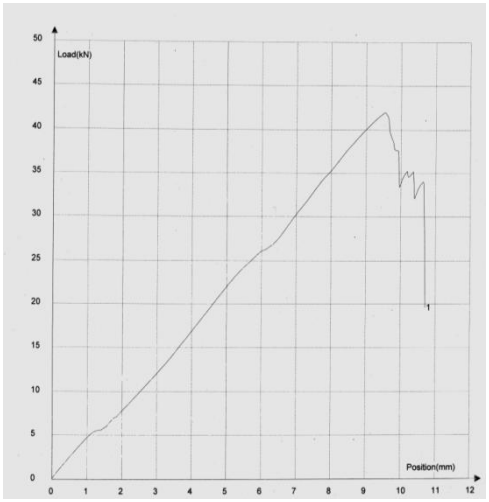

(1)

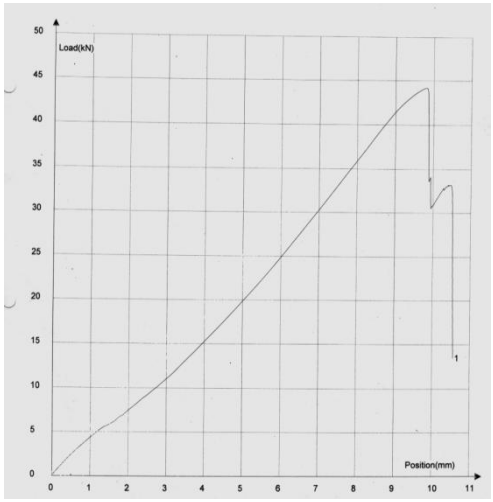

(2)

Table C3 Results values

Items	Maximum Load (kN)	Tensile Strength (MPa)
Sample 1	41.95	534.11
Sample 2	44.17	562.39

b) CFRP re-bars:

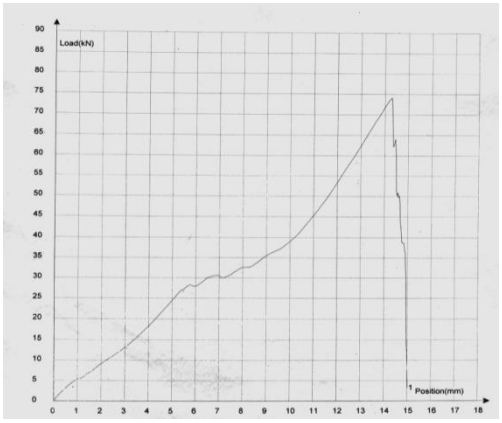

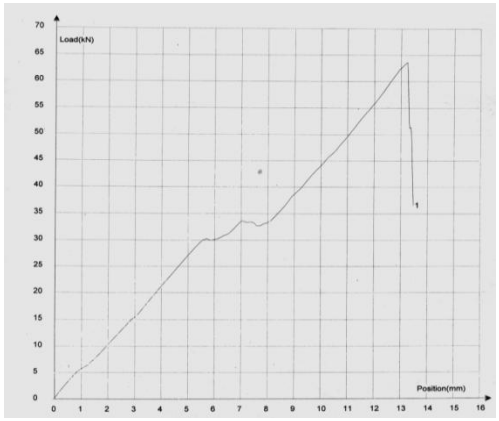

(1) (2)

Table C4 Results values

Items	Maximum Load (kN)	Tensile Strength (MPa)
Sample 1	74.08	943.18
Sample 2	63.60	809.82

C.3 Tensile Tests Results of steel re-bars.

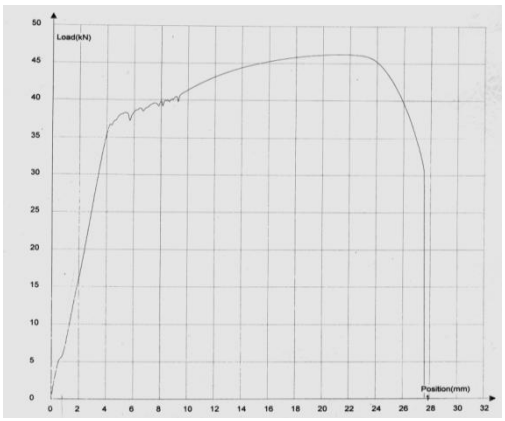

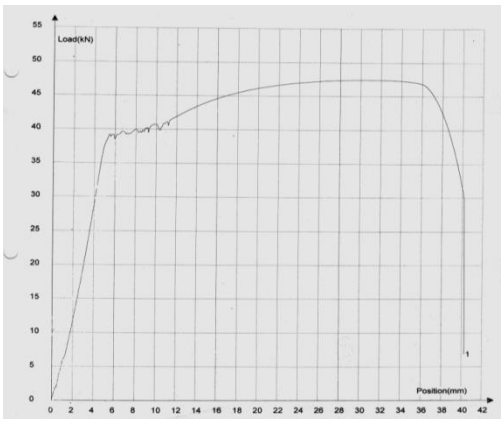

(1) (2)

Table C5 Results values

Items	Maximum Load (kN)	Tensile Strength (MPa)
Sample 1	46.23	588.62
Sample 2	47.39	603.40

APPENDIX D

Samples Curves

In the graphs below, the red colour represents the strain gauges on the reinforcement; the green, orange and violet colours represent the strain gauges placed on concrete.

However, the sudden variation of green, orange and violet colours in the graphs were due to the cracks passing on the strain gauges; the latter broken down.

The X – axis represents the time in second and the Y – axis represents the variation of output voltage in Volt.

Steel 1 D28 curve: Ultimate loads = 439.3 kN

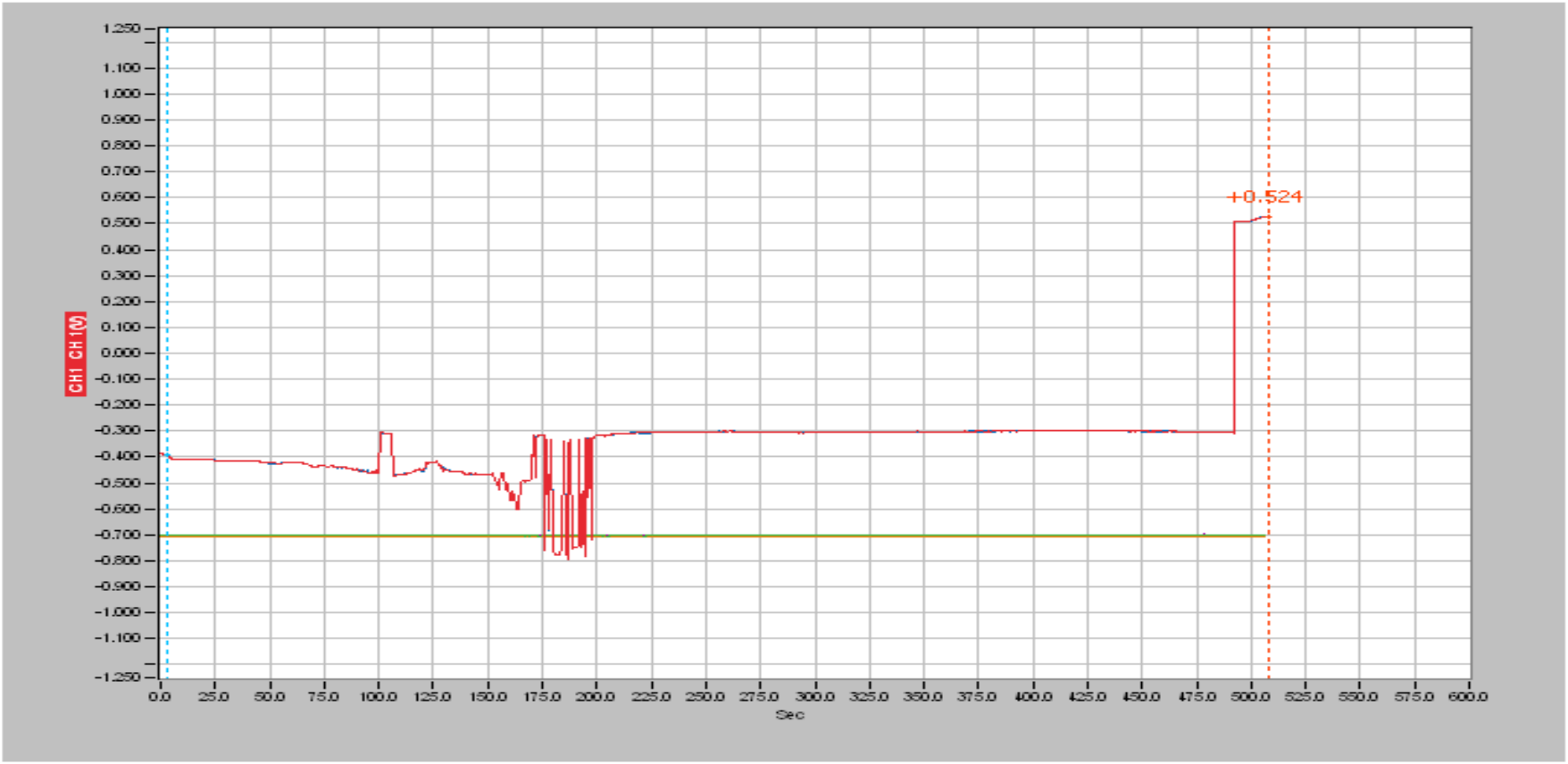

Figure D1 Strain curve diagram for steel at 28 days test

CFRP 1 D28 curve: Ultimate loads = 428.7 kN

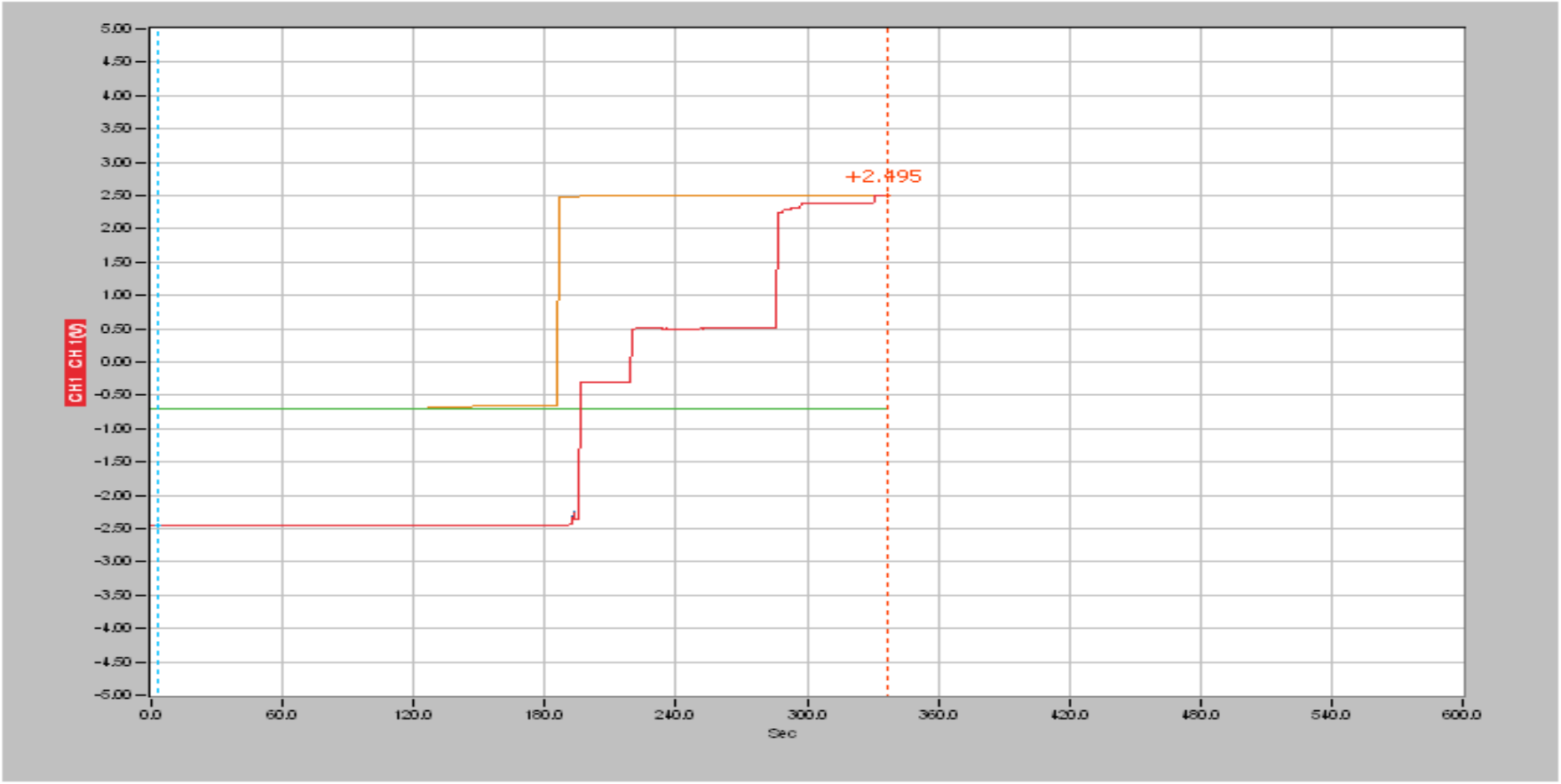

Figure D2 Strain curve diagram for CFRP at 28 days test

GFRP 3 D28 curve: ultimate loads = 426 kN

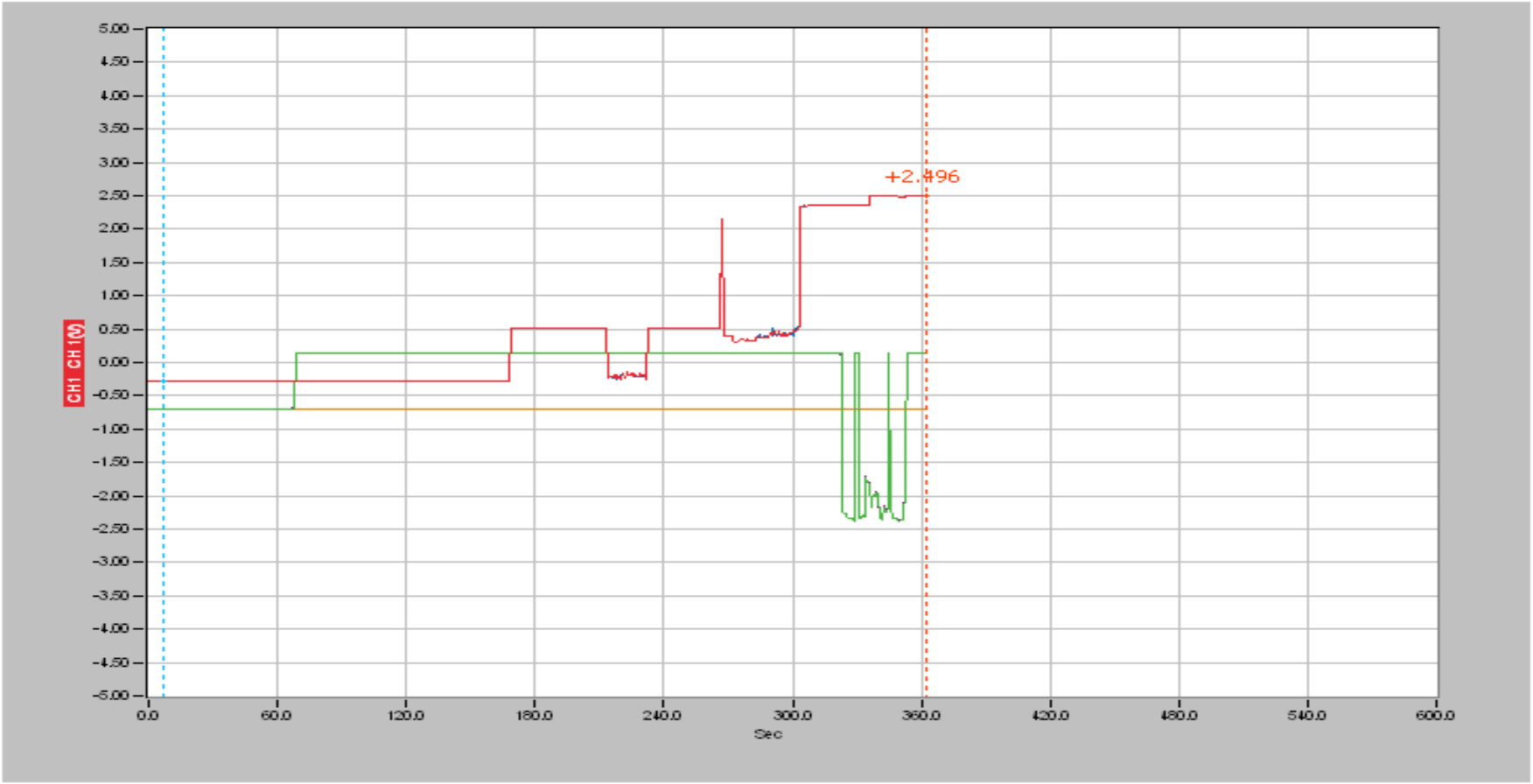

Figure D3 Strain curve diagram for GFRP at 28 days test

Steel 1 D21 curve: Ultimate loads = 435.8 kN

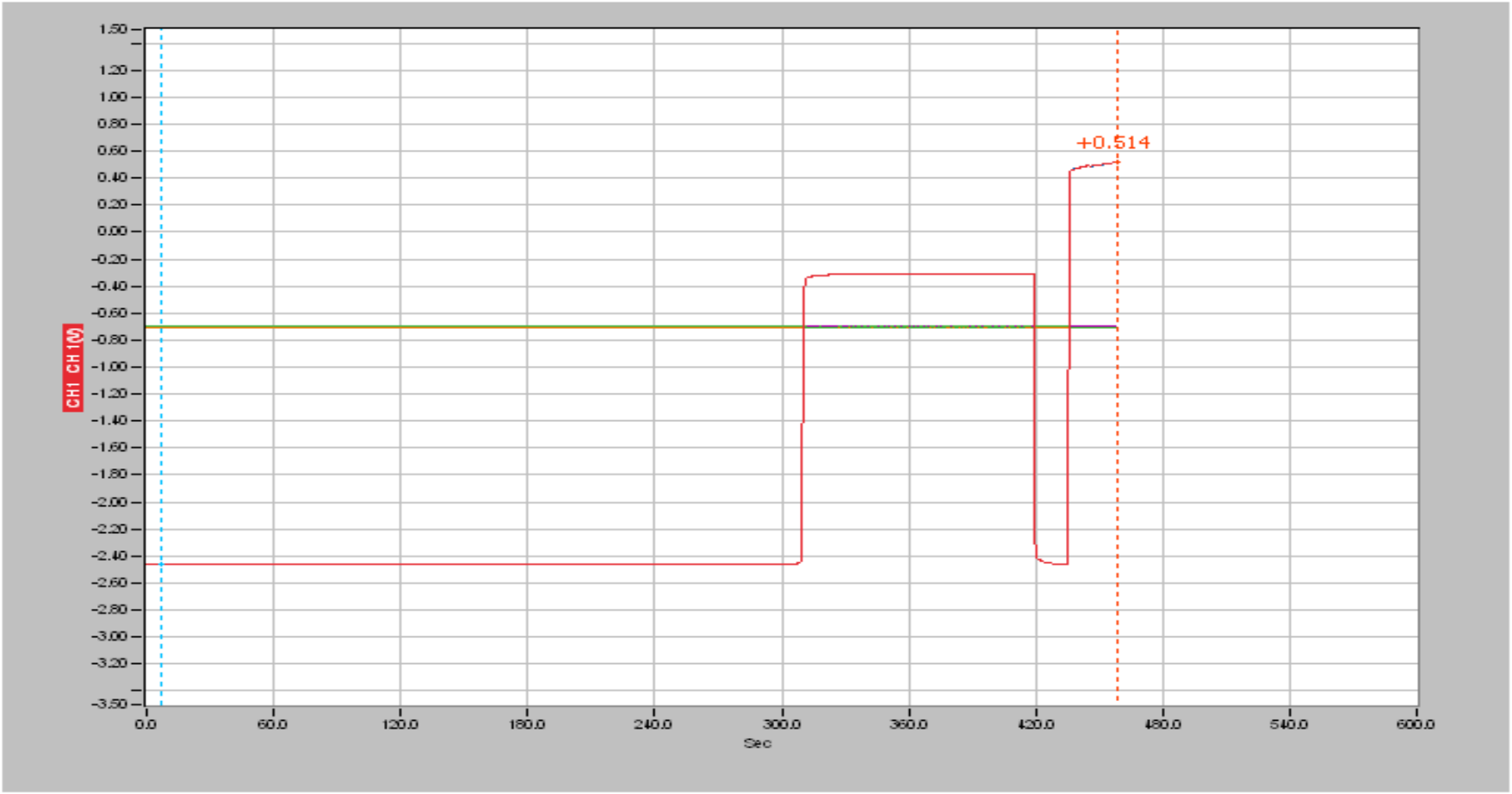

Figure D4 Strain curve diagram for steel at 21 days test

CFRP 1 D21 curve: ultimate loads = 430kN

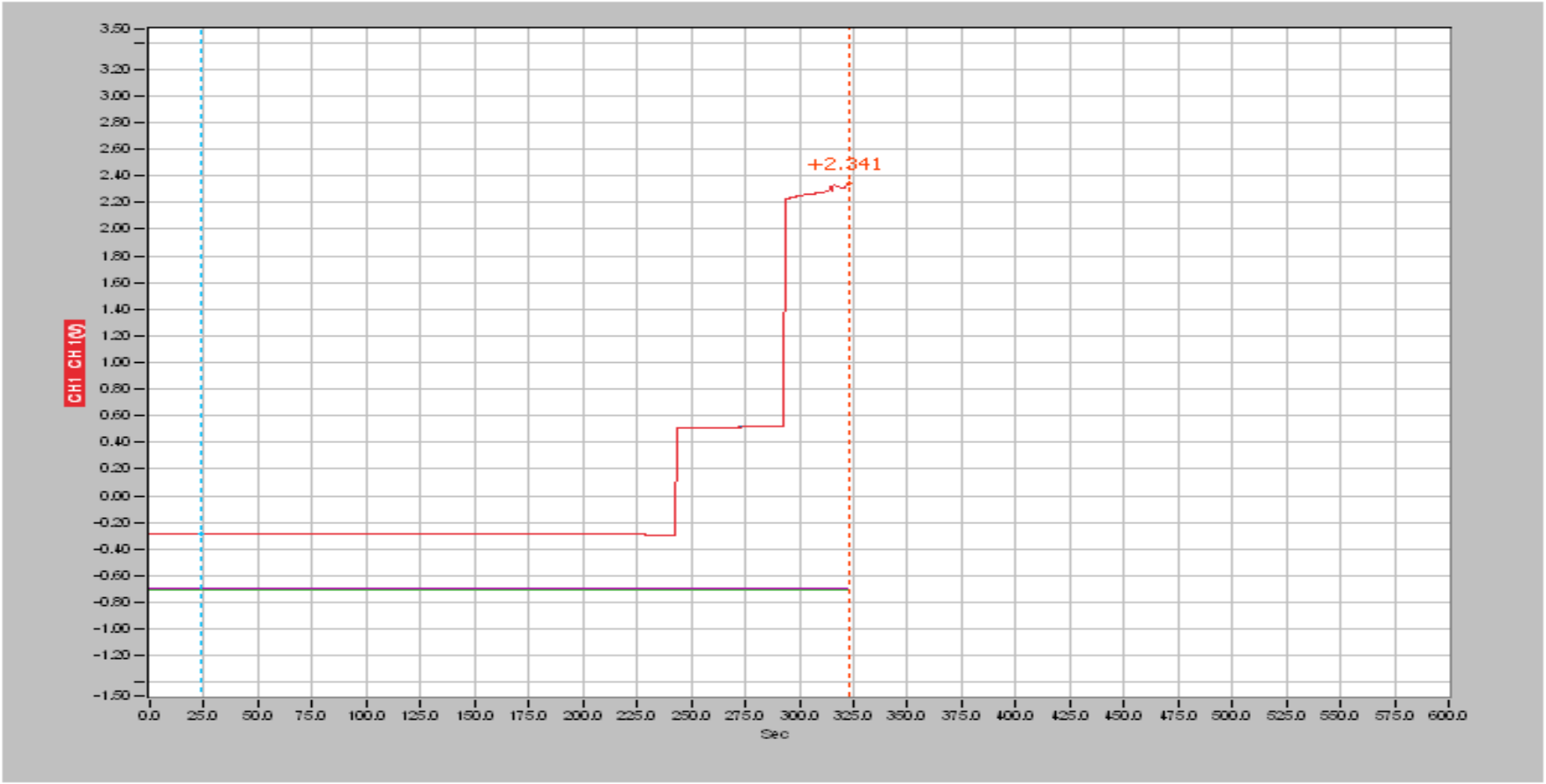

Figure D5 Strain curve diagram for CFRP at 21 days test

GFRP 1 D21 curve: Ultimate loads = 425.4 kN

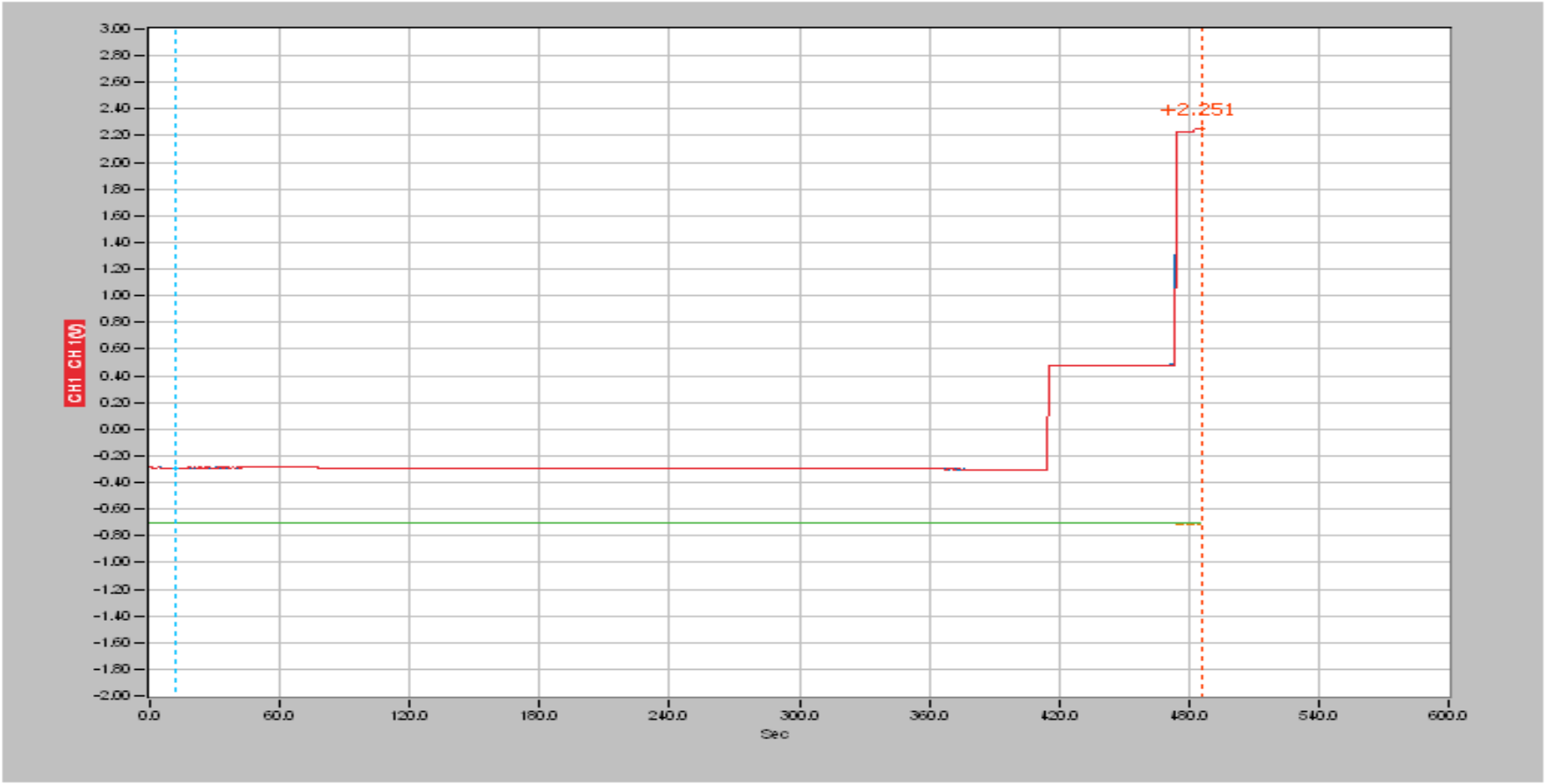

Figure D6 Strain curve diagram for GFRP at 21 days test

Steel 1 D14 curve: Ultimate loads = 397 kN

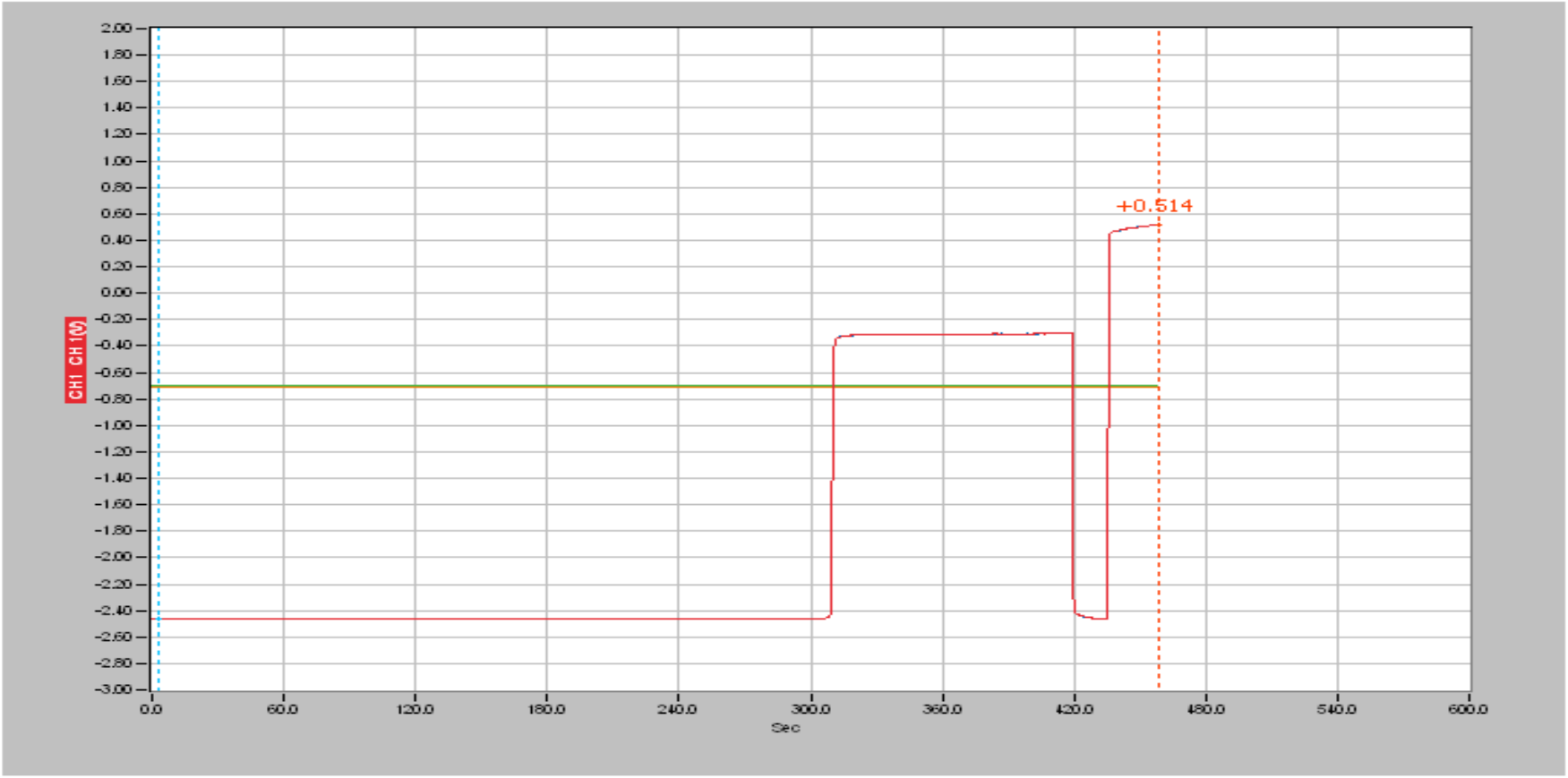

Figure D7 Strain curve diagram for steel at 14 days test

CFRP 2 D14 curve: Ultimate loads = 375.6 kN

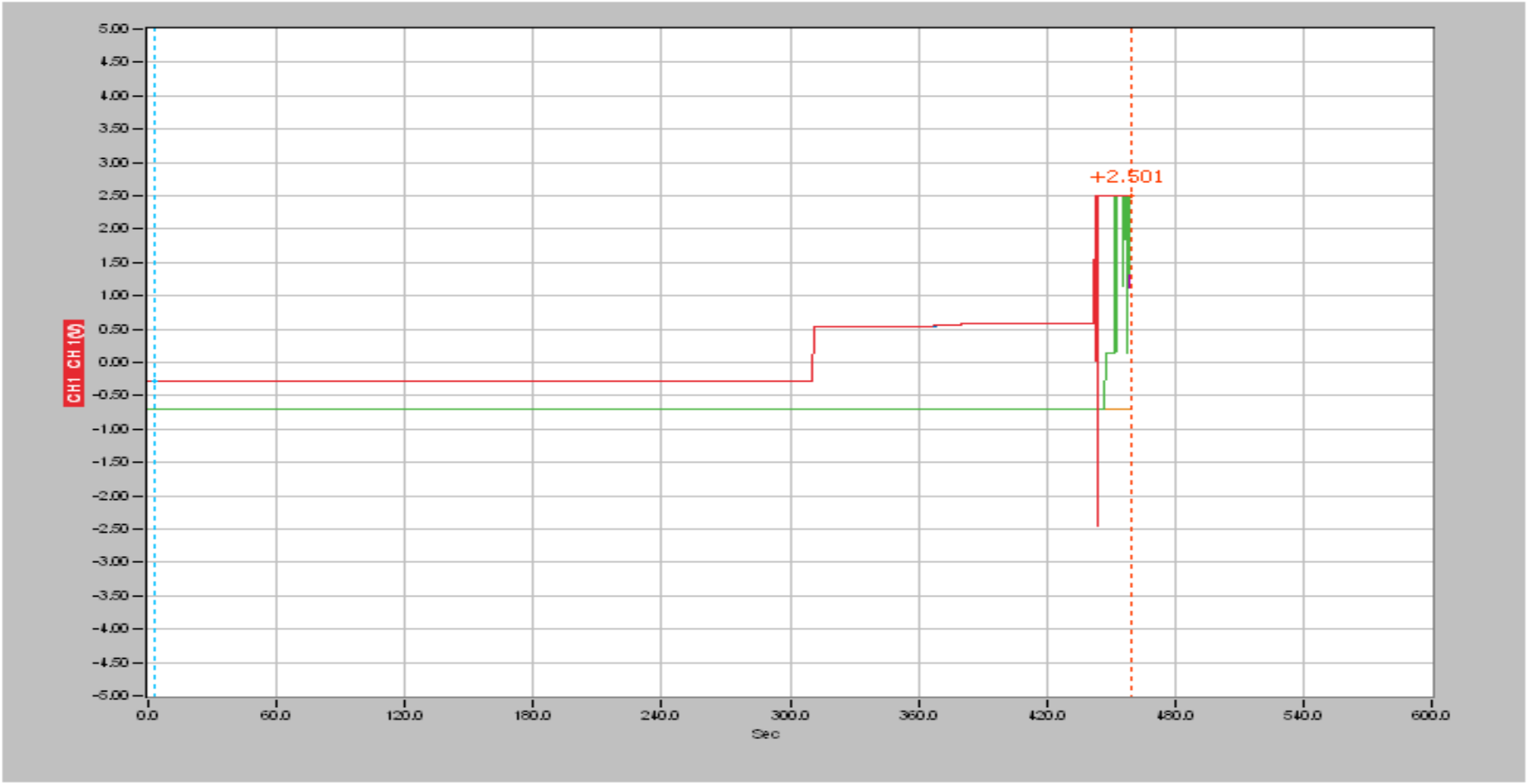

Figure D8 Strain curve diagram for CFRP at 14 days test

GFRP 3 D14 curve: Ultimate loads = 370 kN

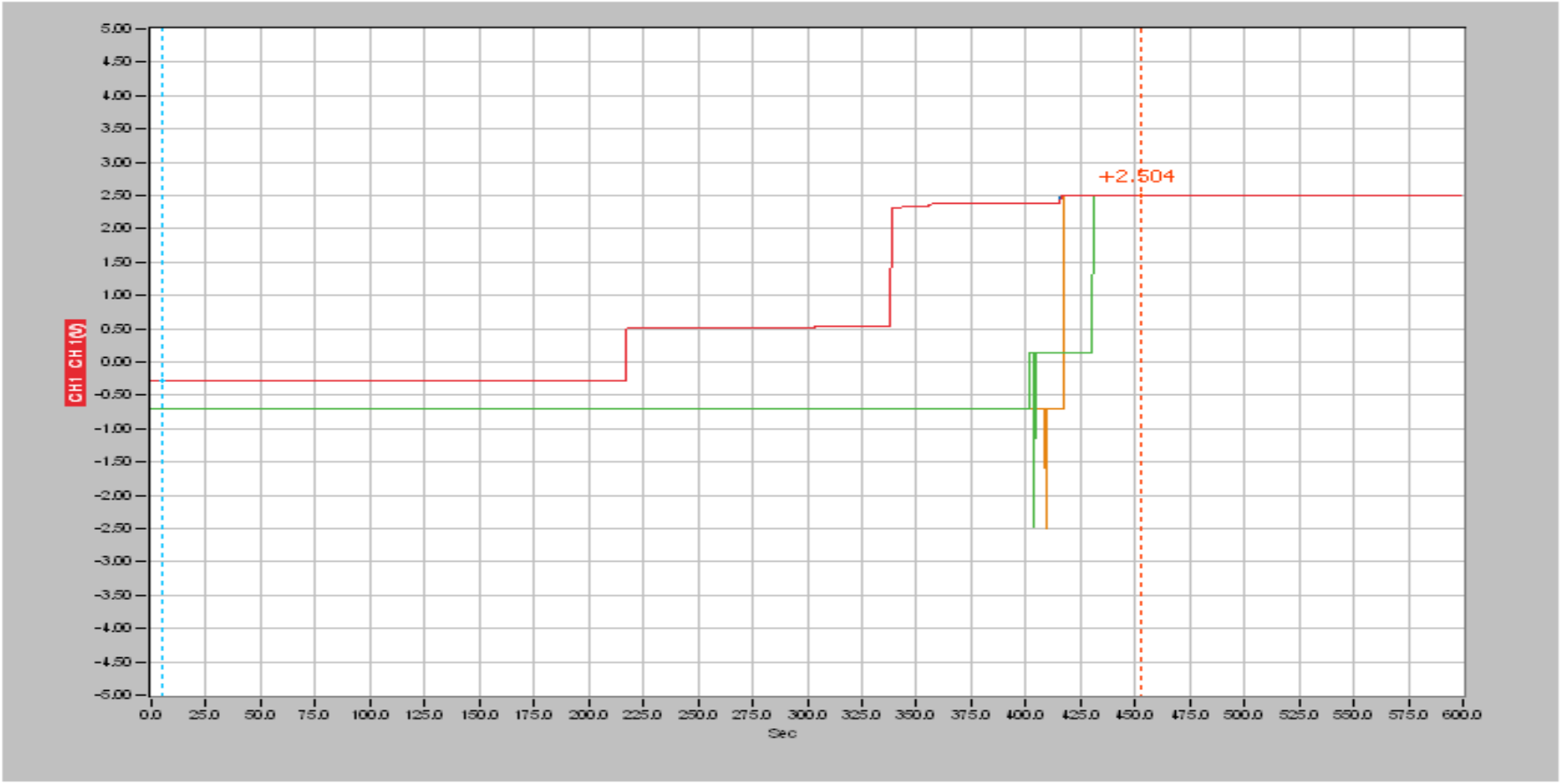

Figure D9 Strain curve diagram for GFRP at 14 days test

Steel 2 D7 curve: Ultimate loads = 350 kN

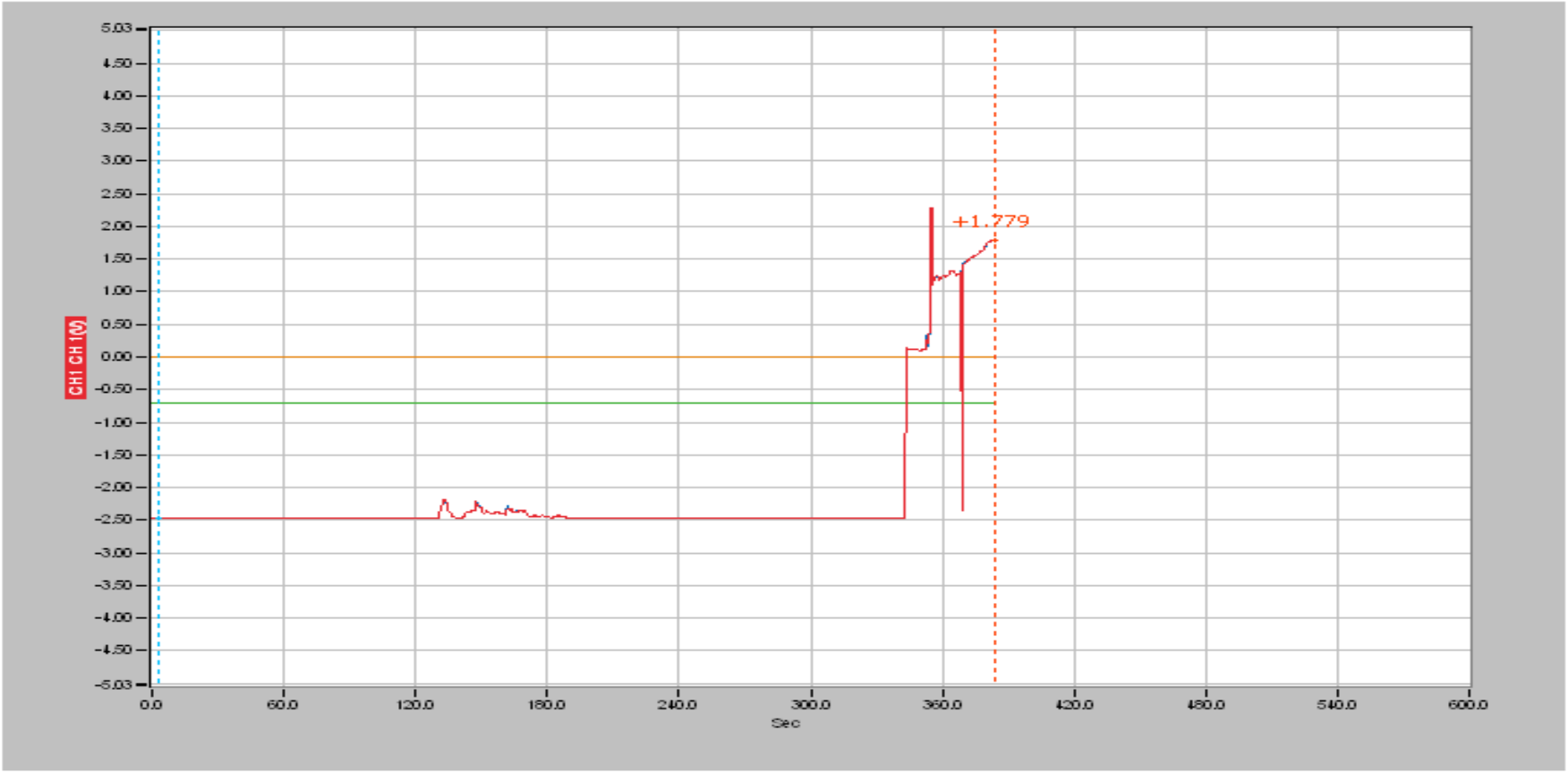

Figure D10 Strain curve diagram for steel at 7 days test

CFRP 1 D7 curve: Ultimate loads = 380 kN

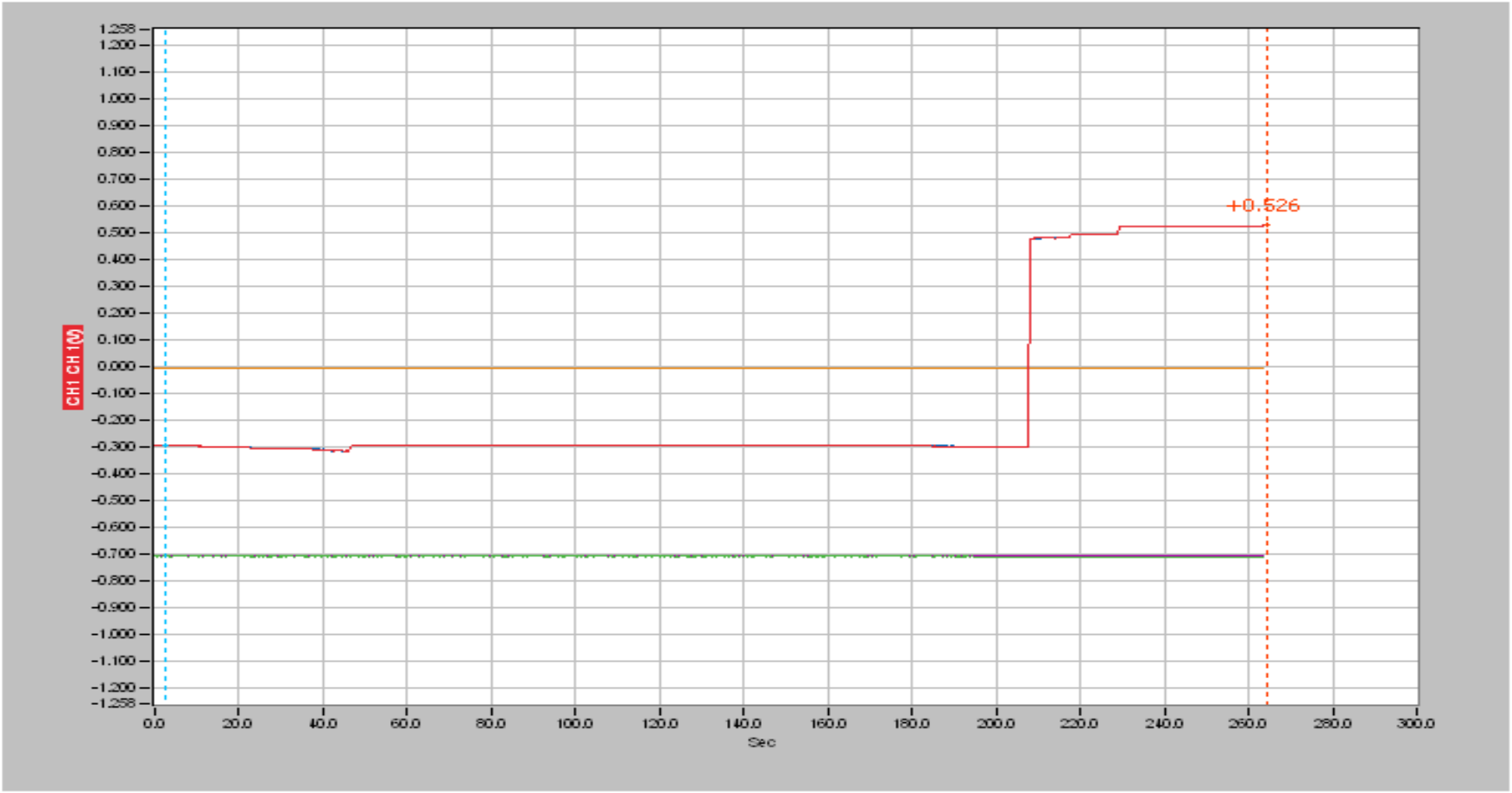

Figure D11 Strain curve diagram for CFRP at 7 days test

GFRP 1 D7 curve: Ultimate loads = 321 kN

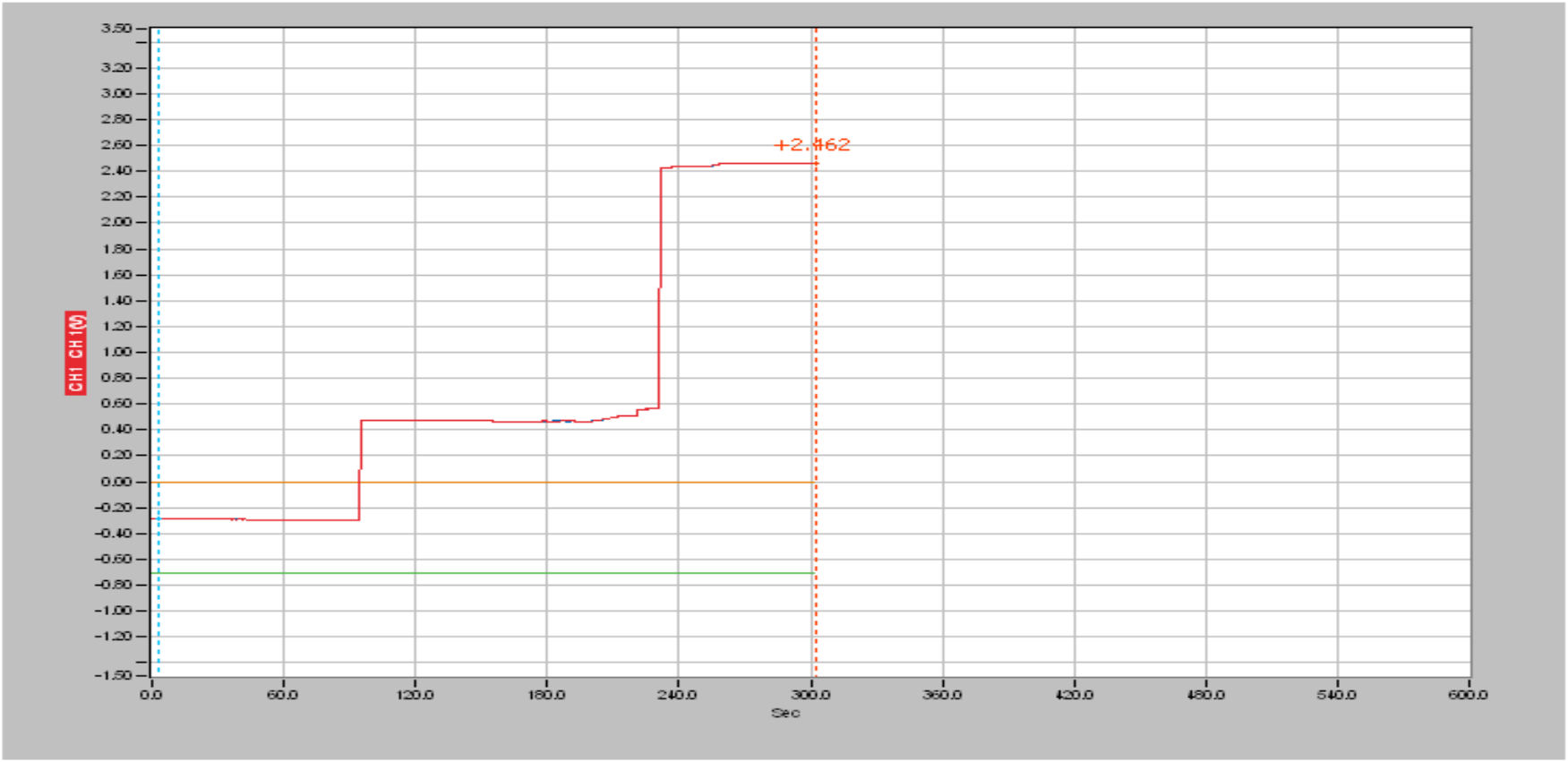

Figure D12 Strain curve diagram for GFRP at 7 days test